THE DEVELOPMENT OF FLUORESCENT PROBES AND SLOW-RELEASING H_2S DONORS FOR STUDYING BIOLOGICAL H_2S

by

MATTHEW D. HAMMERS

A DISSERTATION

Presented to the Department of Chemistry and Biochemistry
and the Graduate School of the University of Oregon
in partial fulfillment of the requirements
for the degree of
Doctor of Philosophy

June 2016

DISSERTATION APPROVAL PAGE

Student: Matthew D. Hammers

Title: The Development of Fluorescent Probes and Slow-Releasing H_2S Donors for Studying Biological H_2S

This dissertation has been accepted and approved in partial fulfillment of the requirements for the Doctor of Philosophy degree in the Department of Chemistry and Biochemistry by:

Michael M. Haley	Chairperson
Michael D. Pluth	Advisor
David R. Tyler	Core Member
Peter M. O'Day	Institutional Representative

and

Scott L. Pratt	Dean of the Graduate School

Original approval signatures are on file with the University of Oregon Graduate School.

Degree awarded June 2016

DISSERTATION ABSTRACT

Matthew D. Hammers

Doctor of Philosophy

Department of Chemistry and Biochemistry

June 2016

Title: The Development of Fluorescent Probes and Slow-Releasing H_2S Donors for Studying Biological H_2S

Hydrogen sulfide (H_2S) is an essential small molecule in human physiology. Although quite toxic, H_2S is produced endogenously and performs important regulatory functions in the cardiovascular, immune, nervous, and respiratory systems. Varied interactions with intracellular thiols, reactive oxidants, and protein transition-metal centers are highly dynamic and sensitive to fluctuations in redox homeostasis. Furthermore, H_2S is implicated in a number of diseases such as cancer, neurodegeneration, and heart disease. Hence, exogenously delivered H_2S as a therapeutic agent is an active area of intrigue and research. The complexity and interconnectivity of these processes has stimulated the development of advanced chemical tools with which to study biological H_2S, including reaction-based fluorescent probes and slow-releasing H_2S donors.

Toward these goals, I present several significant advances in the fields of H_2S detection and delivery. An azide reduction-based probe, MeRho-Az, provides a rapid >1,000-fold fluorescence response when treated with H_2S. MeRho-Az is sufficiently sensitive to detect endogenous H_2S in C6 cells and was used to image H_2S in live

zebrafish larvae using light sheet fluorescence microscopy, representing the first analyte-responsive experiments with this imaging technology. Using a ratiometric dual-fluorophore fragmentation strategy, NBD-Coum simultaneously detects, differentiates, and measures relative concentration ratios of H_2S versus cysteine/homocysteine, two important metabolites in H_2S biosynthesis. NBD-Coum was used to monitor changes in redox homeostasis in a simulated sulfur pool and is useful for studying H_2S-thiol dynamics. The synthesis and amide-coupling conditions of ADT-NH_2, a highly sought dithiolethione H_2S donor, allow for hydrolytically stable, H_2S-releasing non-steroidal anti-inflammatory drug hybrids. Finally, inspired by polysulfide-containing natural products, functionalized tetrasulfides are a new class of accessible, customizable, and versatile H_2S donors with controllable H_2S release rates. I hope that by using these investigative tools, chemists and biologists are able to refine our understanding of physiological H_2S and exploit H_2S activities in disease treatments.

This dissertation includes previously published and unpublished coauthored materials.

CURRICULUM VITAE

NAME OF AUTHOR: Matthew D. Hammers

GRADUATE AND UNDERGRADUATE SCHOOLS ATTENDED:

University of Oregon, Eugene, OR
University of Wisconsin – Eau Claire, Eau Claire, WI

DEGREES AWARDED:

Doctor of Philosophy, 2016, University of Oregon
Bachelor of Science, 2011, University of Wisconsin – Eau Claire
Bachelor of Business Administration, 2007, University of Wisconsin – Eau Claire

PROFESSIONAL EXPERIENCE:

Graduate Student Researcher, Department of Chemistry & Biochemistry, University of Oregon, Eugene, 2011-2016

Undergraduate Student Researcher, Department of Chemistry & Biochemistry, University of Wisconsin – Eau Claire, Eau Claire, 2010-2011

GRANTS, AWARDS, AND HONORS:

Graduate Teaching Fellowship 2011-2016

ACS Division of Organic Chemistry Travel Award, 2016

Honorable Mention, National Science Foundation Graduate Research Fellowship, 2013

PUBLICATIONS:

Hammers, M. D.; Singh, L.; Montoya, L. A.; Moghaddam, A. D.; Pluth, M. D. *Synlett* **2016**, eFirst online. [DOI: 10.1055/s-0035-1560603].

Pluth, M. D.; Bailey, T. S.; Hammers, M. D.; Hartle, M. D.; Henthorn, H. A.; Steiger, A. K. *Synlett* **2015**, *26*, 2633-2643.

Hammers, M. D.; Taormina, M. J.; Cerda, M. M.; Montoya, L. A.; Seidenkranz, D. T.; Parthasarathy, R.; Pluth, M. D. *J. Am. Chem. Soc.* **2015**, *137*, 10216-10223.

Sonke, E.; Verrydt, M.; Postenka, C.O.; Pardhan, S.; Willie, C. J.; Mazzola, C. R.; Hammers, M. D.; Pluth, M. D.; Lobb, I.; Power, N. E.; Chambers, A. F.; Leong, H. S.; Sener, A. *Nitric Oxide* **2015**, *49*, 26-39.

Hammers, M. D.; Pluth, M. D. *Anal. Chem.* **2014**, *86*, 7135-7140.

Pluth, M. D.; Bailey, T. S.; Hammers, M. D.; Montoya, L. A. *Biochalcogen Chemistry: The Biological Chemistry of Sulfur, Selenium, and Tellurium*; ACS Symposium Series 1152; University of Oregon, Eugene, OR **2013**, 15-32.

Hammers, M. D.; Wichman, J. J.; Wiegel, K. N. *Liquid Crystals* **2011**, *38*, 581-587.

ACKNOWLEDGMENTS

I wish to thank Professor Pluth for his tireless support every step of the way. I also give special thanks to Loveprit Singh and Mary Earp for their hard work and intellectual contributions. Finally, thanks to Mr. Sergei Rachmaninoff for his beautiful and stimulating music.

For my parents.

TABLE OF CONTENTS

LIST OF FIGURES

Figure Page

LIST OF TABLES

Table Page

LIST OF SCHEMES

Scheme Page

CHAPTER I

INTRODUCTION

Sulfur is an essential element for executing the human body's operational plan. In proteins, cysteine (Cys) amino acid thiols participate in enzymatic operations as a nucleophile, and oxidation of cysteine residues to form disulfide bridges help maintain the integrity of tertiary protein structure. Glutathione (GSH), a common Cys-containing tripeptide often present at up to 5 mM concentrations in the body, is an important antioxidant protecting cellular environments from harmful reactive oxygen and nitrogen species. Finally, hydrogen sulfide (H_2S), which contains fully reduced sulfur, performs signal transduction operations throughout the body, notably in heart, brain, and liver tissues. The rich chemical biology associated with physiological sulfur continues to evolve with our understanding of how these molecules interact among themselves and with other cellular machinery. To better facilitate research into these areas and to situate H_2S within this context, advanced chemical tools and methodologies are being developed for H_2S detection and delivery which provide important spatial and temporal information in both *in vitro* and *in vivo* experiments.

The perception of H_2S has been transformed from existing as merely a toxic, odorous environmental pollutant. This important small molecule is now recognized as an essential mammalian gasotransmitter, meaning H_2S is an endogenously produced gaseous signaling molecule with regulated biosynthetic, translocation, and metabolic pathways.[1-4] H_2S is generated enzymatically from Cys and homocysteine (Hcy) feedstocks primarily

by the enzymes cystathionine β-synthase (CBS),[5] cystathionine γ-lyase (CSE),[6] and 3-mercaptopyruvate sulfurtransferase (3-MST) (Figure 1.1).[7] The rate of H_2S biosynthesis is sensitive to concentration fluctuations of any of these feedstocks, and thus these pathways are tightly regulated. Generated H_2S then exerts regulatory influence in a number of systems within the body.[4] In the cardiovascular system, H_2S interacts with K_{ATP} channels and modulates vasorelaxation, angiogenesis, and cell proliferation/apoptosis.[8-11] H_2S elicits either pro- or anti-inflammatory responses in the immune system depending on experimental conditions, which is an intriguing and controversial aspect of current H_2S research.[12-15] H_2S is a neuromodulator, and its stimulation of NMDA receptors induces hippocampal memory formation in the central nervous system (CNS).[1,16] Furthermore, CNS diseases such as Alzheimer's and Parkinson's disease, as well as Down syndrome have been linked with abnormal H_2S production levels.[17-19] Much of the toxicity associated with H_2S is due to its effects on the respiratory system, where H_2S can inhibit cytochrome c oxidase and disrupt the electron transport chain in mitochondria.[20] The complexity and interconnectivity of these varied physiological implications require that advanced tools and technologies for H_2S detection be developed to differentiate the activities of H_2S from other biologically relevant analytes and to truly refine our understanding of physiological H_2S.

Although there is substantial evidence establishing the importance of H_2S in biology, historically the main challenge to fully elucidating its role has been a lack of detection and quantification methods that provide sufficient sensitivity, selectivity, *in vivo* compatibility, and ease of use. Because of this challenge, estimations of physiological H_2S levels have varied widely, over a five order of magnitude range.[21]

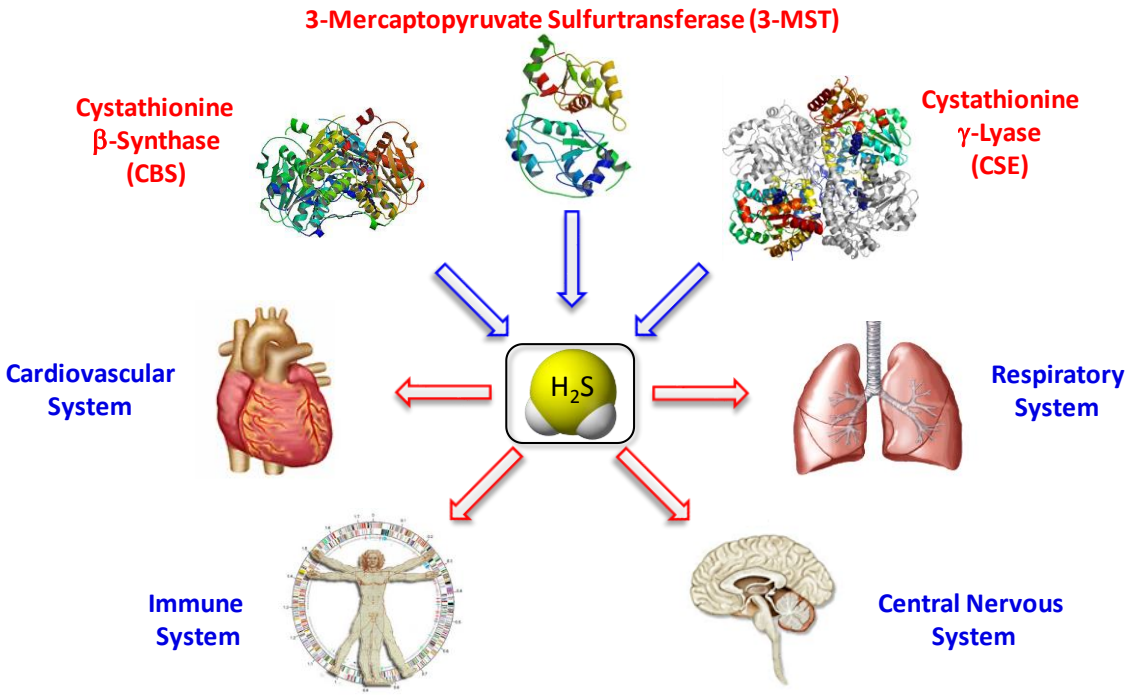

Figure 1.1. Endogenous biosynthesis and signaling targets of H_2S.

Until recently, the two most commonly used methods for H_2S detection and quantification have been the methylene blue (MB)[22] and monobromobimane (MBB)[23] assays (Figure 1.2a). In the MB assay, an experimental sample is treated with $Zn(OAc)_2$ and *p*-dimethylaminoaniline under acidic conditions to form methylene blue, which has a characteristic absorbance at 670 nm. Unfortunately, the harshly acidic conditions present in the MB workup liberate acid-labile sulfur from sources such as iron-sulfur clusters, which limits the selectivity of this method.[23] Alternatively, the MBB assay improves upon this limitation by analyzing the reaction products of an experimental sample with monobromobimane using fluorescence HPLC. H_2S undergoes nucleophilic substitution with two equivalents of monobromobimane to form sulfide-dibimane (SdB). SdB is fluorescent at 478 nm and can be quantified. Furthermore, a more elaborate workflow

used in concert with this strategy is able to differentiate sulfide from among different sulfur pools including free, sulfane, and acid-labile sulfide.[24] Homogenization of experimental tissue samples is required using either the MB or MBB assays, however, which precludes any live-cell or -animal imaging experiments. Other more classical technologies such as gas chromatography, polarography, and H_2S-selective electrodes also have similar limitations in sensitivity, response rate, selectivity, and/or require complex workups.[25-27] To overcome these challenges in H_2S detection, chemists have shifted their focus toward developing new methodologies including fluorescence detection.

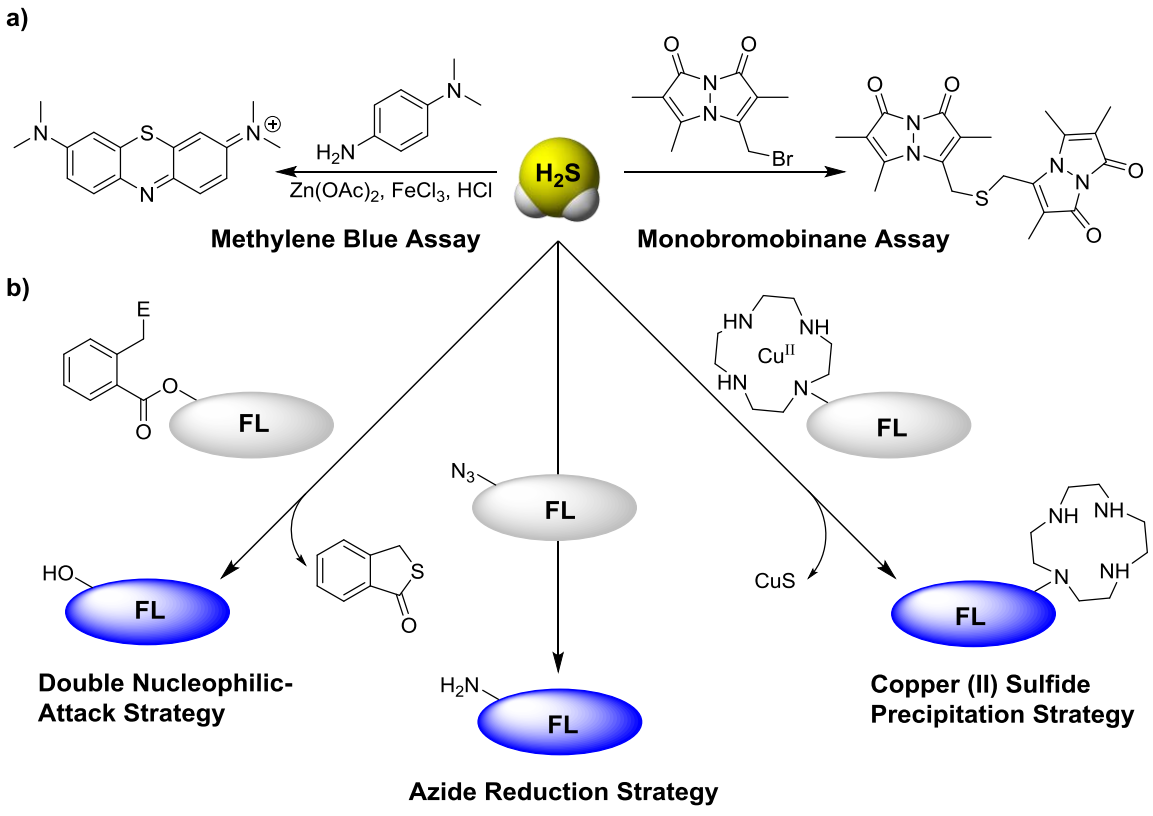

Figure 1.2. a) Traditional methods for H_2S detection including the methylene blue and monobromobimane assays. b) Fluorescence detection strategies for H_2S including double nucleophilic attack, copper (II) sulfide precipitation, and azide reduction.

Reaction-based, small-molecule fluorescent probes provide a number of advantages over previously developed H_2S detection strategies. Fluorescence detection experiments using these probes do not require harsh reaction conditions or tissue destruction for effective H_2S visualization and are thus amenable to both live-cell and *in vivo* environments. Furthermore, fluorescence imaging techniques may be performed with real-time spatiotemporal resolution. As chemists explore fluorescence-based H_2S detection, there are several important requirements to consider. The probe must react rapidly with H_2S, generate a strong and sensitive fluorescence response, and exhibit excellent selectivity for H_2S over other biologically relevant analytes (Cys and GSH in particular).

Toward these goals, three main reaction-based strategies (Figure 1.2b) have been developed which exploit unique characteristics of H_2S reactivity: utilizing 1) the dual-nucleophilicity of H_2S to liberate an ester-bound fluorophore adjacent to a nearby electrophilic site through an initial nucleophilic attack and successive intramolecular cyclization, 2) the propensity of H_2S to form insoluble salts with metal cations to precipitate CuS from Cu^{II}-ligated fluorophores, and 3) the reducing power of H_2S to reduce azide-modified fluorophores and regenerate their respective fluorogenic amines. In each of these strategies, a fluorophore is structurally modified such that its fluorescence is quenched. Reaction with H_2S removes this quenching mechanism and results in a fluorescence turn-on. This topic has been reviewed extensively,[28-39] and the reader is directed to Chapters II and III for additional discussion. Of these fluorescence-

based H_2S detection strategies, azide reduction has been the most broadly applied, partly due to the ease of azide functionalization of amine-containing fluorophores and the plethora of amine-containing fluorophores from which to functionalize. As such, this strategy has been extended to include over 70 fluorophore scaffolds in only the past several years. Taken together, the advent of reaction-based fluorescent probes for H_2S has provided chemical biologists with a new class of tools with which to perform live-cell and *in vivo* experiments not possible using previously developed assays. With the added knowledge that these experiments provide, scientists look toward application-driven development of new research tools.

As we refine our understanding of the physiological roles of H_2S, it becomes clear that H_2S activity and disease are closely related. Therefore, there is motivation for chemists to construct synthetic donor molecules that deliver 'caged' H_2S into biological systems within the context of therapeutic application for diseases such as cancer, inflammation, neurodegeneration, heart disease, and HIV (Figure 1.3).[13,40-43] Injecting H_2S gas or its sodium salt, NaHS, into a biological system results in an immediate, large burst of H_2S; however, and the abrupt homeostatic perturbation likely has erroneous effects unrelated to the specific H_2S activity of interest. Delivering H_2S in a more controlled manner akin to endogenous production rates would be more advantageous when isolating cause and effect relationships. Several classes of slow-releasing H_2S donors have been developed for this purpose,[42,43] including dithiolethione-containing compounds such as ADT-OH, phosphinodithioate GYY4137, thiol-mediated *N*-mercaptobenzamides and perthiols, light-activated geminal dithiols, and even polysulfide-containing natural products. Many of these compounds have been

investigated for their therapeutic potential. In particular, ADT-OH has been investigated in conjunction with bound non-steroidal anti-inflammatory drugs (NSAIDs) for their synergistic antioxidant and anti-inflammatory activities. It has been functionalized with a number of NSAIDs through ester linkages, such as aspirin and naproxen,[44,45] and several of these H_2S-donating NSAIDs are in clinical trials.[46] GYY4137 has also been investigated extensively in cancer and cardiovascular disease research.[47] The reader is directed to Chapters IV and V for additional discussion of these compounds and their application in drug therapeutics. Overall, the observed physiological effects of H_2S often vary significantly depending upon which H_2S donor is used in the experiment, and judicious selection of H_2S donor appears essential to eliciting a desired physiological response.

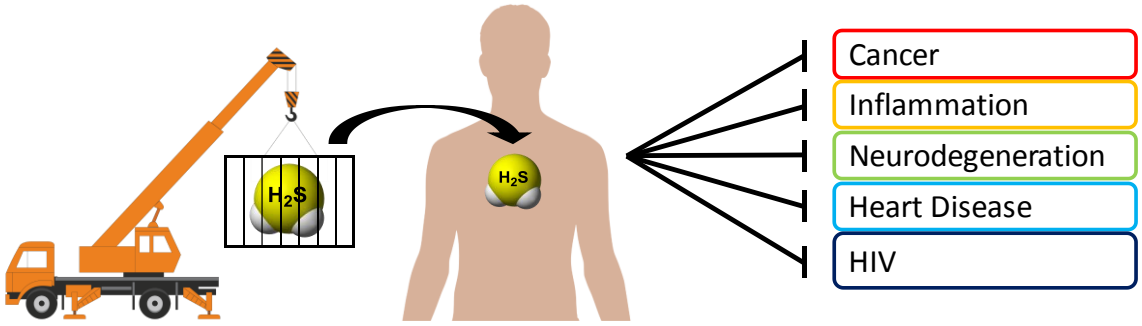

Figure 1.3. Synthetic H_2S donors deliver caged sulfide for the treatment of a number of diseases, including inflammation, neurodegeneration, cancer, heart disease, and HIV.

In this dissertation, I have created and investigated chemical tools for assisting chemists, biochemists, and biologists in their study of the two main areas of H_2S research: identifying the physiological roles of H_2S and utilizing exogenous H_2S in drug

therapeutic applications. In Chapters II and III, I describe the development of an azide-reduction strategy for H_2S detection which represents the strongest fluorescence response reported to date and a dual-fluorophore fragmentation system which simultaneously detects and differentiates H_2S and Cys/Hcy. Then in Chapters IV and V, I present the synthesis and amide-coupling of ADT-NH_2 with various NSAIDS which exhibits significantly improved hydrolytic stability over ester-bound analogs and tetrasulfides as a new easily-accessible class of H_2S donors.

These chapters include both previously published and unpublished coauthored works of the following:

CHAPTER II: A BRIGHT FLUORESCENT PROBE FOR H_2S ENABLES ANALYTE-RESPONSIVE, 3D IMAGING IN LIVE ZEBRAFISH USING LIGHT SHEET FLUORESCENCE MICROSCOPY

- **Hammers, M. D.**; Taormina, M. J.; Cerda, M. M.; Montoya, L. A.; Seidenkranz, D. T.; Parthasarathy, R.; Pluth, M. D. *J. Am. Chem. Soc.* **2015**, *137*, 10216-10223.
- Co-authors: Michael J. Taormina, Matthew M. Cerda, Leticia A. Montoya, Daniel T. Seidenkranz, Rahuveer Parthasarathy, and Michael D. Pluth

CHAPTER III: RATIOMETRIC MEASUREMENT OF H_2S AND CYSTEINE/HOMOCYSTEINE RATIOS USING A DUAL-FLUOROPHORE FRAGMENTATION STRATEGY

- **Hammers, M. D.**; Pluth, M. D. *Anal. Chem.* **2014**, *86*, 7135-7140.

- Coauthors: Michael D. Pluth

CHAPTER IV: SYNTHESIS OF AMINO-ADT PROVIDES ACCESS TO HYDROLYTICALLY-STABLE AMIDE-COUPLED H_2S-RELEASING DRUG TARGETS

- **Hammers, M. D.**; Singh, L.; Montoya, L. A.; Moghaddam, A. D.; Pluth, M. D. *Synlett* **2016**, eFirst online. [DOI: 10.1055/s-0035-1560603].
- Coauthors: Loveprit Singh, Leticia A. Montoya, Alan D. Moghaddam, Michael D. Pluth

CHAPTER V: FUNCTIONALIZED TETRASULFIDES AS EASILY ACCESSABLE H_2S DONORS

- Unpublished, *manuscript in preparation*
- Coauthors: Mary S. Earp, Michael D. Pluth

CHAPTER II

A BRIGHT FLUORESCENT PROBE FOR HYDROGEN SULFIDE ENABLES ANALYTE-RESPONSIVE, 3D IMAGING IN LIVE ZEBRAFISH USING LIGHT SHEET FLUORSCENCE MICROSCOPY

This work includes previously published and coauthored material from Hammers, M. D.; Taormina, M. J.; Cerda, M. M.; Montoya, L. A.; Seidenkranz, D. T.; Parthasarathy, R.; Pluth, M. D. *J. Am. Chem. Soc.* **2015**, *137*, 10216-20223.

Introduction

The perception of hydrogen sulfide (H_2S) in the scientific community has shifted dramatically in the 21st century.[4] No longer viewed as merely a toxic geological and environmental pollutant, H_2S is now at the center of a rich and expanding field focused on investigating its biological and physiological significance. Since 1996, when Abe and Kimura first suggested that H_2S acts as a neuromodulator in hippocampal long-term potentiation,[1] H_2S has been recognized as an essential gasotransmitter that regulates many important physiological functions in the cardiovascular, nervous, endocrine, immune, and gastrointestinal systems.[4,8,16,48-50] Biosynthesized by three main enzymes, cystathionine-β-synthase (CBS), cystathionine-γ-lyase (CSE), and 3-mercaptopyruvate sulfurtransferase (3-MST), H_2S is generated enzymatically in the heart, brain, liver, and kidneys; however, localized H_2S concentrations in the body are tissue-dependent,

suggesting differential activation and action in various H_2S-producing pathways.[51] Once generated, H_2S undergoes complex catabolism through its interactions with cellular oxidants, protein transition-metal centers, and reactive sulfur, oxygen, and nitrogen species (RSONs), all of which are sensitive to internal and external redox stimuli. For example, oxidative *S*-sulfhydration (or persulfidation) of protein cysteine residues is proposed to constitute a significant sulfide storage mechanism, which modifies protein function and the signaling activity of H_2S.[52-55] The intricacy of physiological H_2S reactivity requires that researchers utilize advanced chemical and technological tools for H_2S detection and imaging in order to gain a more detailed understanding of the interconnectivity of these networks.

In recent years chemists have answered the call for improved tools for H_2S detection by developing small-molecule fluorescent probes and similar methods to investigate biological H_2S.[28,56] Historically the most widely utilized assay for H_2S detection and quantification has been the methylene blue assay.[22] This technique, however, requires sample homogenization and a harshly acidic workup that precludes real-time detection or live-animal imaging. These conditions also liberate sulfur from acid-labile sulfur pools and are thus not selective for H_2S.[24] By contrast, H_2S quantification using monobromobimane (mBB) has better detection limits and enables separation of free, sulfane, and acid-labile sulfide pools.[23] Although the mBB method offers a robust platform for H_2S quantification, this technique still requires sample destruction and additional HPLC analysis. Similarly, the usefulness of other techniques including gas chromatography and sulfur-selective electrodes are limited by complex workups and/or insufficient sensitivity.[25,27] Alternatively, reaction-based fluorescent

probes offer the potential for *in vivo* compatibility, high sensitivity, and high spatiotemporal resolution while maintaining selectivity for H_2S over other RSONs including free thiols, which are abundant in much higher concentrations than H_2S in cellular milieu. Based on these requirements, three main reaction-based strategies for H_2S imaging have been developed: using the dual-nucleophilicity of H_2S to liberate ester-bound fluorophores with nearby reactive electrophilic sites,[57-63] formation and displacement of CuS from Cu^{II}-ligated fluorophores,[64-66] and reduction of nitro- and azide-functionalized fluorophores.[67-82] Among these strategies, H_2S-mediated azide reduction has been the most broadly reported due to the plethora of amine-functionalized fluorophores available for modification and the ease of azide functional group installation. Azide reduction is often rapid and produces large (10–100-fold) fluorescence turn-ons, with the resultant probes exhibiting functional low micromolar detection limits and excellent selectivity profiles. One limitation of such methods, however, is the potential photoreduction of azides to amines, which can lead to unwanted photoactivation in long-term imaging experiments.[76]

Despite the rapidly-advancing progress in H_2S probe development, few examples of live-animal imaging and application of these tools in biological studies exist[80,83-85] due to the substantial challenges associated with transitioning from cell culture to whole organisms. Additionally, the innate sensitivity of fluorophores to high energy excitation must be considered against tissue penetration requirements for *in vivo* imaging, thus complicating problems with azide photoactivation. Laser scanning confocal microscopy, a popular technique in three-dimensional fluorescence imaging, inherently sacrifices illumination efficiency in order to achieve highly resolved, focused images. This process

often results in photobleaching (or photoactivation). An alternative imaging strategy with significantly reduced photobleaching and phototoxicity by comparison to confocal or even 2-photon illumination is light sheet fluorescence microscopy (LSFM), in which excitation light is confined to a thin sheet coinciding with the focal plane of a wide field imaging system.[86-90] LSFM also provides access to significantly larger samples (> 1 mm) than conventional confocal microscopy, while maintaining fast imaging times. Highlighting the impact of this emerging imaging technique, LSFM of larval zebrafish, a useful model for many aspects of vertebrate development,[91] enables the imaging of intestinal tract contents with three-dimensional spatial resolution of microns, temporal resolution of seconds, and durations of tens of hours. Such contents can include bacterial communities colonizing the gut of the fish, a particularly interesting target for future investigations of microbial sulfur metabolism and the role of H_2S and associated sulfur-containing species in gut microbiota.[92,93] A key unmet step toward bridging this gap, however, is the utilization of analyte-responsive imaging tools in combination with LSFM. Combining these application-driven approaches would enable significant new avenues of investigation, such as small-molecule and secondary messenger trafficking, by providing access to real-time, analyte-responsive imaging in whole organisms. Toward this goal, we report herein the development of a bright fluorescent probe for selective H_2S imaging and demonstrate for the first time analyte-responsive detection experiments in combination with LSFM in live zebrafish. Supplemental information can be found in Appendix A.

Results and Discussion

Because of the small sample volume excited during LSFM experiments, a high dynamic range and a bright fluorophore are key probe requirements for analyte detection studies. Although fluorescein and rhodamine are common platforms in the design of reaction-based probes because of their excellent photophysical properties, including high extinction coefficients and quantum yields,[94] their susceptibility to photobleaching and pH sensitivity can limit their versatility in certain biological environments. Additionally, although reaction-based probes for H_2S detection based on azido-fluorescein or rhodamine conjugates have provided useful tools for investigations of H_2S in context,[67,79] the dynamic range of these scaffolds (typically < 25-fold turn-on) remains insufficient for LSFM investigations. To overcome these limitations, we reasoned that the rhodol (or rhodafluor) family of fluorophores would provide an attractive platform well suited for LSFM with improved pH insensitivity and photostability, while retaining many of the key photophysical advantages of their parent structures.[95] Additionally, *O*-alkylation of rhodols provides a potential handle for structural modification, and unlike fluorescein, *O*-alkylation typically does not appreciably mitigate the quantum yield. Consequently, rhodol derivatives have been adopted as sensors for hydrogen peroxide, hydrolase activity, nitroxyl, and thiols in recent years.[96-99] We envisioned that an *O*-methylrhodol (MeRho) modified by an azide-functionalized xanthene core (MeRho-Az) would be locked in a *non-fluorescent* spirocyclic lactone tautomer. H_2S-mediated azide reduction would unmask fluorophore fluorescence by regenerating the amine and unlocking the *fluorescent* open tautomer (Scheme 2.1). Given the inherent brightness of rhodols and the rapidity of H_2S-mediated azide reduction, we reasoned that MeRho-Az would produce a

strong fluorescent response to H_2S when reduced, thus providing a high fidelity functional tool for studying H_2S *in vivo* that is compatible with LSFM.

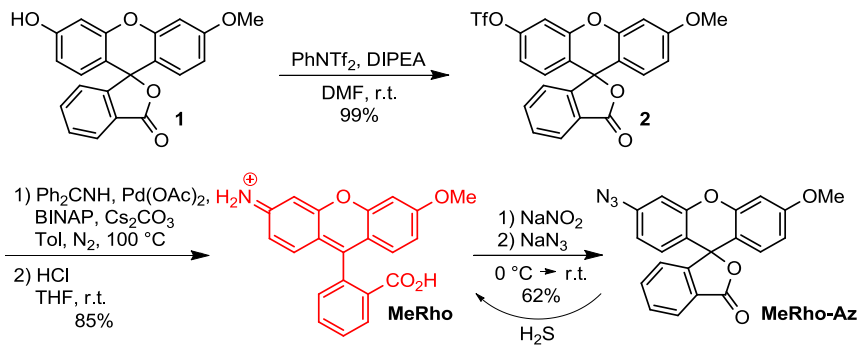

Scheme 2.1. Synthesis and H_2S-mediated activation of MeRho-Az.

To test this design hypothesis, we first prepared the rhodol scaffold by adapting the modular rhodol synthesis reported by Yang and co-workers[100] to convert methylfluorescein (1) to MeRho in two steps. Triflation of 1 with *N*-phenyl-*bis*(trifluoromethanesulfonamide) to form triflated methylfluorescein (2), and subsequent Buchwald-Hartwig amination with benzophenone imine as an ammonia equivalent, followed by acid hydrolysis, affords MeRho in 84% overall yield. During reaction optimization, we found that initially heating the amination reaction to 140 °C increased the yield significantly, presumably by either facilitating efficient formation of the L–Pd^0 active catalyst or by accelerating oxidative addition of 2. Finally, diazotization of MeRho and azidification under Sandmeyer conditions affords MeRho-Az.

With both MeRho and MeRho-Az in hand, the photophysical properties of each compound were characterized (Table 2.1). MeRho displays excellent solubility in aqueous buffer (50 mM PIPES, 100 mM KCl, pH 7.4), with absorption and fluorescence bands centered at 476 nm and 516 nm, respectively (Figure A.1). As predicted, MeRho exhibits a high quantum yield (Φ_{MeRho} = 0.57), whereas the quantum yield of the closed lactone form of MeRho-Az is essentially zero when excited at either the λ_{max} (286 nm) or that of MeRho (476 nm). To establish the fidelity of the MeRho scaffold under physiological conditions, we investigated the pH-dependent fluorescence. By performing a pH titration and monitoring the fluorescence, we established that the MeRho fluorophore maintains a constant emission between pH 4.5 and 10 (Figure 2.1), with apparent pK_a values of 3.3 and 12.2, making the biologically viable pH range superior to that of fluorescein (Figure A.2). Additionally, the MeRho fluorophore maintains 75% of its maximum fluorescence under highly-acidic conditions.

	λ_{max} (nm)	ε (M^{-1} cm^{-1})	λ_{em} (nm)	Φ
MeRho	476	30,800	516	0.57
MeRho-Az	286	13,900	N/A	< 0.01

Table 2.1. Spectroscopic properties of MeRho and MeRho-Az in PIPES buffer (50 mM, 100 mM KCl, pH 7.4). Quantum yield are presented relative to fluorescein (0.1 M NaOH).

Having established that MeRho offers a bright, biocompatible fluorophore platform, we next investigated the viability of MeRho-Az as a fluorescent H_2S sensor. MeRho-Az (5 μM) exhibits a rapid increase in fluorescence when treated with 50 equiv.

of NaHS (250 μM) in aqueous PIPES buffer (50 mM, 100 mM KCl, pH 7.4). Owing to the stark contrast in brightness between the azide- and amine-functionalized rhodol scaffolds, reduction of MeRho-Az to the parent amine produces a 1200-fold fluorescence turn on (F/F_0) over 60 minutes (440-fold without any background correction) (Figure 2.2a). This represents one of the strongest fluorescent responses from H_2S detection recorded to date.

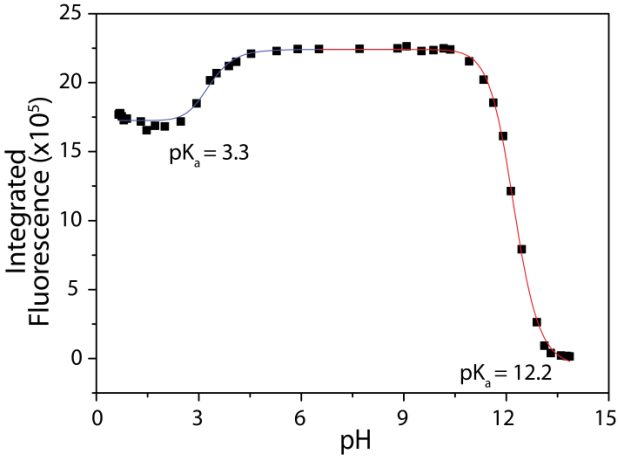

Figure 2.1. Integrated MeRho fluorescence (20 μM, λ_{ex} = 476 nm, λ_{em} = 480-650 nm) in aqueous solution at various pH (100 mM KCl).

While the reaction of some probes with H_2S may reach completion more quickly, the magnitude of response with MeRho-Az after merely five minutes is significant. Furthermore the fluorescence turn-on characteristics of MeRho-Az are faster and stronger than a recently reported nitro-reduction rhodol platform,[101] which is consistent with previous findings from our group in which azide reduction on a naphthalimide scaffold proceeds faster and has a stronger turn-on than the corresponding nitro-functionalized analogue.[102] After determining that MeRho-Az effectively reports on H_2S, the sensitivity

and detection limit of the probe was examined. A linear, concentration-dependent fluorescence relationship was observed between MeRho-Az fluorescence and increasing H_2S concentrations (Figure 2.2b, Table A.1). The detection limit was calculated to be the concentration at which the fluorescence equals that of [blank + 3σ] according to a linear regression fit of the data and determined to be 86 ± 7 nM. Supporting the validity of this detection limit, the MeRho-Az probe can differentiate between 1.0 and 0.10 μM H_2S with a *p* value < 0.01. Finally, to test the photostability of MeRho-Az, we prepared three common azide-based H_2S detection probes HSN2, DNS-N_3, and C7-Az,[68,77,102] which are based on naphthalimide, dansyl, and coumarin fluorophores, respectively, and compared the photoactivation of each azide under identical conditions in the absence of H_2S. As expected, the rhodol system in MeRho-Az exhibits significantly less photoactivation than the other azide-based systems (Figure 2.2c). Taken together, these data demonstrate the reactivity of MeRho-Az with H_2S and highlights its sensitivity and potential for use in biological applications.

After establishing the concentration-dependent reactivity for MeRho-Az with H_2S, we examined the reactivity of various RSONs toward the probe to establish a selectivity profile (Figure 2.3). No fluorescence was observed upon introduction of 50 equiv. (250 μM) of biological thiols cysteine (Cys), homocysteine (Hcy), or glutathione (GSH) over 60 minutes. Sulfur anions thiosulfate, ($S_2O_3^{2-}$), sulfite (SO_3^{2-}), and sulfate (SO_4^{2-}), as well as hydrogen peroxide (H_2O_2) and nitric oxide (NO) also all proved to be chemically inert toward the probe. Additionally, MeRho-Az exhibits 32-fold preferential reactivity with H_2S relative to 5 mM GSH loading, thus reinforcing the excellent selectivity of the H_2S-mediated azide-reduction mechanism.

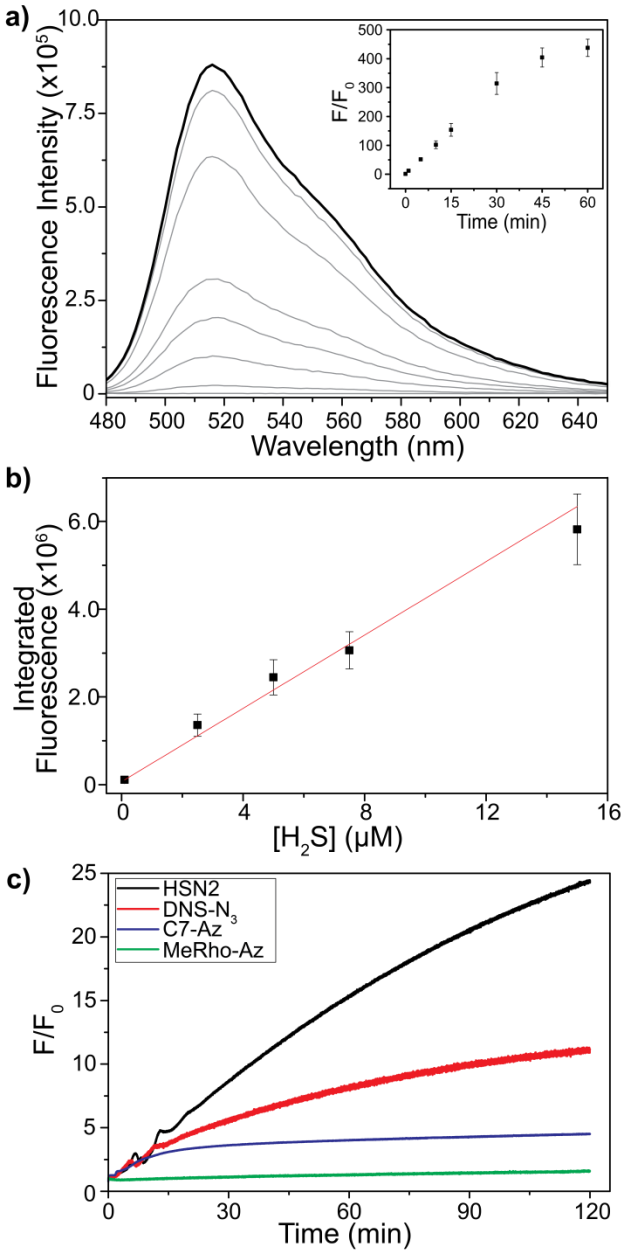

Figure 2.2. a) Uncorrected fluorescent response of MeRho-Az to NaHS treatment over 60 minutes. Conditions: 5 μM MeRho-Az, 250 μM NaHS, PIPES buffer (50 mM, 100 mM KCl, pH 7.4), λ_{ex} = 476 nm, λ_{em} = 480-650 nm, 37 °C. b) Concentration-dependent fluorescence of MeRho-Az when treated with 0.10, 2.5, 5.0, 7.5, and 15 μM NaHS and incubation for 90 minutes at 37 °C. Each data point represents the average of at least three trials. Error bars were calculated as standard deviation. c) Fluorescence photoactivation response of HSN2 (λ_{ex} = 432 nm, λ_{em} = 542 nm), DNS-N_3 (λ_{ex} = 340 nm, λ_{em} = 550 nm), C7-Az (λ_{ex} = 340 nm, λ_{em} = 445 nm), and MeRho-Az (λ_{ex} = 476 nm, λ_{em} = 516 nm). Excitation slits: 2.6 nm. Data measured at 4 s^{-1}.

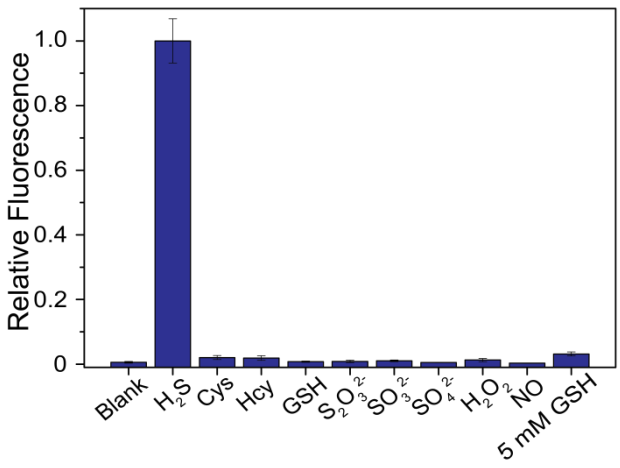

Figure 2.3. Selectivity profile of MeRho-Az toward reactive sulfur, oxygen, and nitrogen species. From left to right: blank, NaHS, L-cysteine, DL-homocysteine, glutathione, $Na_2S_2O_3$, Na_2SO_3, Na_2SO_4, H_2O_2, and DEA NONOate. Conditions: 5 µM MeRho-Az, 250 µM RSONs, PIPES buffer (50 mM, 100 mM KCl, pH 7.4), λ_{ex} = 476 nm, λ_{em} = 480-650 nm, 37 °C. Data were acquired after 60 minute incubation at 37 °C.

Based on the excellent H_2S sensing properties of MeRho-Az, we sought to establish the efficacy of MeRho-Az for detecting endogenously produced H_2S in cells. After incubation of C6 rat glial cells, which express the H_2S-producing CBS enzyme, with 5 µM MeRho-Az for 45 minutes, the cells were fixed and imaged using a fluorescence microscope (Figure 2.4). We then compared this fluorescence response with cells that had been pretreated with either a slow-releasing H_2S donor (AP39, 100 nM)[103] or a common CBS inhibitor (aminooxyacetic acid, AOAA, 20 µM).[104] We observed a significant reduction in fluorescence in cells treated with AOAA by contrast to untreated cells, suggesting that MeRho-Az is sufficiently sensitive to detect endogenous levels of enzymatically-produced H_2S. Furthermore, cells treated with low concentrations of AP39 showed enhanced fluorescence, highlighting the sensitivity of the system. These results demonstrate the applicability of the MeRho-Az platform in cellular environments, which

can likely be extended to assays involving biological fluids such as serum, blood, or tissue homogenates.

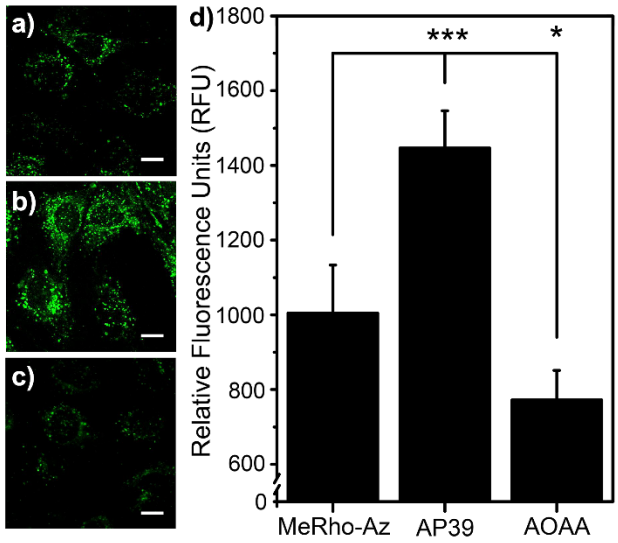

Figure 2.4. Fluorescence imaging of H_2S in C6 cells. Cells were imaged after incubation with 5 µM MeRho-Az for 45 minutes after pretreatment with a) no pretreatment, b) 100 nM AP39 for 60 minutes, or c) 20 µM AOAA for 45 minutes. Scale bars = 5 µm. d) Quantified cellular fluorescence after reaction of MeRho-Az with endogenous H_2S (MeRho-Az, N=3), after addition of exogenous H_2S (AP39, N=3), and after inhibition of enzymatic H_2S production (AOAA, N=3).

To further establish MeRho-Az as an *in vivo* H_2S reporter, we next examined its biocompatibility using LSFM. Because little is known about endogenous sulfide dynamics in developing zebrafish, we focused our initial efforts on H_2S release from a commonly used slow-releasing H_2S donor, diallyl trisulfide (DATS). To confirm, as previously reported, that a thiol such as GSH is required to achieve H_2S release from DATS,[105] we used MeRho-Az with DATS to detect liberated H_2S and observed a dose-dependent release of H_2S in response to [GSH] (Figure A.3). To expand on the use of

MeRho-Az and to establish its validity for use with LSFM in live organisms, we chose to use larval (7 days post fertilization) zebrafish for imaging studies. At this stage in their development, zebrafish are approximately 3 mm in length and maintain a high level of transparency. Also, a key benefit of LSFM is that the collection of illuminated sheets that make up the three-dimensional images is obtained on a time scale (~10 seconds in total) significantly faster than the timescale of gut peristalsis (~ 1 min), which allows for direct analysis of the actual gut volume with minimal artifacts from translational movement. We first tested the toxicity of MeRho-Az in larval zebrafish by orally gavaging[106] 7 nL of buffered solutions (50 mM PIPES, 100 mM KCl, pH 7.4) containing 5 μM MeRho-Az, and monitored the fish over time. No toxicity was observed for 20 hours, and although this cannot completely rule out unwanted biological effects in longer term experiments, it suggests the safe use of MeRho-Az as a viable *in vivo* fluorescent reporter over the time scale of hours. To test the ability of MeRho-Az to provide an analyte-responsive signal toward H_2S, larval zebrafish were orally gavaged with buffered solutions containing: buffer only, 5 μM MeRho-Az, 5 μM MeRho-Az + 250 μM DATS, 5 μM MeRho-Az + 250 μM DATS + 250 μM GSH, or 5 μM MeRho. After 60 minutes of recovery time, a three dimensional image of the intestinal bulb for each fish was acquired using LSFM (Figure 2.5).

No difference in fluorescence was observed when comparing the signal between a vehicle-gavaged control group and fish gavaged with either MeRho-Az alone or MeRho-Az + DATS, confirming that LSFM was not causing photoactivation of the azide and that H_2S release from DATS was GSH-dependent (Figure 2.6). By utilizing a control of buffer-gavaged fish instead of un-gavaged fish, the relative strength and variability of

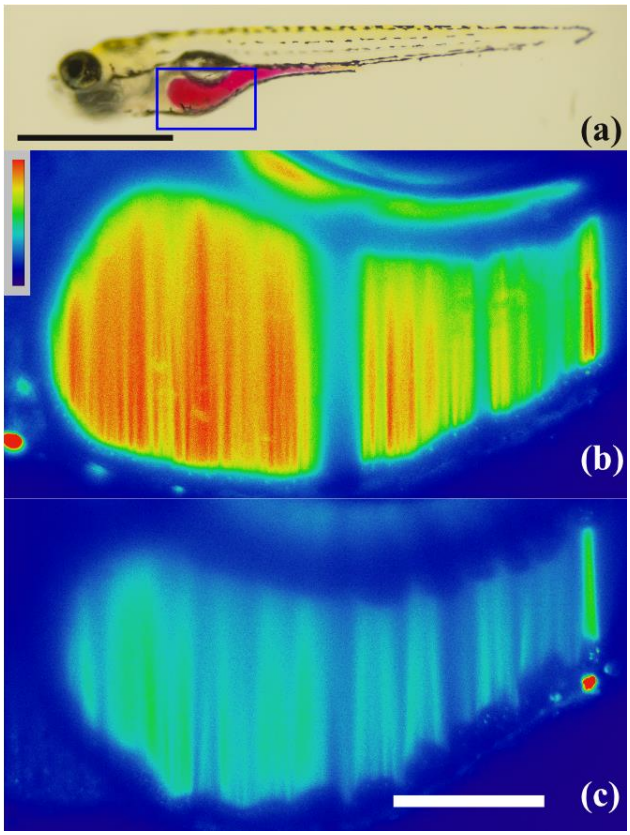

Figure 2.5. 2D slices of LSFM images of live zebrafish 60 minutes after gavage. a) Larval zebrafish (7 dpf) gavaged with phenol red to highlight the intestine (scale bar = 1 mm). The boxed region corresponds to the intestinal bulb expanded below in b,c). Zebrafish gavaged with b) 5 µM MeRho-Az + 250 µM DATS + 250 µM GSH or c) 5 µM MeRho-Az. Scale bar in b) and c) = 10 µm.

mucosal autofluorescence is suppressed. Additionally, any morphological changes to the gut cavity upon gavage are accounted for in buffer-gavaged fish. In contrast, fish gavaged with MeRho-Az and DATS/GSH were measurably brighter than the vehicle or MeRho-Az alone (Figure 2.6), confirming that H_2S was being captured by MeRho-Az and visualized using LSFM (Figure 2.5, see DOI: 10.1021/jacs.5b04196 for a link to video compiling 2D image slices into a 3D representation). To compare the relative intensity of the fully activated probe, we also gavaged fish with the fluorophore, MeRho, alone,

which resulted in an identical intensity to that observed with MeRho-Az with DATS/GSH, which is consistent with efficient H_2S-mediated activation of MeRho-Az in the zebrafish gut. To the best of our knowledge, these data demonstrate the first use of analyte-responsive reaction-based probes in live-animal imaging experiments using LSFM, thus opening the door for new investigations of whole-organism imaging in the context of reactive small molecule analytes. In a broader context, the three-dimensional imaging capability afforded by LSFM is crucial for accurately determining fluorescence intensity in a whole organism due to the heterogeneity of basal autofluorescence, reflection, and absorption of various tissues and organs. Differentiation and separation of these different signals would not be possible without the 3D intensity map afforded by LSFM imaging.

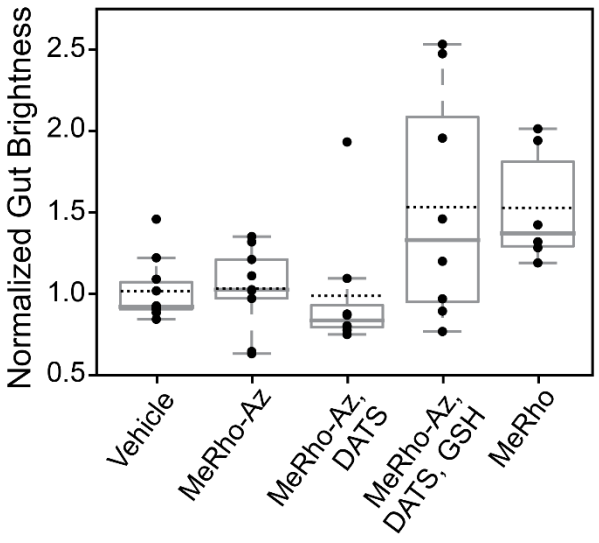

Figure 2.6. Average fluorescence intensity in zebrafish intestinal bulb, normalized to the mean of the buffer-gavaged set. Each dot represents one fish, each of which provided ~10^7 intensity measurements. Boxes extend to the first and third quartile; whiskers enclose data within 1.5 times the inter-quartile range. Solid lines denote median, and

dashed lines denote mean values. Shown are measurements for fish orally gavaged with 6.9 nL of buffered solutions (50 mM PIPES, pH 7.4): buffer (N=5), 5 µM MeRho-Az (N=9), 5 µM MeRho-Az + 250 µM DATS (N=8), 5 µM MeRho-Az + 250 µM DATS + 250 µM GSH (N=8), and 5 µM MeRho (N=6).

Conclusion and Bridge

Motivated by enabling new whole-animal imaging techniques for H_2S, we have developed a bright, selective fluorescent probe for H_2S detection based on a rhodol platform and demonstrated its application both in cells and in LSFM experiments with live zebrafish. This new application of LSFM for use with reaction-based analyte-responsive probes is enabled by the large dynamic range, high photostability, and excellent selectivity afforded by MeRho-Az and would not have been possible with previously-reported H_2S sensing systems.

In addition to the fluorescence detection of H_2S, we've also developed a strategy for studying H_2S-thiol dynamics by fluorescence. By using a dual-fluorophore fragmentation strategy, we're able to simultaneously detect and determine relative concentration ratios of H_2S relative to Cys/Hcy. This strategy will be described in its entirety in Chapter III.

Experimental

Materials and methods. Reagents were purchased from Sigma-Aldrich or Tokyo Chemical Industry (TCI) and used as received. Methylfluorescein (1), HSN2, DNS-N_3, and C7-Az were synthesized as reported previously.[68,77,102,103,107] Deuterated solvents

were purchased from Cambridge Isotope Laboratories and used as received. Silica gel (SiliaFlash F60, Silicycle, 230 - 400 mesh) was used for column chromatography. Preparatory chromatography was performed on Silicycle SiliaPlates (1 mm thickness). ^{1}H and $^{13}C\{^{1}H\}$ NMR spectra were recorded on a Varian INOVA 500 MHz NMR instrument. Chemical shifts are reported in ppm relative to residual protic solvent resonances. UV–visible spectra were acquired on a Cary 100 spectrometer equipped with a Quantum Northwest TLC-42 dual cuvette temperature controller at 37.00 ± 0.05 °C. Fluorescence spectra were obtained on a Quanta Master 40 spectrofluorometer (Photon Technology International) equipped with a Quantum Northwest TLC-50 temperature controller at 37.0 ± 0.05 °C.

Spectroscopic materials and methods. Piperazine-*N*,*N*′-bis(2-ethanesulfonic acid) (PIPES) and potassium chloride (99.999%) were used to make buffered solutions (50 mM PIPES, 100 mM KCl, pH 7.4) in Millipore water. Buffer solutions were sparged with N_2 to remove dissolved oxygen. Anhydrous sodium hydrosulfide (NaHS) was purchased from Strem Chemicals and handled under nitrogen. DEA NONOate (used to generate NO) was purchased from Cayman. Stock solutions of MeRho-Az were prepared in an N_2-filled glovebox and stored at -25 °C until immediately before use. Aqueous stock solutions of L-cysteine, homocysteine, glutathione, NaS_2O_3, Na_2SO_3, Na_2SO_4, and H_2O_2 were freshly prepared in an N_2-filled glovebox prior to use. Stock solutions of DEA NONOate were prepared in degassed 0.01 M NaOH immediately prior to use. Spectroscopic measurements were obtained under anaerobic conditions using septum-sealed cuvettes obtained from Starna Scientific.

General procedure for fluorescence and selectivity measurements. A septum-sealed cuvette was charged with 3.00 mL of buffer (50 mM PIPES, 100 mM KCl, pH 7.4) in a glovebox. After injection of a MeRho-Az (15 μL, 1.0 mM in DMSO) stock solution via syringe, an initial fluorescence spectrum was recorded (λ_{ex} = 476 nm, λ_{em} = 480-650 nm). A NaHS stock solution (15 μL, 50 mM in PIPES buffer) was then injected via syringe, and the fluorescence was recorded after 1, 5, 10, 15 30, 45, and 60 minutes. The reaction cuvette was incubated at 37 °C during the experiment.

pK_a Determination. An aqueous MeRho solution (20 μM, 100 mM KCl, 10 mL) was prepared in a centrifuge tube and acidified to pH 0.656 using 12.1 M HCl. After transferring 3.00 mL of this solution to a cuvette, the MeRho fluorescence was recorded (λ_{ex} = 476 nm, λ_{em} = 480-650 nm). The solution in the cuvette was then returned to the centrifuge tube, and the MeRho solution was basified incrementally to pH 13.859 using stock solutions of KOH at various concentrations (10 M, 5 M, 1 M, 0.1 M). A fluorescence spectrum was recorded at each pH increment.

Determination of detection limit. The fluorescence of seven blank cuvettes containing MeRho-Az (5 μM, λ_{ex} = 476 nm, λ_{em} = 480-650 nm) was recorded after incubation at 37 °C for 90 minutes in PIPES buffer (50 mM, 100 mM KCL, pH 7.4). Then MeRho-Az was treated with NaHS at various concentrations (0.10, 2.5, 5.0, 7.5, 15 μM), and the fluorescence spectra were measured after incubation for 90 min at 37 °C. Each data point represents at least three trials. A linear regression curve was constructed using the background-corrected fluorescence measurements, and the detection limit was determined to be concentration at which the fluorescence equals that of [blank + 3σ].

Cell culture. C6 cells were obtained from ATTC and cultured in Dulbecco's Eagle Medium (DMEM, GIBCO) supplemented with 10% fetal bovine serum (FBS, Hyclone) and 1% penicillin/streptomycin. Cells were seeded on a 22 mm diameter glass coverslip at ~2.3 x 10^6 cells per well in a six-well culture dish and allowed to adhere for 24 h in 2.0 mL DMEM (37 °C, 5% CO_2) prior to experiment. Cells were then washed with 1x Dulbecco's Phosphate Buffered Saline (1x DPBS, 3x) and treated with 2.0 mL of DMEM containing either 100 nM AP39 or 20 μM AOAA. After incubation for 1 h or 45 min, respectively, the cells were washed with 1x DPBS (3x) and treated with 2.0 mL of DMEM containing 5 μM MeRho-Az and incubated at 37 °C for an additional 45 min. as a blank, cells were treated with 5 μM MeRho-Az and incubated in DMEM media for 45 min. after incubation, cells were washed with 1x DPBS (3x) and fixed in 3.7% paraformaldehyde in 1x DPBS at 37 °C for 15 min followed by two rinses and one wash with 1x DPBS. Coverslips containing fixed cells were mounted in Vectashield Hardset Mounting Medium (Vector Laboratories).

Fluorescence microscopy and statistical analysis. Images were acquired on a confocal microscope (Olympus Fluoview 1000) using oil-immersion 60x (1.4 NA) objective. All images were processed with ImageJ software and all statistical comparisons were performed using Prism. (One-way ANOVA with Dunnett's post-test was performed using GraphPad Prism version 7.0 for Windows; GraphPad Software: San Diego, CA www.graphpad.com)

Light sheet fluorescence microscopy. Light sheet fluorescence microscopy was performed using a home-built instrument similar in design to that of Keller *et al*.[87] and described previously.[92] In brief: fluorescence excitation illumination was provided by a

488 nm Coherent sapphire laser (Coherent, Santa Clara, California), shaped into a thin sheet by a mirror galvanometer (Cambridge Technology, Bedford, MA) and telecentric scan lens (Sill Optics). Detection was performed with a Zeiss W Plan-Apochromat 40x/1.0 DIC objective lens and a pco.Edge scientific CMOS camera (PCO, Kelheim, Germany). This LSFM setup can image the volume containing the intestinal bulb used in this study (400 x 350 x 300 μm^3), with 1 μm steps between planes, in approximately 10 seconds, leading to images un-blurred by gut peristalsis. All microscope control, image acquisition, and analysis software were custom-written in MATLAB, C++, and Python.

Specimen mounting and imaging protocols. Larval zebrafish were mounted for imaging as described previously.[93] In brief: specimens were held in 0.5% agarose gel, and suspended in a temperature controlled specimen chamber containing embryo medium, held at 28 °C. All experiments involving zebrafish were performed according to protocols approved by the University of Oregon Institutional Animal Care and Use Committee (protocol #12-18RR).

Zebrafish imaging. Larval zebrafish (7 days post fertilization) were orally gavaged as described[106] with either vehicle (50mM PIPES, pH 7.4), 5 μM MeRho-Az, 5 μM MeRho-Az + 250 μM DATS + 250 μM GSH, or 5 μM MeRho with a total injection volume of 6.9 nL. This injection volume is sufficient to fill the intestinal space. After 60 minutes of recovery time, a three dimensional image (z spacing of 1 μm) of the intestinal bulb of each fish was acquired. Fish in all experimental groups remained alive and healthy for the duration of the experiment, with no indication of toxicity for tens of hours afterward. Excitation light was provided by a 488 nm laser, delivering 10 mW of power

to the sample. Emission light was filtered through a 525/50 nm bandpass filter and collected on a sCMOS camera.

Data Analysis. For each three-dimensional data set, the average background intensity was measured in a region of tissue outside of the intestinal tract and used to provide a minimum threshold value for pixel intensity. Next, a 20 μM thick section within the intestinal bulb was selected at a depth where the bulb was visible in its fullest extent. Voxels from these sections with an average voxel intensity greater than the background threshold were used to measure the integrated gut brightness.

Synthesis of 2. Compound 1 (0.400 g, 1.15 mmol) was combined with *N*-phenyl-bis(trifluoromethanesulfonamide) (0.412 g, 1.15 mmol), and diisopropylethylamine (0.80 mL, 4.60 mmol) in DMF (3 mL) and stirred at room temperature for 15 hr. The reaction mixture was then diluted with water and extracted into EtOAc. The organic phase was washed with brine and dried using Na_2SO_4. After removal of the solvent under reduced pressure, the crude product was purified using column chromatography (100% DCM) to afford the pure product 2 as a white crystalline solid (0.550 g, 99% yield). ^{1}H NMR (500 MHz, $CDCl_3$) δ (ppm): 8.04 (d, J = 7.6 Hz, 1H), 7.66 (m, 2H), 7.24 (d, J = 4.7 Hz, 1H), 7.16 (d, J = 7.5 Hz, 1H), 6.94 (d, J = 8.8 Hz, 1H), 6.89 (d, J = 8.8 Hz, 1H), 6.79 (s, 1H), 6.71 (d, J = 8.8 Hz, 1H), 6.65 (d, J = 9.7 Hz, 1H), 3.84 (s, 3H). ^{13}C{^{1}H} NMR (125 MHz, $CDCl_3$) δ (ppm): 169.1, 161.8, 152.8, 152.2, 152.2, 135.5, 130.3, 130.2, 129.1, 126.4, 125.5, 124.0, 120.1, 120.0, 117.5, 116.8, 112.6, 110.7, 110.6, 101.1, 81.8, 55.8.

Synthesis of MeRho. In a glovebox, compound 2 (0.368 g, 0.769 mmol), $Pd(OAc)_2$ (17 mg, 77 μmol), BINAP (72 mg, 120 μmol), and Cs_2CO_3 (0.752 g, 2.31 mmol) were dissolved in toluene (20 mL) in a three-neck flask fitted with a reflux

condenser. After the reaction vessel was sealed under N_2 and removed from the glovebox, benzophenone imine was added via syringe (0.152 mL, 0.923 mmol). The reaction was heated and stirred at 140 °C for 5 min, and then the temperature was reduced to 100 °C for an additional 8 hr. After heating, the reaction mixture was allowed to cool to room temperature and was filtered through a plug of celite. After removal of the solvent under reduced pressure, the residue was dissolved in a solution of THF (20 mL) and 1 M HCl (2 mL) and stirred at room temperature overnight. The THF was removed under reduced pressure, the crude product was diluted with water, and the pH was neutralized. The aqueous solution was extracted into EtOAc, and the organic phase was washed with brine and dried using Na_2SO_4. The crude product was purified using column chromatography (hexanes: EtOAc gradient from 1:4 to 4:1) to afford MeRho as a pale orange powder (0.226 g, 85% yield). ^{1}H NMR (500 MHz, DMSO) δ (ppm): 7.97 (d, J = 7.7 Hz, 1H), 7.78 (t, J = 8.0 Hz, 1H), 7.70 (t, J = 7.6 Hz, 1H), 7.24 (d, J = 7.6 Hz, 1H), 6.90 (d, J = 2.5 Hz, 1H), 6.66 (dd, J = 8.8, 2.5 Hz, 1H), 6.60 (d, J = 8.8 Hz, 1H), 6.44 (d, J = 2.0 Hz, 1H), 6.37 (d, J = 8.5 Hz, 1H), 6.33 (dd, J = 8.6, 2.0 Hz, 1H), 5.66 (s, 2H), 3.80 (s, 3H). ^{13}C{^{1}H} NMR (125 MHz, DMSO) δ (ppm): 168.7, 160.9, 152.5, 152.1, 151.9, 151.3, 135.5, 129.9, 128.8, 128.5, 126.4, 124.5, 124.0, 111.5, 111.3, 111.2, 105.2, 100.7, 99.0, 83.6, 55.6. HRMS (*m/z*): $[M + H]^+$ calcd for $[C_{21}H_{16}NO_4]^+$ 346.1079, found 346.1096.

Synthesis of MeRho-Az. A solution of $NaNO_2$ (31 mg, 0.45 mmol) in water (2.5 mL) was chilled in an ice bath under foil. A suspension of MeRho (0.100 g, 0.289 mmol) in 6 M HCl (2 mL) was added dropwise, and the reaction was stirred at 0 °C for 30 min. A solution of NaN_3 (58 mg, 0.89 mmol) in water (2 mL) was then added dropwise, and the reaction was allowed to warm to room temperature and stir for 4 hr. While taking care

to shield the crude material from light, water was added, and the pH was neutralized. The crude product was extracted into EtOAc, and the organic phase was washed with brine and dried using Na_2SO_4. Purification of the crude product by preparatory chromatography (3:2 hexanes: EtOAc) afforded pure MeRho-Az as a white solid (54 mg, 50% yield). ^{1}H NMR (600 MHz, $CDCl_3$) δ (ppm): 8.05 (d, J = 7.6 Hz, 1H), 7.68 (m, 2H), 7.17 (d, J = 7.6 Hz, 1H), 6.97 (d, J = 2.2 Hz, 1H), 6.80 (m, 2H), 6.73 (m, 2H), 6.65 (dd, J = 8.8, 2.5 Hz, 1H), 3.87 (s, 3H). $^{13}C\{^1H\}$ NMR (125 MHz, $CDCl_3$) δ (ppm): 169.3, 161.5, 153.0, 152.3, 152.2, 142.5, 135.1, 129.9, 129.7, 129.1, 126.6, 125.2, 123.8, 115.8, 114.9, 112.0, 110.9, 107.2, 100.9, 82.4, 55.6. FTIR (ATR, cm^{-1}): 2110 (s), 1761 (s), 1608 (s), 1260 (m), 1495 (s), 1420 (s), 1282 (m), 1250 (m), 1215 (s), 1161 (m), 1097 (s), 1080 (s), 1030 (m), 828 (s), 757 (s), 691 (m). HRMS (*m/z*): $[M + H]^+$ calcd for $[C_{21}H_{14}N_3O_4]^+$ 372.0984, found 372.0975.

CHAPTER III

RATIOMETRIC MEASUREMENT OF HYDROGEN SULFIDE AND CYSTEINE/HOMOCYSTEINE RATIOS USING A DUAL-FLUOROPHORE FRAGMENTATION STRATEGY

This work includes previously published and coauthored material from Hammers, M. D.; Pluth, M. D. *Anal. Chem.* **2014**, *86*, 7135-7140.

Introduction

Hydrogen sulfide (H_2S) has emerged as an integral biological signaling molecule since its discovery as the third gasotransmitter.[1-4,108] Produced endogenously from cysteine (Cys), homocysteine (Hcy), and cystathionine, enzymatic H_2S biosynthesis occurs primarily from cystathionine-β-synthase (CBS) in the brain, cystathionine-γ-lyase (CSE) in the liver and kidneys, and 3-mercaptopyruvate sulfurtransferase (3-MST) in mitochondria. Once produced, H_2S exerts important effects on vasorelaxation, inflammation, cell angiogenesis, hippocampal memory formation, and hepatic circulation.[1,6-8,10,16,109] Additionally, abnormal H_2S levels are implicated in central nervous system diseases such as Down syndrome and Alzheimer's disease.[19,110] Paralleling these diverse biological roles, basal concentrations of free H_2S are dynamic, interdependent with biological thiol concentrations, and sensitive to changes in redox homeostasis. As substrates in H_2S biosynthesis, fluctuations in Cys and Hcy

concentrations can dramatically affect the kinetics of H_2S generation in enzymatic trans-sulfuration pathways.[111] Posttranslational oxidative modification of Cys protein residues via *S*-sulfhydration to form hydrodisulfides (-SSH) is also postulated to be an important H_2S storage mechanism, which modifies the antioxidant and signal transduction activity of H_2S.[41,52,112,113] Deconvoluting cellular H_2S generation, translocation, and metabolism steps is difficult, however, and chemists have been challenged to develop more accurate experimental methodologies for observing these processes. In particular, methods for the simultaneous detection and differentiation of H_2S and thiols would provide new insight into these multifaceted biological interactions.

Heightened research interest into the physiological properties of H_2S has led to the development of small molecule fluorescent probes which are able to more easily detect and quantify H_2S. Historical techniques for H_2S detection including gas chromatography, colorimetry, the methylene blue assay, and sulfur-selective electrodes all have limitations such as complex workups, slow response rates, and limited sensitivity.[22,25-27,114] One major challenge is differentiating between H_2S and thiols due to their similar modes of chemical reactivity. Recognizing and exploiting particular differences in H_2S and thiol reactivity, however, has been a key driver towards developing the rapidly emerging suite of small molecule fluorescent probes for H_2S. For example, although H_2S and thiols are both reducing agents, H_2S reduces azide and nitro groups at a much faster rate than do thiols. Consequently, the selective H_2S-mediated reduction of azide- and nitro-functionalized fluorophores to elicit a fluorescent response has been used as one strategy for H_2S detection and imaging.[67-77,79-82,102] Other strategies, including the double-nucleophilic attack of H_2S to release or change the photophysical

properties of a bound fluorophore[23,57-59,61,63] and H_2S-mediated metal sulfide precipitation from fluorophore-ligated metals,[64-66,115-117] have also been utilized for sulfide detection.

Several ratiometric probes have been developed for H_2S, which have appealing characteristics compared with chemodosimeter probes.[84,118-122] The magnitude of fluorescence response with chemodosimeters is dependent on probe concentration, meaning that spatial variations in probe concentration caused by differential probe association with components of cellular milieu will reduce the accuracy and reliability of these platforms. Reaction-based ratiometric probes help to alleviate the problem of differential probe distribution by providing monitorable fluorescence emissions at two separate wavelengths, often corresponding to the unreacted probe and its subsequent reaction product. The ratio of these two fluorescence signals functions as an inherent self-calibration, decoupling the observed fluorescence response from probe concentration. A desirable extension of this strategy would be to monitor an additional species by fluorescence, thus allowing for the ratiometric determination of two different analytes simultaneously. To help unravel the intricacies of sulfur redox homoeostasis involving H_2S and thiol chemistry, a platform that could report on both H_2S and thiols simultaneously would provide a way to differentiate between their respective concentrations, with long term potential applications in diseases in which H_2S and thiol concentrations are correlated.

As a proof of concept toward these long term goals, we report herein the development and application of a platform for the ratiometric detection of H_2S and Cys or Hcy based on a dual-fluorophore fragmentation strategy. Supplemental information can be found in Appendix B.

Results and Discussion

Although several ratiometric fluorescent probes for H_2S have been reported, there are no examples of such constructs that report on the direct measurement of relative H_2S and thiol concentrations. To address this unmet need, we envisioned a reaction-based strategy that takes advantage of the nucleophilicity of H_2S and Cys/Hcy to cleave a covalent link between two bound fluorophores, nitrobenzofurazan (NBD) and coumarin. The key design principle is that reaction with sulfhydryl-containing nucleophiles results in fragmentation of NBD and coumarin. We demonstrated previously that H_2S and thiols readily undergo nucleophilic aromatic substitution (S_NAr) with electrophilic NBD derivatives to produce NBD-SH and NBD-SR compounds.[123] Upon reaction with Cys or Hcy, both coumarin and NBD-Cys/Hcy are fluorescent, whereas reaction with H_2S generates coumarin and non-fluorescent NBD-SH. Coumarin functions as an internal standard and allows for the ratiometric measurement of NBD-Cys/Hcy vs. NBD-SH, and thus the Cys/Hcy to H_2S concentration ratios (Scheme 3.1).

If each reaction product after reaction with H_2S or Cys/Hcy provides distinct spectral features, we hypothesized that each could be monitored independently and used to determine relative concentrations of H_2S and Cys/Hcy in mixed-analyte environments. Although NBD-SH and NBD-SR are both non-fluorescent, NBD-adducts of Cys and Hcy undergo subsequent intermolecular rearrangement with adjacent amine functionalities to form fluorescent amino-bound NBD-NHR compounds (Scheme 3.2a, b).[124-126] The coumarin fluorophore appended to the NBD scaffold through an ether linkage provides an additional fluorescent reporter that is liberated upon any nucleophilic substitution. Based on this design, coumarin fluorescence is directly proportional to the combined H_2S

and Cys/Hcy concentrations in solution upon fragmentation of the probe, whereas the NBD component is proportional to the Cys/Hcy concentration exclusively, given that NBD-SH is non-fluorescent. Conveniently, the ratiometric probe NBD-Coum was prepared with good yield in one step from commercially available 4-chloro-7-nitrobenzofurazan (NBD-Cl) and 4-methylumbelliferone (coumarin) in DMF, using NEt_3 as a base (Scheme 3.2c).

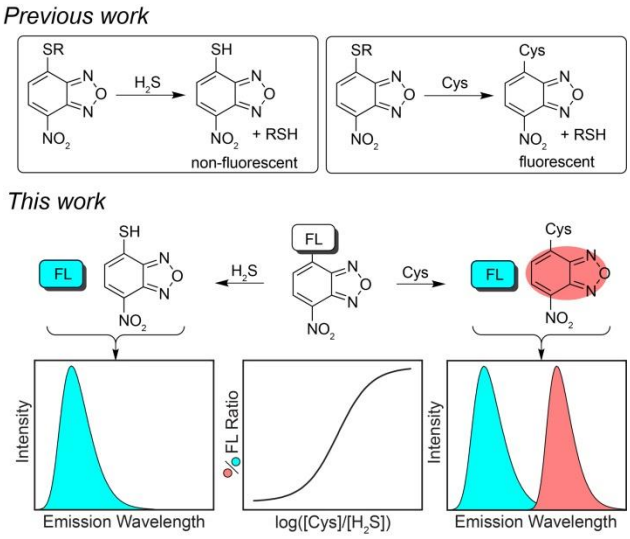

Scheme 3.1. General strategy employed in this work for generating a ratiometric response to H_2S and Cys/Hcy levels.

To evaluate the suitability of our design strategy and NBD-Coum as a platform for ratiometric determination of H_2S and Cys/Hcy levels, we first examined its reactivity with sulfhydryl-containing nucleophiles by UV-vis spectroscopy. Treatment of NBD-Coum (5 μM) with 50 equiv. of NaHS, a common H_2S source, in PIPES buffer (50 mM, 100 mM KCl, pH 7.4) resulted in the rapid disappearance of NBD-Coum absorbance at

380 nm (< 1 min) with concomitant appearance of two absorbances at 322 nm and 535 nm, corresponding to coumarin and NBD-SH respectively. These results confirm that reaction of NBD-Coum with H_2S results in nearly instantaneous probe fragmentation into coumarin and NBD components. Treatment of NBD-Coum with either Cys or Hcy resulted in new absorbances centered at 475 nm, consistent with formation of amino-bound NBD.[127] By contrast, reaction of NBD-Coum with either glutathione (GSH) or N-acetylcysteine (NAC), two thiols lacking the proximal amines required to undergo the intramolecular rearrangement, generated an absorbance at 425 nm, consistent with formation of NBD-SR adducts (Figure 3.1).

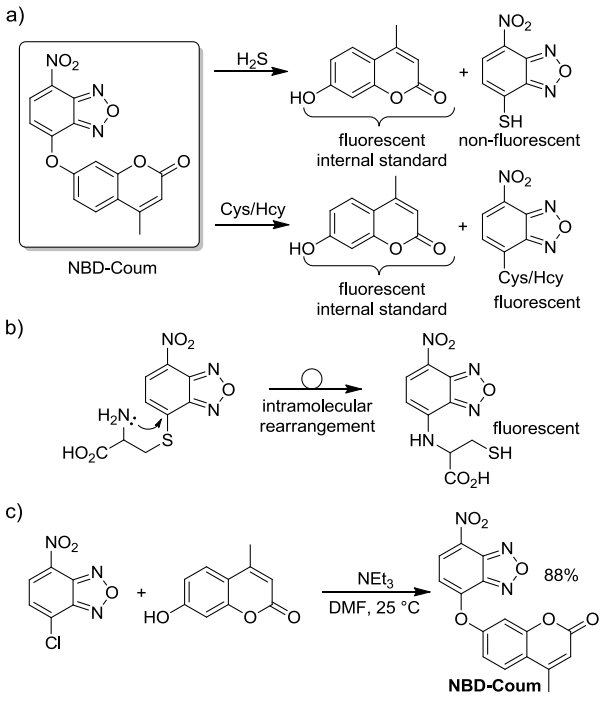

Scheme 3.2. a) The differential reactivity of NBD-Coum with H_2S and Cys/Hcy allows for the ratio of H_2S and Cys/Hcy in a sample to be determined, b) Non-fluorescent *S*-bound NBD-Cys/Hcy undergoes an intramolecular rearrangement to form the fluorescent *N*-bound adducts, c) Synthesis of NBD-Coum.

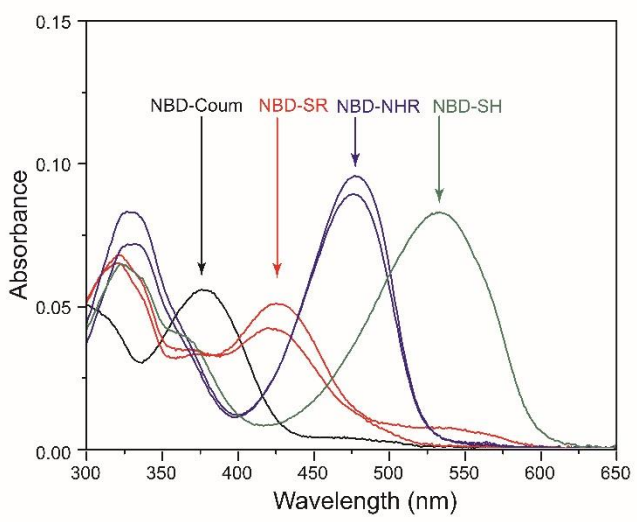

Figure 3.1. Comparison of the UV-vis spectra of NBD-Coum (5 μM, black) and the *HS*-, *RHN*-, and *RS*-bound NBD products from reactions with 50 equiv. of NaHS (250 μM, green), Cys or Hcy (250 μM, blue), and GSH or NAC (250 μM, red) in PIPES buffer (50 mM, 100 mM KCl, pH 7.4) after incubation for 15 minutes at 25 °C.

We next examined the reactivity of NBD-Coum with H_2S and Cys/Hcy by fluorescence spectroscopy to determine whether differentiable fluorescent products are produced in each case. In its unreacted state, NBD-Coum is non-fluorescent due to self-quenching of the bound coumarin and NBD fluorophores. Treatment of NBD-Coum with 50 equiv. of NaHS resulted in ejection of the coumarin fluorophore and generation of a strong emission band centered at 449 nm. As established previously, NBD-SH is non-fluorescent due to the high acidity of the sulfhydryl proton and consequent deprotonation at pH 7.4.[123] By contrast to the reactivity observed with NaHS, reaction of NBD-Coum with Cys or Hcy generated two fluorescent products corresponding to coumarin and the *N*-bound Cys/Hcy NBD adducts. Consecutive excitations at 322 nm and 475 nm resulted in two discrete fluorescence signals centered at 449 nm and 549 nm corresponding to coumarin and NBD-Cys/Hcy, respectively. These results are again consistent with the

dual-fluorophore fragmentation design, liberating coumarin upon reaction of NBD-Coum with either H_2S or Cys/Hcy, providing an internal standard for ratiometric differentiation. The resulting NBD product, however, is non-fluorescent from reaction with H_2S and fluorescent with Cys/Hcy reaction. The 100 nm separation between coumarin and NBD-Cys/Hcy fluorescence maxima allows for unambiguous measurement of each signal.

To further validate our design strategy, we next investigated the dynamic range of the system by treating NBD-Coum (5 μM) with mixed Cys:H_2S solutions with stoichiometries ranging from 1:75 to 75:1, while keeping the total sulfur concentration constant in all samples (50 equiv.). Under these experimental conditions, the two terminal data points represent 3 μM:247 μM in Cys:H_2S and H_2S:Cys, respectively; however, lower analyte detection limits should be accessible using lower probe and/or analyte concentrations. In each experiment, the fluorescence intensities at 449 nm (coumarin) and 549 nm (NBD-Cys) were measured. When excited at their respective λ_{max} values, coumarin has >15-fold stronger fluorescence than NBD-Cys. To set the two baseline fluorescence intensities at the same order of magnitude, coumarin was excited at 400 nm.As the [Cys]/[H_2S] ratio increases, more NBD-Cys is formed relative to NBD-SH, thus generating a stronger fluorescent signal at 549 nm. Consistent with our design hypothesis, the F_{549}/F_{449} ratio increased accordingly with higher [Cys]/[H_2S]. Furthermore, measurement of the ratio of the fluorescence intensities from coumarin and NBD-Cys generated a sigmoidal response (R^2 = 0.997), which allows for the ratiometric determination of relative H_2S and Cys concentrations with a dynamic range of nearly four orders of magnitude (Figure 3.2).

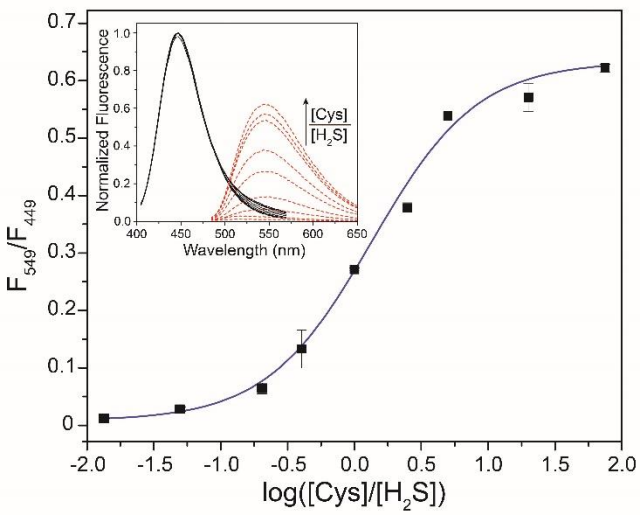

Figure 3.2. Ratiometric response (F_{549}/F_{449}) of NBD-Coum to varying Cys:H_2S stoichiometries (75:1, 20:1, 5:1, 2.5:1, 1:1, 1:2.5, 1:5, 1:20, and 1:75). Inset: Resultant fluorescence spectra from varying Cys:H_2S ratios. Normalized coumarin fluorescence (λ_{ex} = 400 nm, λ_{em} = 449 nm) remains constant while NBD-Cys fluorescence (λ_{ex} = 475 nm, λ_{em} = 549 nm) increases with [Cys]/[H_2S]. Conditions: 5 µM NBD-Coum, 250 µM combined NaHS + Cys, PIPES buffer (50 mM, 100 mM KCl, pH 7.4). Data were acquired after 15 minute incubation at 25 °C. Each data point represents the average of three trials. Error bars were calculated as standard error.

Having demonstrated the efficacy of the NBD-Coum platform in detecting different H_2S:Cys ratios, we next investigated the selectivity of probe for H_2S and Cys/Hcy over other biologically relevant nucleophiles and reactive sulfur, oxygen, and nitrogen species (RSONs). NBD-Coum (5 µM) was treated with 10 equiv. of nucleophilic amino acids (Ser, Tyr, Lys, and Thr), oxidizing agents (H_2O_2), sulfur anions (SO_3^{2-}, SO_4^{2-}, and $S_2O_3^{2-}$), and reactive nitrogen species (NO and HNO). In all cases, incubation for 15 minutes resulted in a negligible fluorescence response at both 449 nm and 549 nm (Figure 3.3). Treatment of NBD-Coum with GSH released the coumarin fluorophore and generated *S*-bound NBD-GSH, which was essentially non-fluorescent, and no turn-on at 549 nm was observed. Although high levels of GSH would likely

interfere with the ability of NBD-Coum to effectively differentiate H_2S and Cys/Hcy in many live-cell experiments, studies in blood plasma may still be accessible due to much lower concentrations of free GSH. Oxygen and nitrogen nucleophiles were insufficiently nucleophilic at physiological pH to react with NBD-Coum, which indicates that fragmentation of NBD-Coum into its respective NBD and coumarin components requires S_NAr by stronger sulfhydryl-containing nucleophiles. Taken together, these selectivity studies highlight the selectivity of the NBD-Coum scaffold for differentiating between H_2S and Cys/Hcy.

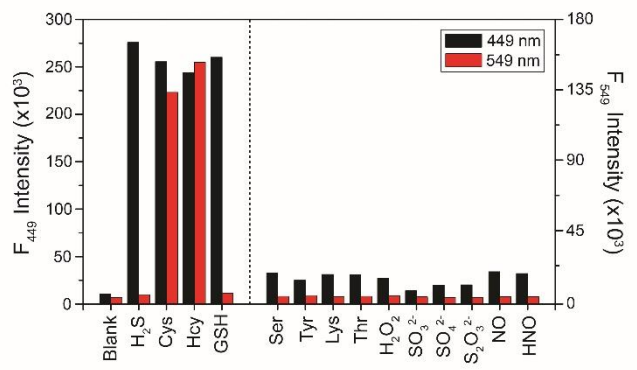

Figure 3.3. Selectivity profile of NBD-Coum toward nucleophilic amino acids and reactive sulfur, oxygen, and nitrogen species. From left to right: blank, NaHS, L-cysteine, DL-homocysteine, glutathione, L-serine, L-tyrosine, L-lysine, L-threonine, H_2O_2, Na_2SO_3, Na_2SO_4, $Na_2S_2O_3$, DEA NONOate, and Angeli's salt. Conditions: 5 μM NBD-Coum, 50 μM RSONs, PIPES buffer (50 mM, 100 mM KCl, pH 7.4), $\lambda_{ex}/\lambda_{em}$ = 400 nm/449 nm and 475 nm/549. Data were acquired after 15 minute incubation at 25 °C.

Sulfur pools of H_2S and sulfhydryl-containing amino acids and peptides respond continuously to various levels of oxidative stress in biological systems by undergoing changes in their redox states. To simulate such changes, we investigated whether NBD-Coum could detect changes in oxidative stress levels in a simulated sulfur pool consisting

of H_2S (125 µM), Cys (125 µM), and cystine (250 µM) (Figure 3.4). All experiments were compared to a control case in which the sulfur species were combined in an N_2-purged cuvette. To enhance oxidizing conditions, the sample was bubbled with either air or O_2, or alternatively treated with NaOCl. Treatment of the sample with tris(2-carboxyethyl)phosphine (TCEP), a common reductant used to reduce disulfides, was used to mimic reductive conditions. In all cases of induced oxidative stress, the relative ratio of Cys/H_2S decreased, which is consistent with Cys oxidation. By contrast, under reductive conditions, the ratio of Cys/H_2S increased, which is consistent with TCEP-mediated reduction of cystine to Cys. Taken together, these results demonstrate that NBD-Coum is able to effectively monitor changes in redox state in the sulfur pool.

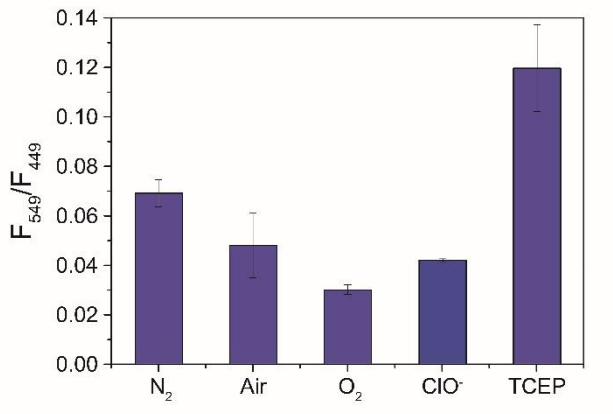

Figure 3.4. Response of the sulfur pool containing H_2S, Cys, and cystine to oxidative and reductive influences. Relative Cys:H_2S ratios decrease under oxidative conditions and increase under reducing conditions. Conditions: The initial sulfur pool (125 µM H_2S, 125 µM Cys, 250 µM cystine) was incubated in PIPES buffer (50 mM, 100 mM KCl, pH 7.4) for 60 minutes at 25 °C under each redox condition and treated with 5 µM NBD-Coum.

Conclusion and Bridge

We have demonstrated the design and application of a platform to effectively measure H_2S and Cys/Hcy ratios using a dual-fluorophore fragmentation strategy. The mechanism of action relies not only on the differences in reactivity of H_2S and Cys/Hcy to provide differentiable reaction products with NBD-Coum, but also in their similarity as potent nucleophiles capable of undergoing S_NAr with the electrophilic scaffold. The strategy described here introduces a new class of compounds that could offer insights into thiol-H_2S dynamics such as redox homeostasis or enzymatic metabolism.

In addition to developing new strategies for the detection of H_2S, developing new methods and compounds that controllably deliver H_2S into biological systems is an important field of study. Toward this goal, we developed the synthesis of an amine-functionalized dithiolethione-based H_2S donor, which we functionalized with non-steroidal anti-inflammatory drugs. These drug conjugates are hydrolytically stable, offering an improved alternative to ester-functionalized conjugates which are hydrolytically unstable. This strategy will be described in its entirety in Chapter IV.

Experimental

Materials and Methods. Reagents were purchased from Sigma-Aldrich or Tokyo Chemical Industry (TCI) and used as received. Deuterated solvents were purchased from Cambridge Isotope Laboratories and used as received. Silica gel (SiliaFlash F60, Silicycle, 230 - 400 mesh) was used for column chromatography. ^{1}H and $^{13}C\{^{1}H\}$ NMR spectra were recorded on a Varian INOVA 500 MHz NMR instrument. Chemical shifts

are reported in ppm relative to residual protic solvent resonances. UV–visible spectra were acquired on a Cary 100 spectrometer equipped with a Quantum Northwest TLC-42 dual cuvette temperature controller at 25.00 ± 0.05 °C. Fluorescence spectra were obtained on a Quanta Master 40 spectrofluorometer (Photon Technology International) equipped with a Quantum Northwest TLC-50 temperature controller at 25.0 ± 0.05 °C.

Spectroscopic Materials and Methods. Piperazine-*N*,*N*′-bis(2-ethanesulfonic acid) (PIPES, Aldrich) and potassium chloride (99.999%, Aldrich) were used to make buffered solutions (50 mM PIPES, 100 mM KCl, pH 7.4) in Millipore water. Anhydrous sodium hydrosulfide (NaHS) was purchased from Strem Chemicals and handled under nitrogen. Angeli's salt and DEA NONOate were purchased from Cayman and used to generate HNO and NO, respectively. Stock solutions of NBD-Coum in DMSO were prepared in an N_2-filled glovebox and stored at -25 °C until immediately prior to use. Stock solutions of L-cysteine, homocysteine, glutathione, serine, lysine, threonine, H_2O_2, Na_2SO_3, Na_2SO_4, and $Na_2S_2O_3$ in buffer, and tyrosine in 0.1 M NaOH were freshly prepared in a glovebox. Stock solutions of NaHS in degassed buffer, and Angeli's salt and DEA NONOate in degassed 0.01 M NaOH, and L-cystine in degassed 1 M HCl were prepared under nitrogen immediately prior to use. All absorption and fluorescence measurements were made under anaerobic conditions, and cuvette solutions were prepared under an inert atmosphere in septum-sealed cuvettes obtained from Starna Scientific.

General Procedure for Fluorescence and Selectivity Measurements. A cuvette containing 3.0 mL of PIPES buffer (50 mM, 100 mM KCl, pH 7.4) and a septum cap was prepared in a glovebox. An NBD-Coum stock solution (15 μL, 1.0 mM) was added via syringe to the cuvette, and initial fluorescence spectra were recorded with

excitation/emission at 400/405-600 nm and 475/485-650 nm. After addition of a NaHS stock solution (15 μL, 50 mM) via syringe and incubation for 15 minutes at 25 °C, fluorescence scans were again recorded. For selectivity and ratiometric experiments, the emission maxima at 449 nm and 549 nm were compared.

General Procedure for the Ratiometric Detection of H_2S and Cysteine. Stock solutions of NaHS (15 μL, 100 mM) and cysteine (15 μL, 100 mM) were combined and diluted with PIPES buffer (50 mM, 100 mM KCl, pH 7.4, 30 μL) to prepare a second stock solution containing 50 mM total sulfur content at a desired 1:1 H_2S:Cys ratio. The fluorescence response of NBD-Coum was measured upon treatment with this second solution following the general procedure described above. The H_2S:Cys stoichiometry in each experiment was controlled by varying the isolated H_2S or Cys stock solution volumes used to prepare secondary stock solutions accordingly at the desired ratio.

Procedure for Redox Comparisons. A stock solution of L-cystine was prepared (25 mM) in 1 M HCl. Preliminary stock solutions of NaHS (15 μL, 100 mM) and cysteine (15 μL, 100 mM) were combined and diluted with PIPES buffer (50 mM, 100 mM KCl, pH 7.4, 30 μL) to prepare a second stock solution containing equimolar concentrations of NaSH and Cys (25 mM). A cuvette containing 3.0 mL of PIPES buffer (50 mM, 100 mM KCl, pH 7.4) and a septum cap was prepared under ambient atmosphere and purged with N_2, air, or O_2 for 15 minutes. The cuvette was then charged with the NaHS/Cys (15 μL) and cystine (15 μL) stock solutions and incubated for 60 minutes at 25 °C to allow for equilibration of the sulfur pool. The cuvette was then injected with a NBD-Coum stock solution (15 μL, 1.0 mM), incubated an additional 15 minutes, and the fluorescence response of NBD-Coum at 449 nm and 549 nm was recorded. For the redox comparisons

with NaOCl or TCEP, a cuvette containing 3.0 mL of PIPES buffer (50 mM, 100 mM KCl, pH 7.4) and a septum cap was prepared under ambient atmosphere. The cuvette was then charged with stock solutions of TCEP or NaOCl (15 μL, 50 mM), NaHS/Cys, and cystine and incubated for 60 minutes at 25 °C. The cuvette was injected with a NBD-Coum stock solution, incubated for 15 minutes, and the fluorescence response of NBD-Coum was measured.

Synthesis of NBD-Coum. A solution of 4-chloro-7-nitrobenzofurazan (60 mg, 0.32 mmol), 4-methylumbelliferone (42 mg, 0.24 mmol), and triethylamine (42 μL, 0.32 mmol) in DMF was stirred at room temperature for one hour. The reaction mixture was then diluted with water and extracted into EtOAc. The organic phase was washed with brine and dried over Na_2SO_4 to yield the crude product. Purification via column chromatography (hex:EtOAc gradient) afforded NBD-Coum as a pure orange solid (72 mg, 88%). ^{1}H NMR (500 MHz, DMSO) δ (ppm): 8.67 (d, J = 8.3 Hz, 1H), 7.98 (d, J = 8.7 Hz, 1H), 7.56 (d, J = 2.4 Hz, 1H), 7.44 (dd, J = 8.7, 2.4 Hz, 1H), 7.00 (d, J = 8.3 Hz, 1H), 6.46 (s, 1H), 2.48 (s, 3H). ^{13}C{^{1}H} NMR (125 MHz, DMSO) δ (ppm): 159.9, 156.1, 154.7, 153.4, 152.3, 145.9, 144.9, 135.6, 131.7, 128.3, 118.6, 117.2, 114.5, 112.3, 110.0, 18.7. HRMS (*m/z*): $[M + H]^+$ calcd for $[C_{16}H_{10}N_3O_6]^+$ 340.0565, found 340.0570.

CHAPTER IV

SYNTHESIS OF AMINO-ADT PROVIDES ACCESS TO HYDROLYTICALLY-STABLE AMIDE-COUPLED HYDROGEN SULFIDE-RELEASING DRUG TARGETS

This work includes previously published and coauthored material from Hammers, M. D.; Singh, L.; Montoya, L. A.; Moghaddam, A. D.; Pluth, M. D. *Synlett* **2016**, eFirst online. [DOI: 10.1055/s-0035-1560603].

Introduction

Hydrogen sulfide (H_2S) has joined carbon monoxide (CO) and nitric oxide (NO) as the third endogenously produced gaseous signaling molecule, or gasotransmitter.[112] Biosynthesized through enzymatic and non-enzymatic pathways, cellular H_2S regulates critical cardiovascular, immune, nervous, respiratory, and gastrointestinal system functions and is implicated in a number of diseases.[4] In addition to central nervous system diseases such as Down syndrome,[19] Alzheimer's,[128] and Parkinson's disease,[129] the role of H_2S in inflammation and angiogenesis has been of particular interest.[12,130] Different studies have shown H_2S to exhibit either anti-inflammatory or pro-inflammatory effects depending on which model is being examined. For example, H_2S-mediated activation of K_{ATP} channels limits leukocyte adherence to vascular endothelium and reduces edema formation in rats, both anti-inflammatory effects.[131] In models of

septic shock, however, inflammatory responses are observed in conjunction with elevated levels of H_2S,[132,133] and inhibition of enzymatic H_2S production during endotoxemia mitigates both inflammation and organ injury.[134] Furthermore, enhanced levels of K_{ATP} activation have been linked with LPS-induced models of hypotension and hyporeactivity.[135] These observations suggest that the interactions of H_2S with K_{ATP} channels during inflammation may be circumstantially either beneficial or deleterious. In addition to inflammation, signaling actions of H_2S have significant effects on angiogenesis. H_2S promotes endothelial cell growth through upregulation of vascular endothelial growth factor (VEGF) expression,[136] and topical H_2S administration to burn wounds has been shown to stimulate wound healing on rats.[137] More recently, H_2S treatment was shown to enhance angiogenesis after ischemic stroke though cooperation of astrocytes and endothelial cells.[138] Taken together, these broad-reaching roles of H_2S highlight the pharmacological potential of exogenously administered H_2S.

Although a variety of H_2S delivery methods exist, conflicting results are often observed depending upon which H_2S donor is used,[12] and developing new types of synthetic H_2S-donating compounds is an active area of investigation.[42,139] By contrast to the more commonly utilized inorganic sulfide sources such as Na_2S and NaHS, which deliver an immediate burst of H_2S into an experimental system, small-molecule donors are designed to more closely resemble continuous, endogenous H_2S release. One of the most extensively studied H_2S donors is 5-(4-hydroxyphenyl)-3*H*-1,2-dithiol-3-thione (ADT-OH), which contains the H_2S-releasing dithiolethione moiety. This phenolic compound is easily functionalized via ester linkages (Scheme 4.1), and indeed a number of ester-bound ADT derivatives of nonsteroidal anti-inflammatory (NSAIDs) and other

drugs are being investigated for their synergistic anti-inflammatory and antioxidant potential. For example, an ADT-functionalized diclofenac derivative, S-diclofenac, not only exhibited greater anti-inflammatory effects than the parent diclofenac in LPS-injected rats, but also displayed reduced gastrointestinal toxicity.[140] Other demonstrations of ester-functionalized ADT drugs include derivatives of naproxen,[45] valproic acid,[141] aspirin,[44] sildenafil,[142] and mesalamine.[143] One practical challenge associated with implementing these ADT derivatives in drug delivery, however, is the potential for hydrolysis of the ester bond linking the two drug components. A recent report demonstrated that hydrolysis of polymeric ester-bound ADT in phosphate buffered saline occurred with a half-life of approximately 30 minutes.[144] Therefore, stomach acid would likely catalyze hydrolysis and component fragmentation, which would be particularly problematic in oral drug delivery systems. One logical solution to this unwanted hydrolysis is to link ADT to the drugs through amide, rather than ester, bonds.{Xie, 2014 #2}

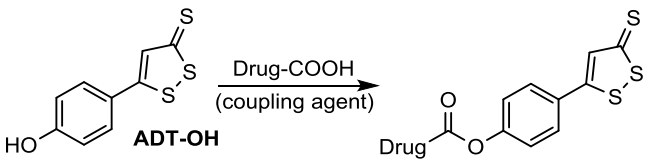

Scheme 4.1. Esterification of ADT-OH to form H_2S-releasing drugs.

To better enable access to more robust ADT-functionalized NSAIDs, we report here a straightforward synthesis and purification of 5-(4-aminophenyl)-3*H*-1,2-dithiol-3-

thione (amino-ADT, ADT-NH_2) and compare the hydrolytic stability between amide- and ester-coupled ADT. We also provide conditions for coupling of ADT-NH_2 with common drugs, including naproxen and valproic acid and demonstrate cytotoxicities for the ester- and amide-linked versions of these drug conjugates. Supplemental information can be found in Appendix C.

Results and Discussion

To access ADT-NH_2, direct conversion of the phenolic group in ADT-OH to an amine would be preferred. Our attempts using a reported one-pot S_NAr-Smiles rearrangement strategy (Scheme 4.2A)[145] or palladium-catalyzed Buchwald-Hartwig amination of triflated ADT (Scheme 4.2B) were unsuccessful. We reasoned that the presence of highly metalophilic sulfur atoms in the dithiolethione moiety, combined with the sulfophilicity of Pd, makes Pd-catalyzed cross-couplings with ADT problematic. Therefore, we reasoned that ADT-NH_2 would need to be constructed from an aniline precursor and that any metal-mediated steps must be incorporated prior to installation of the dithiolethione moiety (Scheme 4.2C).

Fortunately, organotrifluoroborate salts have emerged as excellent substrates for Suzuki-Miyaura reactions due to their improved air-stability and reduced cost.[146,147] In particular for our purposes, they offer an attractive alternative to expensive vinyl boronic acid and boronate substrates.[148,149] Utilizing this strategy, we found that ADT-NH_2 is accessible in two steps from commercially available starting materials with 56% overall yield (Scheme 4.3A). Palladium-catalyzed coupling of 4-chloro-(*N*-Boc)aniline with

potassium *trans*-1-propenyltrifluoroborate installs a propenyl dithiolethione precursor onto the protected aniline to form compound 1. Subsequent reaction with elemental sulfur at 180 °C both forms the dithiolethione and deprotects the aniline to give ADT-NH_2. We note that although the synthesis of ADT-NH_2 is suggested in U.S. Patent 2007/0197479 A1, August 23, 2007, the precursor to compound 1 in the patent application is not a known compound, and no preparation is presented. Methylated ADT-NMe_2 (Scheme 4.3D) was synthesized according to the same scheme using 4-bromo-*N*,*N*-dimethylaniline as starting. ADT-OH and ADT-OMe were synthesized using previously-reported methods,[140] and we report an updated purification method in the Supporting Information. Importantly, dithiolethione formation from reaction of elemental sulfur with an aryl propenyl group appears to be general, as similar reaction conditions may be used to form ADT-NH_2, ADT-NMe_2, and ADT-OMe from their respective propenyl starting materials.

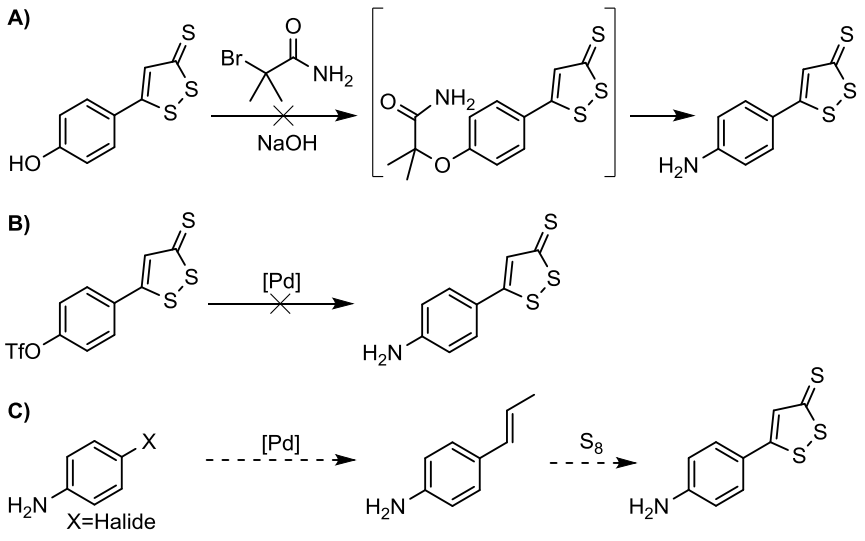

Scheme 4.2. Potential synthetic routes to ADT-NH_2.

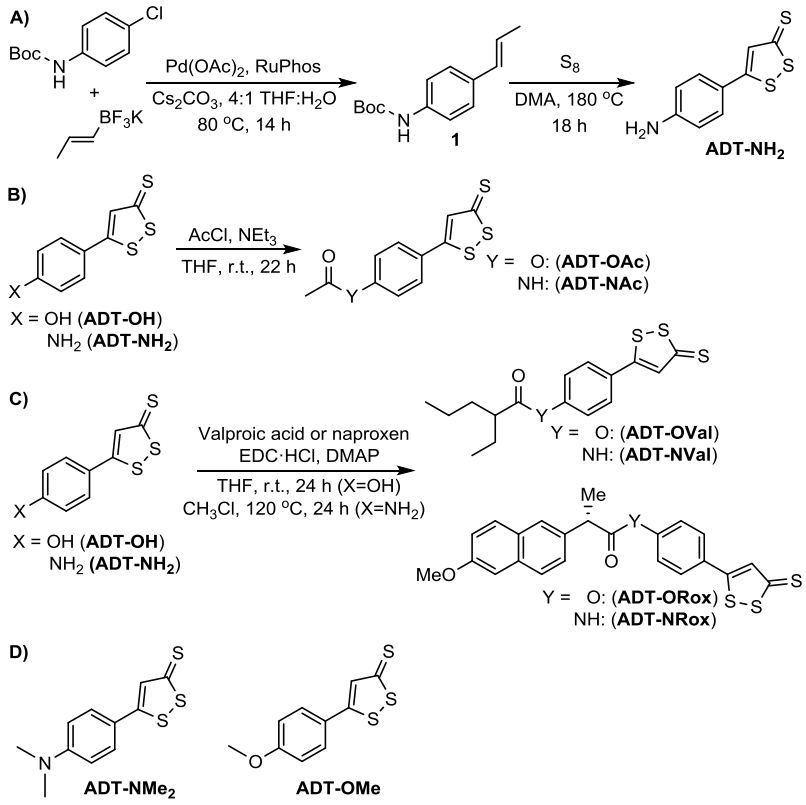

Scheme 4.3. Synthesis of ADT-containing compounds including a) ADT-NH_2, b) ADT-OAc and ADT-NAC, c) ADT drug conjugates, and d) ADT-NMe_2 and ADT-OMe.

Having developed a facile route to access ADT-NH_2, our next objective was to demonstrate effective functionalization of the amine. Acetamide (ADT-NAc) and acetate (ADT-OAc) ADT derivatives were synthesized as model compounds for hydrolysis study, both through reactions with acetyl chloride (Scheme 4.3B). Ester- and amide-coupled ADT derivatives of naproxen and valproic acid (ADT-ORox, ADT-OVal, ADT-NRox, and ADT-NVal) were coupled using 1-ethyl-3-(3-dimethylaminopropyl)carbodiimide (EDC·HCl) and catalytic 4-dimethylaminopyridine

(DMAP) as coupling agents (Scheme 4.3C). Both ADT-NH_2 and ADT-OH are weak nucleophiles, making substitution reactions challenging. The dithiolethione group is inductively electron-withdrawing, as reflected by the increased acidity of ADT-OH compared with phenol (pK_a of 7.86 vs. 10.00), slightly more so than a nitrile group (pK_a of 4-cyanophenol is 7.95).[150] Resonance contributions from lone-pair electron delocalization produce partial zwitterionic character in these compounds, which further decreases their nucleophilicities (Scheme C.1). We found that ADT-NH_2 is less reactive than ADT-OH, which suggests a higher degree of electron delocalization. For example, esterification of ADT to form esters ADT-ORox and ADT-OVal proceed at room temperature, whereas 120 °C temperatures are required for the corresponding amide couplings of ADT-NRox and ADT-NVal. Nonetheless, ADT-NH_2 is readily linked through amide bonds using these standard methodologies, which can likely be extended toward coupling with other carboxylic acid-containing NSAIDs.

To compare the hydrolytic stability of ester- and amide-bound ADT derivatives in an acidic environment akin to the stomach, the hydrolysis of model compounds ADT-OAc and ADT-NAc was investigated in 0.10 M HCl using UV-vis spectroscopy and HPLC. After addition of ADT-OAc (20 μM) to a cuvette containing 0.10 M HCl, a decrease in absorption at 320 nm was observed with concomitant growth of a new peak at 358 nm, which is consistent with formation of ADT-OH after ester hydrolysis (Figure 4.1A). By contrast, treatment of ADT-NAc (20 μM) resulted in only minimal hydrolysis to form ADT-NH_2 (λ_{max}= 311 nm) (Figure 4.1B). Over the course of the 18-hour experiment, 69% of the ester-bound ADT was hydrolyzed, whereas only 9% of the amide was hydrolyzed under identical conditions (Figure 4.1C). ADT-OH and ADT-NH_2

fragments were also identified as reaction byproducts using HPLC analysis. (Figure C.1). As expected, these results clearly demonstrate the enhanced chemical stability of amide linkages toward hydrolysis in ADT derivatives by contrast to ester linkages.

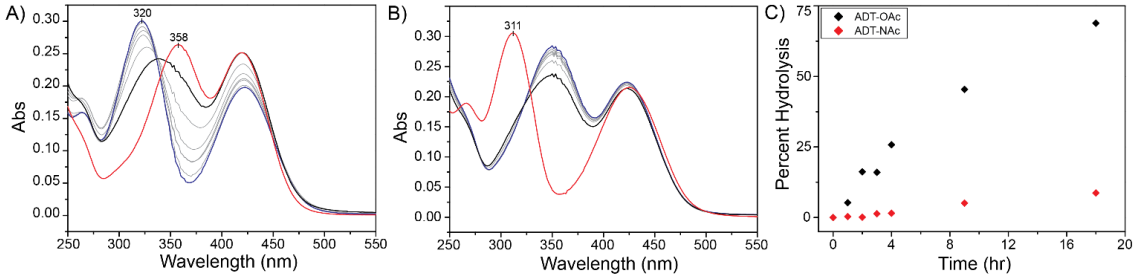

Figure 4.1. Hydrolysis of acyl ADT derivatives (20 µM) in 0.10 M HCl at 37 °C, a) UV-vis timecourse of ADT-OAc (blue = initial, black = final) over 18 hours overlaid with the absorbance spectrum of ADT-OH (red), b) Time course of ADT-NAc (blue = initial, black = final) over 18 hours overlaid with the absorbance spectrum of ADT-NH_2 (red), c) Calculated percent hydrolysis of ADT-OAc and ADT-NAc.

Undesired fragmentation of ADT-functionalized drugs may have toxicological consequences in addition to *in vivo* decomposition. To probe these properties, the effect of ADT functionalization on cytotoxicity was tested in HeLa cells using the MTT assay.[151] Cells were treated with ADT derivatives at 31, 55, 95, 170, 290, 510, and 900 µM to observe the effect of each derivative on cell proliferation. Free ADT-OH and ADT-NH_2 exhibited similar levels of toxicity (Figure 4.2A), whereas alkylated derivatives ADT-OMe and ADT-NMe_2 were considerably more toxic (Figure 4.2.B). At concentrations below 290 µM, naproxen (ADT-ORox, ADT-NRox, Figure 4.2C) and valproic acid (ADT-OVal, ADT-NVal, Figure 4.2D) derivatives all exhibited lower toxicity than the free ADT species. While amide and ester ADT derivatives generally had

similar toxicity profiles, ADT-ORox exhibited the highest level of toxicity among them. All eight derivatives had considerable toxicity at concentrations approaching 1 mM.

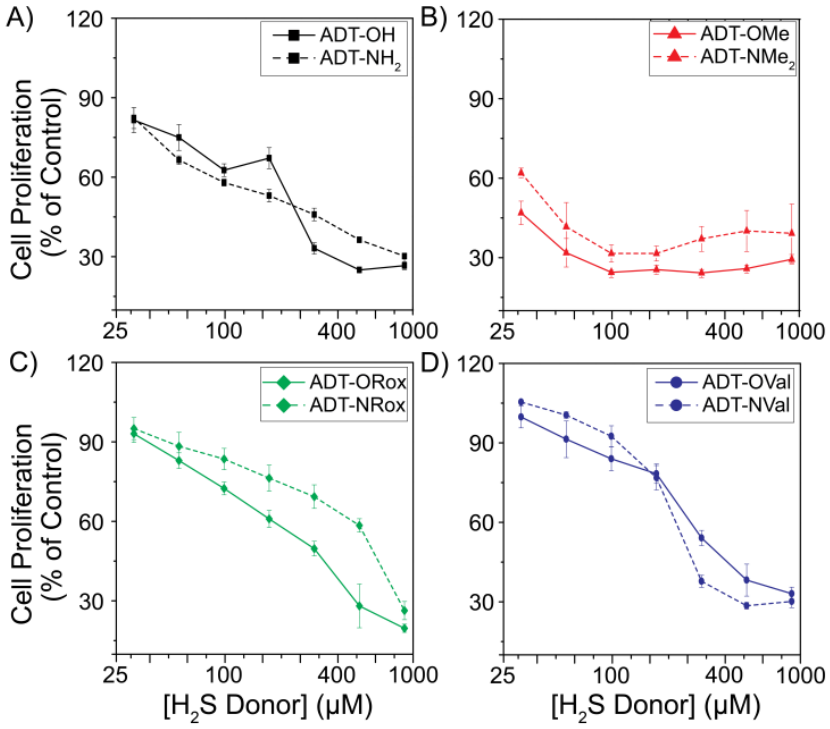

Figure 4.2. MTT cell proliferation assay of ADT derivatives (31-900 μM) in HeLa cells. Cells were treated with a) ADT-OH or ADT-NH_2 (black), b) ADT-OMe or ADT-NMe_2 (red), c) ADT-ORox or ADT-NRox (green), d) ADT-OVal or ADT-NVal (blue) for 24 hours.

Previous experiments using the MTT assay have suggested that free ADT-OH and ADT-OMe are more cytotoxic than ester- or ether-functionalized ADT.[24] The authors attributed this toxicity to possible direct interactions of ADT with intracellular enzymes and organelles. Our results are consistent with those findings (Figure 4.2), where ADT-OH and ADT-NH_2 were both more toxic than either ester- or amide-functionalized ADT.

Methylation further increased the toxicity of the free ADTs. Naproxen has been shown to have anti-proliferative properties in HeLa and osteosarcoma cells,[152,153] which may contribute to our observed enhanced toxicity of ADT-ORox vs. ADT-NRox in the event of intracellular ADT-ORox hydrolysis. This trend was not observed with valproic acid derivatives, and correspondingly, valproic acid was previously shown to have minimal toxicity in glioma or neuroblastoma cells below 1 mM.[154,155]

Conclusion and Bridge

Amide-coupled ADT derivatives help provide a solution to challenges associated with undesired acid-catalyzed hydrolysis of ester-bound ADT-NSAIDs in oral drug delivery applications. By utilizing advances in Suzuki-Miyaura cross-coupling using trifluoroborate salts, we successfully accessed the key intermediate 1 toward our target H_2S donor, ADT-NH_2. We hope that the proof of concept syntheses of ADT-NVal and ADT-NRox will assist future investigations toward unlocking the therapeutic potential of H_2S-releasing drugs.

In addition to dithiolethione-based H_2S-releasing compounds, polysulfide-containing molecules are also known to release H_2S. To understand the chemical reactivity of these compounds, we investigated the H_2S-releasing capabilities of a library of tetrasulfide derivatives with the goal of creating a toolbox of controllable donors for use in biological studies. This strategy will be described in its entirety in Chapter V.

Experimental

Materials and methods. Reagents were purchased from Sigma-Aldrich or Tokyo Chemical Industry (TCI) and used as received. ADT-OH, ADT-OMe, and ADT-OVal were synthesized as reported previously with modifications as described below.{Li, 2007 #114;Isenberg, 2007 #23} Deuterated solvents were purchased from Cambridge Isotope Laboratories and used as received. Silica gel (SiliaFlash F60, Silicycle, 230 - 400 mesh) was used for column chromatography. Preparatory chromatography was performed on Silicycle SiliaPlates (1 mm thickness). ^{1}H and ^{13}C[48] NMR spectra were recorded on a Varian INOVA 500 MHz NMR instrument. Chemical shifts are reported in ppm relative to residual protic solvent resonances. UV–visible spectra were acquired on a Cary 100 spectrometer equipped with a Quantum Northwest TLC-42 dual cuvette temperature controller at 37.00 ± 0.05 °C. HPLC samples were analyzed using reverse-phase HPLC (Akta purifier; Amersham Biosciences) on a C18 column (Hypersil GOLD, 5 mm 4.6/250 mm; Thermo Scientific).

Spectroscopic materials and methods. Stock solutions of ADT-OH, ADT-OMe, ADT-OVal, ADT-ORox, ADT-NVal, and ADT-NRox were prepared in an N_2-filled glovebox and stored at -25 °C until immediately before use. Spectroscopic measurements were obtained using septum-sealed cuvettes obtained from Starna Scientific.

MTT Assay[151] of ADT Derivatives. C6 cells were seeded at 2,500 cells per well on a 96 well plate the night before drug treatment to allow for adherence of the cells to the bottom of the wells. The following day, cells were treated with

ADT derivatives (31, 55, 95, 170, 290, 510, and 900 µM) for 24 hours at 37 °C and 5% CO_2. MTT (3-(4,5-dimethylthiazol-2-yl)-2,5-diphenyl tetrazolium bromide) was dissolved in PBS at 5 mg/mL and filtered to sterilize and remove any insoluble residue present. The MTT solution (10 µL) was added to all wells and was incubated at 37 °C for 3.5 hours. The solution was removed and 100 µL of acidic isopropanol (0.04 M HCl, 0.01% IGEPAL in isopropanol) was added to all wells and placed on a shaker for 15 minutes in the dark at room temperature. After incubation, the plate was read on a Tecan Safire2 UV-vis plate reader at 570 nm.

Synthesis of 5-(4-Methoxyphenyl)-3H-1,2-dithiole-3-thione(ADT-OMe). Anethole (4.15 g, 28.0 mmol) and sulfur (6.00 g, 187 mmol) were dissolved in DMF (25 mL) and refluxed at 170 °C under N_2 for 8 hours. After the reaction flask was cooled to room temperature, the reaction mixture was diluted into water and extracted into toluene. The toluene fractions were dried with Na_2SO_4 and concentrated, and the remaining solid was recrystallized from 5% methanol/DCM. These crystals were then further purified by column chromatography (4:1 Hex:EtOAc) to give pure product as a brownish-red crystalline solid (2.27 g, 34% yield). ^{1}H NMR (500 MHz, DMSO) δ (ppm): 7.87 (d, J = 8.8 Hz, 2H), 7.75 (s, 1H), 7.07 (d, J = 8.8 Hz, 2H), 3.84 (s, 3H). ^{13}C{^{1}H} NMR (125 MHz, DMSO) δ (ppm): 214.70, 173.77, 162.66, 134.11, 128.98, 123.64, 115.02, 55.63.

Synthesis of 5-(4-Hydroxyphenyl)-3H-1,2-dithiole-3-thione (ADT-OH). ADT-OMe (2.00 g, 8.32 mmol), and anhydrous pyridine hydrochloride (5.77 g, 49.9 mmol) were added to an oven-dried pressure vessel under N_2. The apparatus was submerged into an oil bath and stirred at 220 °C. After stirring for 25 minutes,

the reaction flask was cooled to room temperature, and the contents were dissolved in methanol and transferred to a round bottom flask. The methanol was removed, and the contents of the round bottom were dissolved in a 50:50 mixture of 0.5 M HCl and EtOAc in order to solubilize the crude product. This mixture was then further diluted with water and extracted into EtOAc. The organic layer was dried with Na_2SO_4 and purified by column chromatography (3:2 Hex:EtOAc) to afford ADT-OH as a lovely golden orange solid (1.60 g, 85%). ^{1}H NMR (500 MHz, DMSO) δ (ppm): 10.49 (s, 1H), 7.78 (d, J = 7.8 Hz, 2H), 7.69 (s, 1H), 6.89 (d, J = 7.8 Hz, 2H). ^{13}C{^{1}H} NMR (125 MHz, DMSO) δ (ppm): 214.38, 174.39, 161.75, 133.45, 129.19, 122.13, 116.42.

Synthesis of (E)-tert-Butyl (4-(prop-1-en-1-yl)phenyl)carbamate (1). In a glovebox, 4-chloro-(N-Boc)aniline (350 mg, 1.54 mmol), potassium *trans*-1-propenyltrifluoroborate (273 mg, 1.85 mmol), $Pd(OAc)_2$ (35 mg, 0.16 mmol), RuPhos (144 mg, 0.308 mmol), and Cs_2CO_3 (1.5 g, 4.6 mmol) were added to an oven-dried 3-neck round bottom flask fitted with a reflux condenser. The sealed apparatus was removed from the glovebox, and a degassed solvent mixture of 4:1 THF:water (10 mL) was added via syringe; minimal solvent aids with full conversion and overall yield. The reaction mixture was stirred at 80 °C under N_2 for 14 hrs, after which the solvent was removed by rotary evaporation. The residue was dissolved in EtOAc and filtered through celite. The filtrate was washed with water, brine, and dried with Na_2SO_4. The crude product was purified using column chromatography (20-50% Hex:EtOAc gradient) and further purified by recrystallization from hexanes to afford the pure product as a light brown solid

(318 mg, 88% yield). ^{1}H NMR (500 MHz, DMSO) δ (ppm): 9.31 (s, 1H), 7.38 (d, J = 8.5 Hz, 2H), 7.24 (d, J = 8.6 Hz, 2H), 6.31 (dd, J = 15.8, 1.43 Hz, 1H), 6.11-6.18 (m, 1H), 1.81 (dd, J = 6.56, 1.5 Hz, 3H), 1.47 (s, 9H). ^{13}C{^{1}H} NMR (125 MHz, DMSO) δ (ppm): 152.67, 138.26, 131.34, 130.41, 125.94, 123.34, 118.08, 78.95, 28.11, 18.19. HRMS $[M + Na]^+$ calcd for $[NaC_{14}H_{19}NO_2]^+$ 256.1313; found, 256.1309.

Synthesis of 5-(4-Aminophenyl)-3H-1,2-dithiole-3-thione (ADT-NH_2). Compound 1 (100 mg, 0.429 mmol) and sulfur (96 mg, 3.0 mmol) were added to an oven-dried pressure vessel and dissolved in DMAc (6 mL) under N_2, and the reaction was stirred at 180 °C for 18 hours. After stirring, the solvent was removed under vacuum whilst heated at 40 °C. The crude residue was diluted with water, extracted into EtOAc. The combined organic fractions were washed with brine and dried with Na_2SO_4. The compound was purified using column chromatography (3% MeOH:DCM) to afford the pure product as a dark brown solid (66 mg, 68% yield). ^{1}H NMR (500 MHz, CD_2Cl_2) δ (ppm): 7.51 (d, J = 8.7 Hz, 2H), 7.36 (s, 1H), 6.71 (d, J = 8.7 Hz, 2H), 4.27 (br, 2H). ^{13}C{^{1}H} NMR (125 MHz, CD_2Cl_2) δ (ppm): 215.05, 174.86, 151.60, 133.66, 129.25, 121.63, 115.29. HRMS $[M + H]^+$ calcd for $[C_9H_8NS_3]^+$ 225.9819; found, 225.9823.

Synthesis of (E)-N,N-Dimethyl-4-(prop-1-en-1-yl)aniline (N,N-Dimethyl propenylaniline). In a glovebox, 4-bromo-N,N-dimethylaniline (250 mg, 1.25 mmol), potassium *trans*-1-propenyltrifluoroborate (222 mg, 1.50 mmol), $Pd(OAc)_2$ (14 mg, 0.062 mmol), RuPhos (58 mg, 0.12 mmol), and Cs_2CO_3 (1.22 g, 3.75 mmol) were added to an oven-dried 3-neck round bottom flask fitted with a reflux

condenser. The sealed apparatus was removed from the box, and a degassed solvent mixture of 4:1 THF:water (10 mL) was added via syringe. The mixture was stirred at 80 °C under N_2 for 12 hrs, after which the solvent was removed by rotary evaporation. The residue was dissolved in EtOAc and filtered through celite. The filtrate was washed with water, brine, and dried with Na_2SO_4. The compound was purified using column chromatography (20-50% Hex:EtOAc gradient) to afford the pure product as a brown solid (163 mg, 81% yield). ^{1}H NMR (500 MHz, CD_2Cl_2) δ (ppm): 7.20 (d, J = 8.7 Hz, 2H), 6.66 (d, J = 8.8 Hz, 2H), 6.31 (d, J = 17.1 Hz, 1H), 5.96-6.08 (m 1H), 2.92 (s, 6H), 1.84 (d, J = 8.8 Hz, 3H). ^{13}C{^{1}H} NMR (125 MHz, CD_2Cl_2) δ (ppm): 150.17. 131.07, 126.93, 121.53, 112.86, 40.76, 30.15, 18.57.

Synthesis of 5-(4-(Dimethylamino)phenyl)-3H-1,2-dithiole-3-thione (ADT-NMe2). *N*,*N*-dimethyl propenylaniline (163 mg, 1.01 mmol) and sulfur (227 mg, 7.08 mmol) were added to an oven-dried pressure vessel and dissolved in DMAc (6 mL) under N_2, and the reaction was stirred at 180 °C for 18 hours. After stirring, the solvent was removed under vacuum whilst heated at 40 °C. The crude residue was dissolved in EtOAc and washed with water, brine, and dried with Na_2SO_4. The compound was purified using column chromatography (1% MeOH:DCM) to afford the pure product as a brown solid (150 mg, 59% yield). ^{1}H NMR (500 MHz, CD_2Cl_2) δ (ppm): 7.58 (d, J = 8.8 Hz, 2H), 7.37 (s, 1H), 6.7 (d, J = 8.8 Hz, 2H), 3.06 (s, 6H). ^{13}C{^{1}H} NMR (125 MHz, CD_2Cl_2) δ (ppm): 214.23, 175.22, 153.72, 132.72, 128.98, 119.11, 112.30, 40.44. HRMS $[M]^+$ calcd for $[C_{11}H_{11}NS_3]^+$ 253.0053; found, 253.0046.

Synthesis of 4-(3-Thioxo-3H-1,2-dithiol-5-yl)phenyl acetate (ADT-OAc). ADT-OH (50 mg, 0.22 mmol), acetyl chloride (17 mg, 0.22 mmol), and triethylamine (67 mg, 0.66 mmol) were dissolved in dry THF (2 mL) and stirred at room temperature under N_2. After 22 hours the solvent was removed by rotary evaporation, and the residue was purified by preparative chromatography (3:2 Hex:EtOAc) (16 mg, 22% yield). ^{1}H NMR (500 MHz, CD_2Cl_2) δ (ppm): 7.72 (d, J = 8.6 Hz, 2H), 7.42 (s, 1H), 7.25 (d, J = 8.6 Hz, 2H), 2.31 (s, 3H). $^{13}C\{^1H\}$ NMR (125 MHz, CD_2Cl_2) δ (ppm): 216.21, 172.56, 169.38, 154.28, 136.61, 129.75, 128.79, 123.50, 21.48. HRMS $[M]^+$ calcd for $[C_{11}H_8O_2S_3]^+$ 267.9686; found, 267.9694.

Synthesis of N-(4-(3-Thioxo-3H-1,2-dithiol-5-yl)phenyl)acetamide (ADT-NAc). ADT-NH_2 (50 mg, 0.22 mmol), acetyl chloride (17 mg, 0.22 mmol), and triethylamine (67 mg, 0.66 mmol) were dissolved in dry THF (2 mL) and stirred at room temperature under N_2. After 22 hours the solvent was removed by rotary evaporation, and the residue was purified by preparative chromatography (3:1 Hex:EtOAc) (11 mg, 19% yield). ^{1}H NMR (500 MHz, $(CD_3)_2CO$) δ (ppm): 9.53 (br, 1H), 7.85 (m, 4H), 7.56 (s, 1H), 2.13 (s, 3H). $^{13}C\{^1H\}$ NMR (125 MHz, $(CD_3)_2CO$) δ (ppm): 216.54, 174.12, 169.47, 144.35, 135.41, 128.80, 126.97, 120.22, 24.43. HRMS $[M]^+$ calcd for $[C_{11}H_8NOS_3]^+$ 266.9846; found, 266.9843.

Synthesis of (S)-4-(3-Thioxo-3H-1,2-dithiol-5-yl)phenyl 2-(6-methoxynaphthalen-2-yl)propanoate (ADT-ORox). Naproxen (50 mg, 0.22 mmol), ADT-OH (49 mg, 0.22 mmol), EDC·HCl (42 mg, 0.22 mmol), and 4-dimethylaminopyridine (3 mg, 0.03 mmol) were dissolved in dry THF (4 mL) and

stirred at room temperature under N_2 for 24 hours. After stirring, the solvent was removed under vacuum. The crude residue was dissolved in EtOAc and washed with water, brine, and dried with Na_2SO_4. The crude product was purified via preparative TLC (3:2 Hex:EtOAc) to afford the pure product as a dark red solid (14 mg, 15% yield). ^{1}H NMR (500 MHz, CD_2Cl_2) δ (ppm): 7.75-7.79 (m, 3H), 7.77 (m, 2H), 7.50 (dd, J= 8.4, 1.9 Hz, 1H), 7.39 (s, 1H), 7.14-7.17 (m, 4H), 4.11-4.16 (q, J = 7.2 Hz, 1H), 3.92 (s, 1H), 1.69 (d, J = 7.2 Hz, 3H). ^{13}C{^{1}H} NMR (125 MHz, CD_2Cl_2) δ (ppm): 216.18, 173.21, 172.52, 158.48, 154.44, 136.60, 135.38, 134.50, 129.77, 129.52, 128.75, 127.95, 126.70, 126.61, 123.30, 119.70, 110.57, 106.13, 55.87, 46.12, 18.75. HRMS $[M + H]^+$ calcd for $[C_{23}H_{19}O_3S_3]^+$ 439.0496; found, 439.0476.

Synthesis of 4-(3-thioxo-3H-1,2-dithiol-5-yl)phenyl 2-propylpentanoate (ADT-OVal). Valproic acid (32 mg, 0.22 mmol), ADT-OH (52 mg, 0.22 mmol), EDC·HCl (44 mg, 0.22 mmol), and 4-dimethylaminopyridine (2 mg, 0.02 mmol) were dissolved in dry THF (4 mL) and stirred at room temperature under N_2 for 24 hours. After stirring, the solvent was removed under vacuum. The crude residue was dissolved in EtOAc and washed with water, brine, and dried with Na_2SO_4. The crude product was purified via preparative TLC (3:2 Hex:EtOAc) to afford the pure product as a dark red solid (52 mg, 67% yield). ^{1}H NMR (500 MHz, CD_2Cl_2) δ (ppm): 7.72 (d, J = 8.8 Hz, 2H), 7.43 (s, 1H), 7.22 (d, J = 8.8 Hz, 2H), 2.61-2.67 (m, 1H), 1.71-1.78 (m, 2H), 1.55-1.62 (m, 2H), 1.40-1.48 (m, 4H), 0.97 (t, J = 7.3 Hz, 6H). ^{13}C{^{1}H} NMR (125 MHz, CD_2Cl_2) δ (ppm): 216.03, 174.80, 172.46, 154.32, 136.42, 129.49, 128.61, 123.38, 45.74, 34.91, 21.09, 14.19.

Synthesis of (S)-2-(6-methoxynaphthalen-2-yl)-N-(4-(3-thioxo-3H-1,2-dithiol-5-yl)phenyl)propanamide (ADT-NRox). In a glovebox, naproxen (24 mg, 0.10 mmol), ADT-NH_2 (26 mg, 0.12 mmol), EDC·HCl (20 mg, 0.10 mmol), and 4-dimethylaminopyridine (2 mg, 0.02 mmol) were added to an oven-dried pressure vessel and dissolved in dry $CHCl_3$ (4 mL) under N_2, and the reaction was stirred at 120 °C for 27 hours. After stirring, the reaction mixture was diluted with DCM and washed with 0.1 M HCl, 0.5 M K_2CO_3, and brine. The organic layer was dried with Na_2SO_4, and purified by preparative TLC (1:1 Hex:EtOAc) to afford the pure product as a dark red solid (9 mg, 18% yield). ^{1}H NMR (500 MHz, CD_2Cl_2) δ (ppm): 7.74-7.78 (m, 3H), 7.59 (m, 4H), 7.44 (dd, J = 8.5, 1.8 Hz, 1H), 7.38 (br, 1H), 7.37 (s, 1H), 7.15-7.18 (m, 2H), 3.91 (s, 3H), 3.88 (q, J = 7.1 Hz, 1H), 1.64 (d, J = 7.1 Hz, 3H). ^{13}C{^{1}H} NMR (125 MHz, CD_2Cl_2) δ (ppm): 215.84, 173.18, 173.10, 158.54, 142.42, 136.22, 135.62, 134.56, 129.73, 129.58, 128.37, 128.32, 127.43, 126.90, 126.55, 120.31, 119.83, 106.19, 55.88, 48.73, 18.93. HRMS [M + H]$^+$ calcd for $[C_{23}H_{19}NO_2S_3]^+$ 438.0656; found, 438.0645.

Synthesis of 2-Propyl-N-(4-(3-thioxo-3H-1,2-dithiol-5-yl)phenyl)pentanamide (ADT-NVal). In a glovebox, ADT-NH_2 (200 mg, 0.888 mmol), 2-propylpentanoic acid (192 µL, 1.20 mmol), EDC·HCl (230 mg, 1.20 mmol), and 4-dimethylaminopyridine (15 mg, 0.12 mmol) were added to an oven-dried pressure vessel and dissolved in dry $CHCl_3$ (8 mL) under N_2, and the reaction stirred at 120 °C for 2.5 days. The reaction mixture was diluted with DCM and washed with 0.1 M HCl, 0.5 M K_2CO_3, and brine. The organic layer was dried with Na_2SO_4 and purified via column chromatography (20-50% Hex:EtOAc

gradient). Pure product was obtained as an orange-red solid (170 mg, 54% yield). ^{1}H NMR (500 MHz, CD_2Cl_2) δ (ppm): 7.71 (d, J = 8.8 Hz, 2H), 7.66 (d, J= 8.8 Hz, 2H), 7.42 (s, 1H), 7.39 (br, 1H), 2.24 (m, 1H), 1.63-1.70 (m, 2H), 1.45-1.52 (m, 2H), 1.32-1.39 (m, 4H), 0.92 (t, J = 7.3 Hz, 6H). $^{13}C\{^{1}H\}$ NMR (125 MHz, CD_2Cl_2) δ (ppm): 215.90, 175.26, 173.28, 142.48, 135.65, 128.42, 127.41, 120.44, 49.37, 35.76, 21.37, 14.48. HRMS $[M]^+$ calcd for $[C_{17}H_{21}NOS_3]^+$ 351.0785; found, 351.0773.

Hydrolysis of ADT-OAc and ADT-NAc. A cuvette was charged with 3.00 mL of 0.10 M HCl. After addition of an ADT-OAc or ADT-NAc stock solution (60 µL, 1.0 M in DMSO) via syringe, a UV-vis spectrum was recorded at 0, 60, 120, 240, 540, and 1080 minutes. Each reaction cuvette was incubated at 37 °C during the course of the experiment. Percent hydrolysis values were calculated relative to ADT-OH or ADT-NH_2 absorbances (20 µM in 0.10 M HCl) at 358 or 311 nm, respectively.

CHAPTER V

FUNCTIONALIZED TETRASULFIDES AS EASILY ACCESSABLE HYDROGEN SULFIDE DONORS

This work includes unpublished material and involved contributions from Mary S. Earp and Michael D. Pluth. I was the primary researcher and composer of the writing.

Introduction

Hydrogen sulfide (H_2S) is the latest gaseous molecule to be classified as a gasotransmitter because of its importance in cell signaling.[112] Enzymatically produced H_2S regulates physiological function in the immune, nervous, cardiovascular, endocrine, and gastrointestinal systems.[4] Many of these signaling processes proceed through *S*-sulfhydration of protein cysteines,[52] interplay with reactive oxygen and nitrogen species such as nitric oxide (NO),[156] or interactions with heme-containing proteins.[157] The broad-ranging implications of H_2S activity in the body have stimulated interest in administering exogenous H_2S in therapeutic applications. For example, the role of H_2S in inflammation has been well documented, although consistent findings have been elusive.[12-15,158,159] H_2S can act with either anti- or pro-inflammatory effects, and the variability in observed results depends on the specific experimental conditions and mode of H_2S delivery used. In particular, inorganic sulfide sources such as NaHS and synthetic donors usually give markedly different, and often conflicting, results due to contrasting H_2S release kinetics.[12]

Taken together, judicious selection of H_2S donor appears essential to eliciting a desired physiological response.

To diversify the suite of available H_2S donor alternatives for both research and therapeutic applications, a variety of synthetic donors have been developed (Figure 5.1a).[42,43] For example, H_2S-releasing dithiolethiones like ADT-OH and ADT-NH_2 have been functionalized with non-steroidal anti-inflammatory drugs (NSAIDs) through acyl linkages and were studied for their synergistic antioxidant and anti-inflammatory properties.[44,45,140-143] Although these compounds are easily functionalized, ADT-OH is expensive ($5/mg), and ADT-$NH_2$ is not yet commercially available. Furthermore, the mechanism of H_2S extrusion from dithiolethiones in biological milieu remains unclear. GYY4137, another common H_2S donor, was initially prepared as a more water soluble derivative of Lawesson's reagent.[160] GYY4137 releases H_2S through hydrolysis, and this donor motif has been used extensively in cancer and cardiovascular disease research.[47] Unlike ADT-OH, the mechanism of sulfide release from GYY4137 is well-defined and proceeds by slow hydrolysis of its phosphinodithioate functional group in a pH-dependent fashion to release H_2S. This release, however, is inefficient at physiological pH (< 10% release observed over 7 days).[161] Protected *N*-mercaptobenzamides release H_2S after thiol activation through a perthiol intermediate.[162] An extension of the strategy included caged perthiols, which exhibited protective effects in a model of myocardial ischemia-reperfusion injury.[163] Geminal dithiols, another caged H_2S source, were shown to release sulfide after photoactivation.[164] Finally, one naturally-occurring source of H_2S is allyl polysulfides such as diallyl di- and trisulfide (DADS and DATS, respectively), which is found in garlic and is recognized as contributing many of the health benefits of

garlic. These release H_2S in the presence of thiols through a cascade of nucleophilic substitutions and thiol/disulfide exchanges.[105,165]

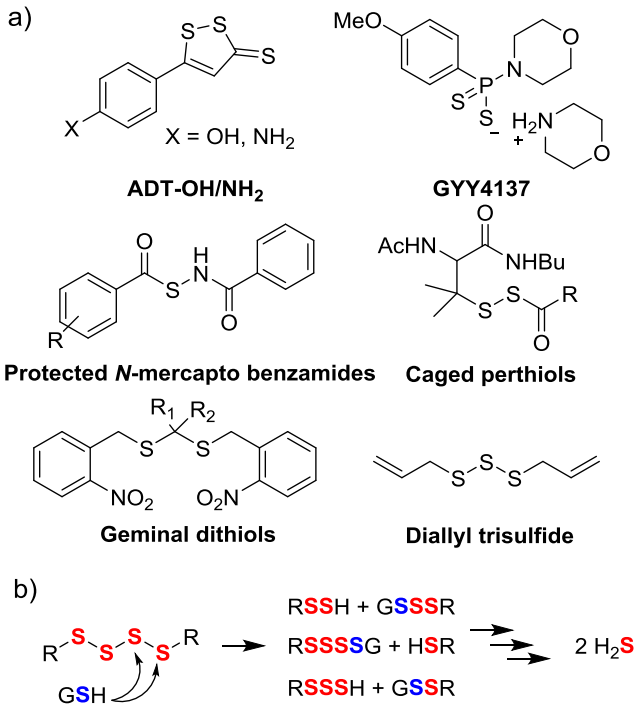

Figure 5.1. a) Examples of established H_2S donor scaffolds, b) Proposed thiol/disulfide exchange cascade which results in H_2S release from tetrasulfide donors.

Inspired by the abundance of polysulfide-containing compounds in nature which release H_2S,[139] we have investigated symmetric tetrasulfide derivatives as an easily accessible sulfane sulfur source for H_2S donation (Figure 5.1b). We hypothesized that tetrasulfides would release H_2S in a similar manner to DATS, and also that such molecules could be easily accessed through simple synthetic methods, thus increasing the diversity of molecules available for different studies. We demonstrate herein the ease and

versatility of tetrasulfide synthesis using commercially available sulfur monochloride (S_2Cl_2) and study the kinetics of H_2S release both as a function of thiol concentration and of tetrasulfide derivatization. Supplemental information can be found in Appendix D.

Results and Discussion

Chemists have created a number of molecular scaffolds for H_2S delivery in biological systems. The structures of donors such as ADT-OH/NH_2 and GYY4137, however, are not easily modified to customize H_2S release rates. Our goal was to develop an accessible, adaptable, and inexpensive strategy for generating H_2S using functionalized polysulfides. We forged our initial hypothesis based on H_2S release from trisulfide-containing DATS. We reasoned that if thiol-mediated H_2S extrusion from trisulfides is general and extendable to a range of functionalized polysulfides, then the scaffold could become modular and broadly functionalized to achieve controllable H_2S release.

First we investigated the viability of polysulfide-based H_2S donor syntheses. Symmetric trisulfides are most easily prepared from substitution reactions of sulfur dichloride (SCl_2) with two equiv. of thiol;[166] however, SCl_2 is not commercially available at high purities and must be prepared from the reaction of hazardous chlorine gas and elemental sulfur or S_2Cl_2.[167] Alternatively, thiols react cleanly with S_2Cl_2 to form tetrasulfides,[168] and S_2Cl_2 is not only more stable and easier to work than SCl_2, it is commercially available at synthetically-viable purities. Therefore, we chose functionalized tetrasulfides as our target H_2S donors. We found that dropwise addition of

a S_2Cl_2 solution into a thiol-containing reaction solution in anhydrous solvents and under N_2, followed by aqueous workup, afforded alkyl tetrasulfides of *N*-acetylcysteine (NAC) and fully protected *N*-acetylcysteine methyl ester (Table 5.1, entries 1 and 2). Reactions to form aryl tetrasulfides bearing both electron-withdrawing and -donating groups (3-7) were all well tolerated, and most products were obtained as analytically pure compounds, but can also be purified by recrystallization if necessary. These results demonstrate the versatility of tetrasulfide syntheses from inexpensive and accessible starting materials.

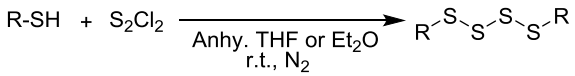

Entry	R	Solvent	Yield
1, $(NAC)_2S_4$	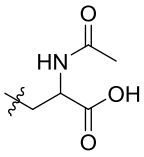	THF	80
2, $(PCys)_2S_4$	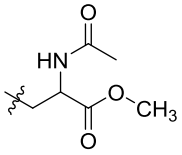	THF	77
3	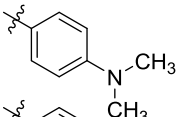	Et_2O	67
4	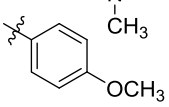	Et_2O	78
5	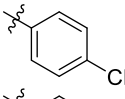	Et_2O	100
6	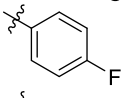	Et_2O	64
7	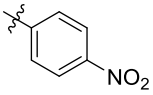	Et_2O	78

Table 5.1. Synthesis of functionalized tetrasulfides.

With a library of functionalized tetrasulfides in hand, we then characterized the thiol-dependence of H_2S release from *N*-acetylcysteine tetrasulfide ($(NAC)_2S_4$) as a model tetrasulfide using an H_2S-selective electrode. No H_2S was observed over 15 minutes after injection of $(NAC)_2S_4$ (10 μM) into aqueous buffer (pH 7.4 PBS, 1 mM CTAB) (Figure D.1), which indicates that water is insufficiently nucleophilic to cleave tetrasulfide S-S bonds. Upon injection of glutathione (GSH), a short induction period with no observed H_2S was followed by a significant increase in signal as $(NAC)_2S_4$ released H_2S (Figure 5.2a). The rate of H_2S evolution increased dramatically with higher concentrations of GSH with a linear dependence according to [GSH] (Figure 5.2b). Minimal H_2S was observed with equimolar amounts of GSH and $(NAC)_2S_4$, and no H_2S was observed when [GSH] < [$(NAC)_2S_4$]. This observation supports the requirement of more than one equiv. of thiol in order to liberate H_2S from polysulfides.

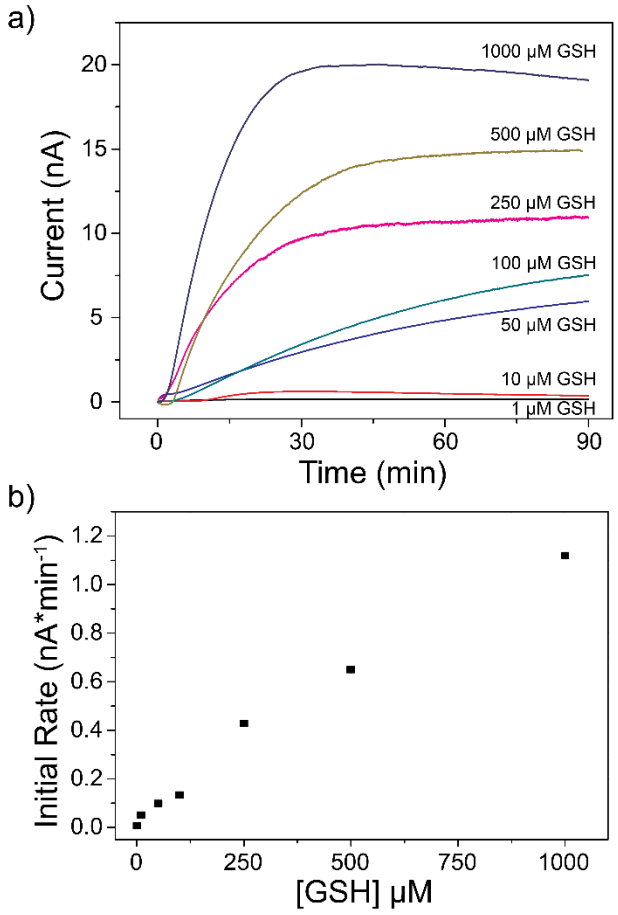

Figure 5.2. a) Thiol-concentration dependence of H_2S release from $(NAC)_2S_4$ (10 µM) after treatment with 1.0, 10, 50, 100, 250, 500, and 1000 µM GSH over 90 minutes in PBS buffer (pH 7.4, 1 mM CTAB), b) Linear relationship between [GSH] and rate of H_2S release. Rates were calculated as initial rates after induction period.

To better understand the mechanism of H_2S release from tetrasulfides, we investigated release rates from *p*-functionalized aryl tetrasulfides. Initially, we expected electron-withdrawn aryl tetrasulfides to react more quickly than electron-rich tetrasulfides. Surprisingly, very little difference in H_2S release rate was observed after treatment of tetrasulfides (10 µM) containing electron-donating ($–N(CH_3)_2$, $–OCH_3$, $–CH_3$) and -withdrawing (–F, $–NO_2$) groups with 10 equiv. GSH (Table 5.2, Figure D.2).

Alkyl derivatives ($(NAC)_2S_4$, $(PCys)_2S_4$), however, reacted one order of magnitude more slowly than the aryl tetrasulfides. Curiously, reaction of the most electron-withdrawn aryl tetrasulfide ($–NO_2$) with GSH was the slowest, with the kinetic profile closely resembling those of $(NAC)_2S_4$ and $(PCys)_2S_4$ (*vida infra*).

p-Substituent	Initial Rate ($nA*min^{-1}$)
$–N(CH_3)_2$	2.9
$–OCH_3$	2.5
$–CH_3$	2.4
–FAr	2.4
$–NO_2$	0.27
$(NAC)_2S_4$	0.13
$(PCys)_2S_4$	0.24

Table 5.2. Rate of H_2S release from functionalized tetrasulfides (10 μM) after addition of GSH (100 μM) in PBS buffer (pH 7.4, 1 mM CTAB). Rates were calculated as initial rates after induction period.

We propose the following mechanistic details supported by these data. Although H_2S release from diallyl polysulfides may involve nucleophilic attack at either the sulfur atoms or the allylic α-carbon,[105] tetrasulfides lacking an allylic position will facilitate attack predominantly at sulfur only. An incoming GSH nucleophile has two distinct pathways with which to initiate reaction with a tetrasulfide: either attack at an interior sulfur atom or at an exterior sulfur atom along the tetrasulfide chain. Internal attack on a symmetric R-S_4-R tetrasulfide includes a non-productive pathway in which the reaction products are a new thiol, R-SH, and G-S_4-R tetrasulfide (Figure 5.3a). G-S_4-R is unable to release H_2S directly and must react with another thiol to move closer to H_2S release.

Only an internal attack producing R-S_3-G and a terminal R-SSH perthiol pushes the tetrasulfide closer toward H_2S release. Reaction of R-SSH with another equivalent of thiol produces H_2S. Inclusion of this non-productive pathway works to effectively decrease the overall rate of H_2S release from tetrasulfides involving nucleophilic attack at an interior sulfur atom. Alternatively, nucleophilic attack at an exterior sulfur will only result in R-SS-G disulfide and R-SSSH persulfide as reaction products (Figure 5.3b), where R-SSSH may directly undergo further reactivity to give H_2S.

Our data suggest that an exterior sulfur bound to the sp^2 carbon of an aryl ring is sufficiently electron-deficient to steer toward external attack, which results in a significantly faster overall release of H_2S for aryl tetrasulfides. It is not altogether clear why modifying the electronics within the aryl substituent does not elicit a stronger effect on the H_2S release rate. Perhaps the rate-determining, H_2S-releasing step from R-SSSH is far enough removed that the process is electronically isolated. By contrast, alkyl tetrasulfides such as our cysteine derivatives undergo nucleophilic attack preferentially on the interior of the tetrasulfide chain and are thus slowed considerably in their H_2S release. In the case of the nitro-functionalized aryl tetrasulfide, resonance stabilization of *p*-nitrothiophenol anion causes GSH to react with two rapid interior attacks to give 2 R-SH and G-S_4-G, which then reacts in a similar fashion as $(NAC)_2S_4$ and $(PCys)_2S_4$. UV-vis data is consistent with this hypothesis. We observed the appearance of *p*-nitrothiophenol more rapidly than H_2S release (Figure D.3). Taken together, these mechanistic insights help dictate the design principles for selecting tetrasulfide H_2S donors to match a desired H_2S-release rate profile.

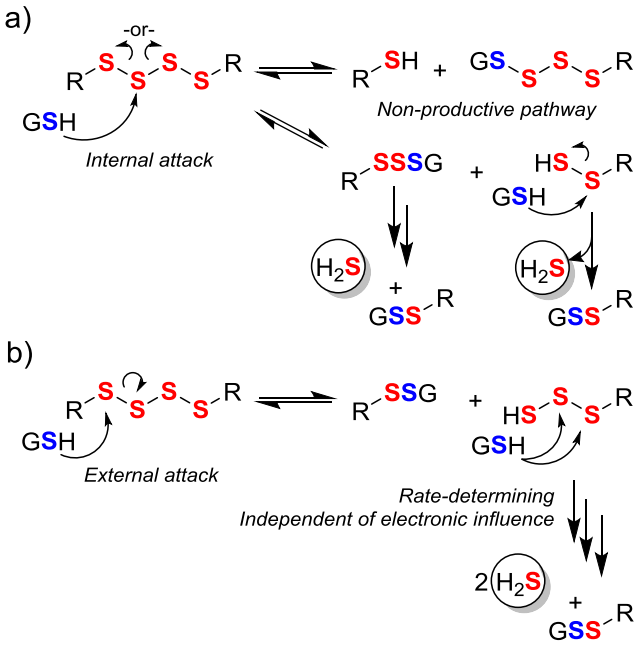

Figure 5.3. a) Interior attack of an incoming GSH nucleophile on the tetrasulfide may result in a non-productive pathway, which slows down the overall rate of reaction, b) Exterior attack leads directly to H_2S-releasing perthiol compounds and gives H_2S more quickly.

Conclusion

Emulating polysulfide-containing compounds found in nature, we've shown that symmetrically-functionalized tetrasulfides represent a straightforward avenue for delivering H_2S. The modular synthesis of these donors offers customizability and makes possible the production of a wide range of donors both quickly and inexpensively, which is a significant improvement upon previously-developed synthetic H_2S donors. By exploiting the two different modes of observed reactivity, users can easily explore the effect of variable H_2S release rates on physiological processes in biological experiments. Because NAC has long been used to protect against oxidative stress,[169] $(NAC)_2S_4$ may provide health benefits from synergistic H_2S and NAC activities. Furthermore, aryl-

tethered tetrasulfides also have application in prodrug-release strategies. Our lab continues to study the mechanism of H_2S release from these and other synthetic donors.

Experimental

Materials and methods. Reagents were purchased from Sigma-Aldrich or Tokyo Chemical Industry (TCI) and used as received. S_2Cl_2 was purchased from Sigma-Aldrich (98% purity). Deuterated solvents were purchased from Cambridge Isotope Laboratories and used as received. Silica gel (SiliaFlash F60, Silicycle, 230 - 400 mesh) was used for column chromatography. Preparatory chromatography was performed on Silicycle SiliaPlates (1 mm thickness). ^{1}H and $^{13}C\{^{1}H\}$ NMR spectra were recorded on a Varian INOVA 500 MHz NMR instrument. Chemical shifts are reported in ppm relative to residual protic solvent resonances. UV–visible spectra were acquired on a Cary 100 spectrometer equipped with a Quantum Northwest TLC-42 dual cuvette temperature controller at room temperature. H_2S-release data were acquired using a World Precision Instruments (WPI) ISO-H2S-2 sensor connected to a TBR Free Radical Analyer.

Spectroscopic materials and methods. Phosphate buffered saline tablets (EMD Millipore) and cetyltrimethylammonium bromide (CTAB) were used to prepare buffered solutions (10 mM phosphate buffer, 140 mM NaCl, 3 mM KCl, 1 mM CTAB, pH 7.4) in Millipore water. Stock solutions of tetrasulfides (10 mM) and GSH (10 mM, 50 mM, 100 mM) were prepared in DMSO and buffer, respectively, in an N_2-filled glovebox and stored at -25 °C until immediately

before use. All electrode experiments were performed using previously degassed buffer, however reaction vessels were briefly exposed to ambient atmosphere during experimental setup.

General procedure for H_2S-release experiments. A scintillation vial containing 20.0 mL of PBS buffer (10 mM phosphate buffer, 140 mM NaCl, 3 mM KCl, 1 mM CTAB, pH 7.4) with stir bar was prepared in a glovebox. The electrode was inserted into the buffered solution, and the signal current was allowed to equilibrate. A $(NAC)_2S_4$ stock solution (20 μL, 10.0 mM) was added via syringe to the vial, and the signal current was again allowed to equilibrate. After addition of a GSH stock solution (20 μL, 50 mM) via syringe, the signal current was recorded over 90 minutes.

General procedure for alkyl tetrasulfide synthesis. A reaction solution of aryl thiol (1.00 mmol) in THF (10 mL) was prepared under N_2 at room temperature. To this solution was added an anaerobic solution of S_2Cl_2 (0.040 mL, 0.495 mmol) in THF (1 mL) dropwise. The reaction was allowed to stir overnight and diluted with THF. After addition of brine and extraction with THF, the organic phases were combined and dried using Na_2SO_4. The solvent was removed under reduced pressure to afford the desired tetrasulfide as pure compound.

General procedure for aryl tetrasulfide synthesis. A reaction solution of aryl thiol (1.00 mmol) in diethyl ether (10 mL) was prepared under N_2 at room temperature. To this solution was added an anaerobic solution of S_2Cl_2 (0.495 mmol) in diethyl ether (1 mL) dropwise. The reaction was allowed to stir overnight and diluted with diethyl ether. After addition of water and extraction with ether, the organic phases were combined and dried

using Na_2SO_4. The solvent was removed under reduced pressure to afford the desired tetrasulfide as pure compound.

3,3'-Tetrasulfanediylbis(2-acetamidopropanoic acid) ($(NAC)_2S_4$, 1). Yield = 80%. Product was recovered as a pure yellowish-white solid. ^{1}H NMR (500 MHz, DMSO) δ (ppm): 12.96 (s, 2H), 8.36 (d, J = 7.9 Hz, 2H), 4.55 (td, J = 8.4, 4.7 Hz, 2H), 3.46-3.07 (m, 4H), 1.86 (s, 6H). ^{13}C{^{1}H} NMR (125 MHz, DMSO) δ (ppm): 171.63, 169.38, 54.90, 51.31, 22.37. HRMS $[M+Na]^+$ calcd for $[NaC_{10}H_{16}N_2O_6S_4]^+$ 410.9789; found, 410.9771.

Dimethyl 3,3'-tetrasulfanediylbis(2-acetamidopropanoate) ($(PCys)_2S_4$, 2). Yield = 77%. Product was recovered as a yellowish-white solid. ^{1}H NMR (500 MHz, DMSO) δ (ppm): 8.49 (d, J = 7.8 Hz, 2H), 4.63 (td, J = 8.3, 5.0 Hz, 2H), 3.66 (s, 6H), 3.42-3.25 (m, 4H), 3.46-3.07 (m, 4H), 1.86 (s, 6H). ^{13}C{^{1}H} NMR (125 MHz, DMSO) δ (ppm): 170.69, 169.48, 52.27, 51.29, 51.14, 22.28.

4,4'-Tetrasulfanediylbis(N,N-dimethylaniline) (3). Yield = 67%. Product was recovered as a yellow solid. ^{1}H NMR (500 MHz, $CDCl_3$) δ (ppm): 7.73 (d, J = 8.4 Hz, 4H), 7.56 (d, J = 8.7 Hz, 4H), 3.20 (s, 12H). ^{13}C{^{1}H} NMR (125 MHz, $CDCl_3$) δ (ppm): 142.52, 138.71, 130.38, 121.81, 46.42.

1,4-Bis(4-methoxyphenyl)tetrasulfane (4). Yield = 78%. Product was recovered as a yellow oil. ^{1}H NMR (500 MHz, $CDCl_3$) δ (ppm): 7.51 (d, J = 8.9 Hz, 4H), 6.86 (d, J = 8.9 Hz, 4H), 3.82 (s, 6H).

1,4-Di-p-tolyltetrasulfane (5). Yield = 100%. Product was recovered as a yellow oil. ^{1}H NMR (500 MHz, $CDCl_3$) δ (ppm): 7.46 (d, J = 8.1 Hz, 4H), 7.14 (d, J = 8.0 Hz, 4H), 2.36 (s, 6H). ^{13}C{^{1}H} NMR (125 MHz, $CDCl_3$) δ (ppm): 139.01, 132.99, 131.21, 130.05, 21.36.

1,4-Bis(4-fluorophenyl)tetrasulfane (6). Yield = 64%. Product was recovered as a yellow oil. ^{1}H NMR (500 MHz, $CDCl_3$) δ (ppm): 7.53 (dd, J = 8.9, 5.2 Hz, 4H), 7.03 (t, J = 8.7 Hz, 4H).

1,4-Bis(4-nitrophenyl)tetrasulfane (7). Yield = 78%. Product was recovered as a yellow solid. ^{1}H NMR (500 MHz, $CDCl_3$) δ (ppm): 8.20 (d, J = 8.9 Hz, 4H), 7.62 (d, J = 8.9 Hz, 4H). $^{13}C\{^{1}H\}$ NMR (125 MHz, $CDCl_3$) δ (ppm): 147.12, 144.19, 126.53, 124.59.

CHAPTER VI

CONCLUDING REMARKS

In recent years, the scientific community has invested substantial intellectual resources in studying physiological H_2S, and we've made great strides toward understanding what this important gasotransmitter does in the human body. A main driver of this progress has been the rapid development of H_2S-selective fluorescent probes and the live-cell/*in vivo* experiments that they facilitate. The enhanced fluorescence response demonstrated herein with MeRho-Az with respect to other azide reduction-based scaffolds (>10-fold improvement) represents another leap forward. MeRho-Az has sufficient sensitivity for cell and whole-animal studies, and we expect that others will build upon our pioneering work with zebrafish larvae and light sheet fluorescence microscopy to investigate sulfide dynamics in other organisms. The ratiometric dual-fluorophore fragmentation strategy with NBD-Coum also provides insight into H_2S-thiol interactions, which are important in redox balance, sulfide biosynthesis and storage, and protein-thiol activity modifications. As we more clearly define the question of "*what* does physiological H_2S do?," fluorescent probes and strategies such as these will be useful in also defining exactly "*how* does H_2S elicit these physiological effects?" One last important question is, "can we effectively *utilize* what we know about physiological H_2S in disease treatments?" Dithiolethione-NSAID conjugates are promising, and coupling of the H_2S-releasing and anti-inflammation components through stable amide linkages will help ensure that the spatial relationship

between the two remains intact after oral drug ingestion. Finally, the simplicity of functionalized tetrasulfides as H_2S donors makes them very versatile and customizable. $(NAC)_2S_4$ is expected to have very low cytotoxicity and is a good candidate for drug screening. Taken together, the chemical tools and strategies developed in this work are facilitators of effective research and experimentation. We continue to work with our collaborators using these compounds to push forward the boundaries of what we know about H_2S in human biology.

APPENDIX A

CHAPTER II SUPPLEMENTARY INFORMATION AND SPECTRA

Supplementary Figures

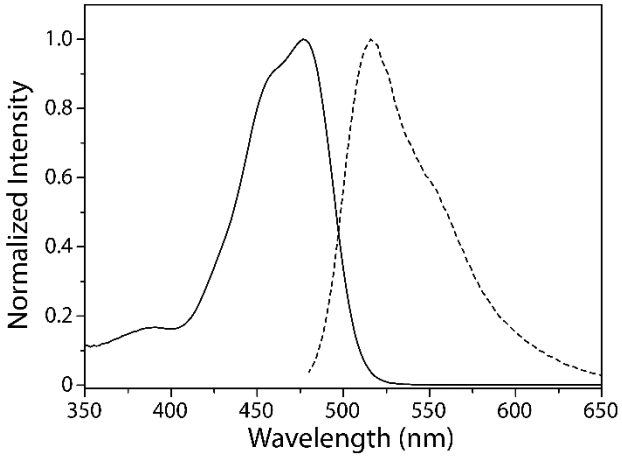

Figure A.1. Normalized absorption (solid line) and emission (dashed line) spectra of MeRho. Conditions: 5 µM MeRho, PIPES buffer (50 mM, 100 mM KCl, pH 7.4), λ_{ex} = 476 nm.

a)

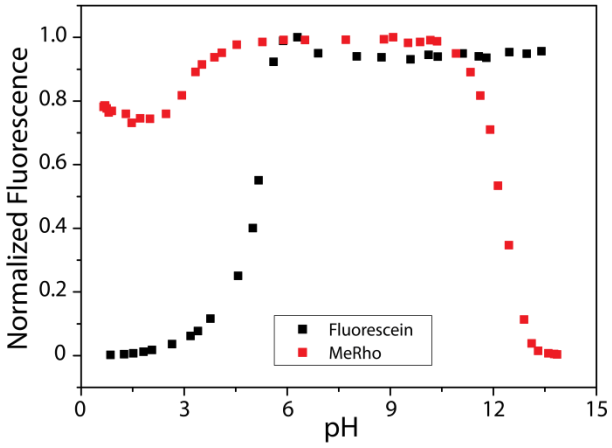

b)

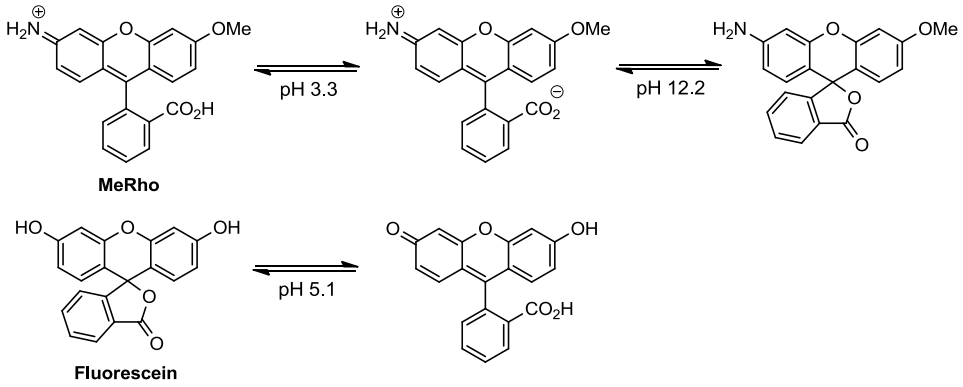

Figure A.2. a) Integrated fluorescein (20 μM, λ_{ex} = 494 nm, λ_{em} = 500-650 nm) and MeRho (20 μM, λ_{ex} = 476 nm, λ_{em} = 480-650 nm) fluorescence in aqueous solution at various pH (100 mM KCl), b) Proposed protonation/deprotonation transitions of MeRho and fluorescein at various pH.

[H_2S] (μM)	Integrated Fluorescence	Standard Deviation
Blank	612234	141173
0.10	1093559	74073
2.5	13564824	2539964
5.0	24469632	4032106
7.5	30622452	4228960
15	58199116	8051924

Table A.1. Tabulated detection limit data of toward H_2S. Conditions: 5 μM MeRho-Az, PIPES buffer (50 mM, 100 mM KCl, pH 7.4), λ_{ex} = 476 nm, λ_{em} = 480-650 nm, 37 °C. Each concentration represents the average of at least three trials.

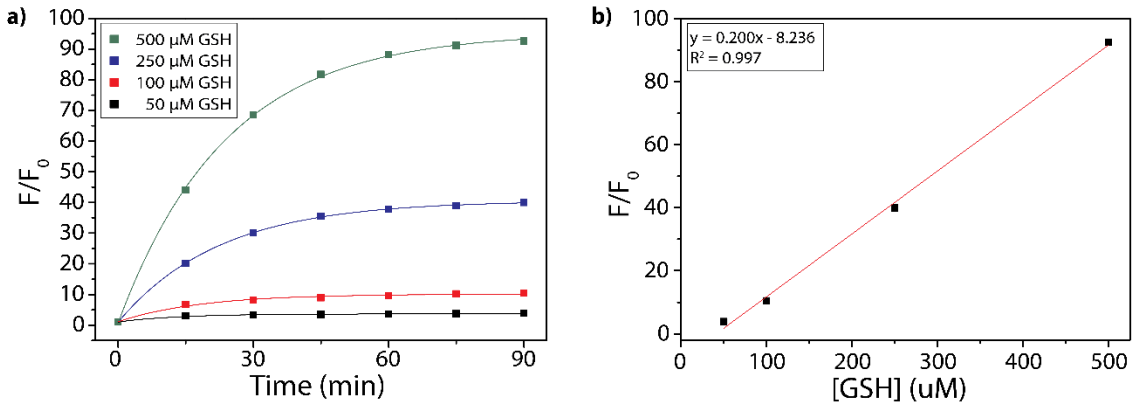

Figure A.3. a) Fluorescent response of MeRho-Az to H_2S released from DATS with various [GSH] over 90 minutes. Conditions: 5 µM MeRho-Az, 300 µM DATS, 50-500 µM GSH, PIPES buffer (50 mM, 100 mM KCl, pH 7.4), λ_{ex} = 476 nm, λ_{em} = 480-650 nm, 37 °C, b) Linear relationship between observed fluorescence turn-on from H_2S release and [GSH].

NMR Spectra

^{1}H (500 MHz, $CDCl_3$) and $^{13}C\{^{1}H\}$ (125 MHz, $CDCl_3$) NMR Spectra of 2

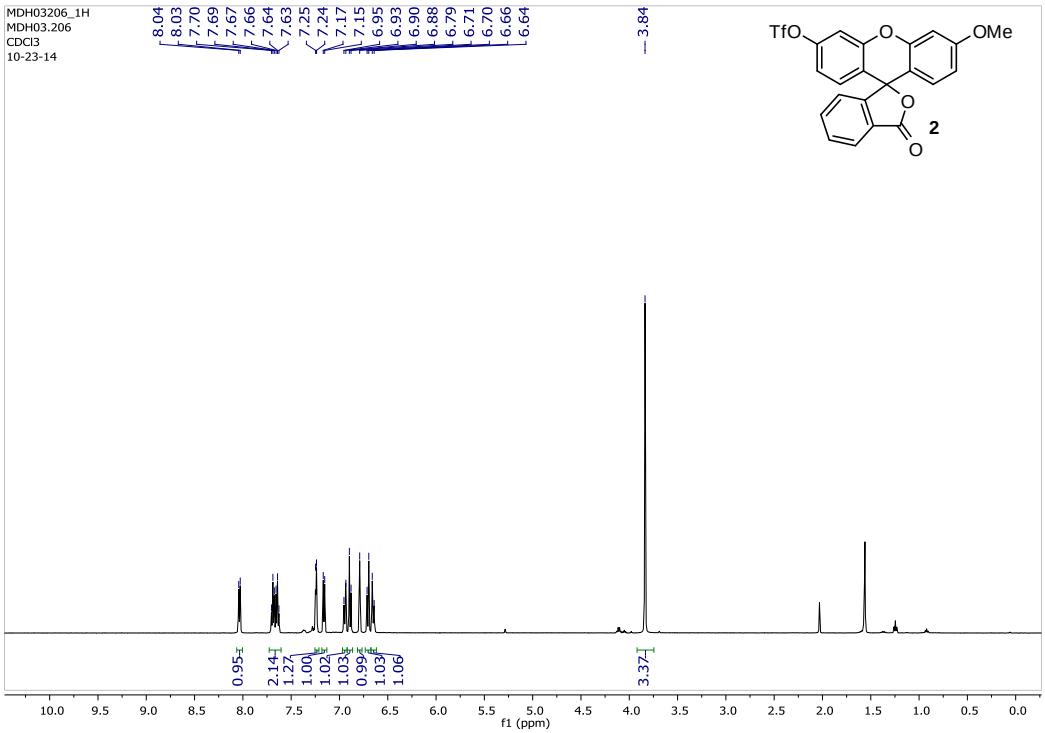

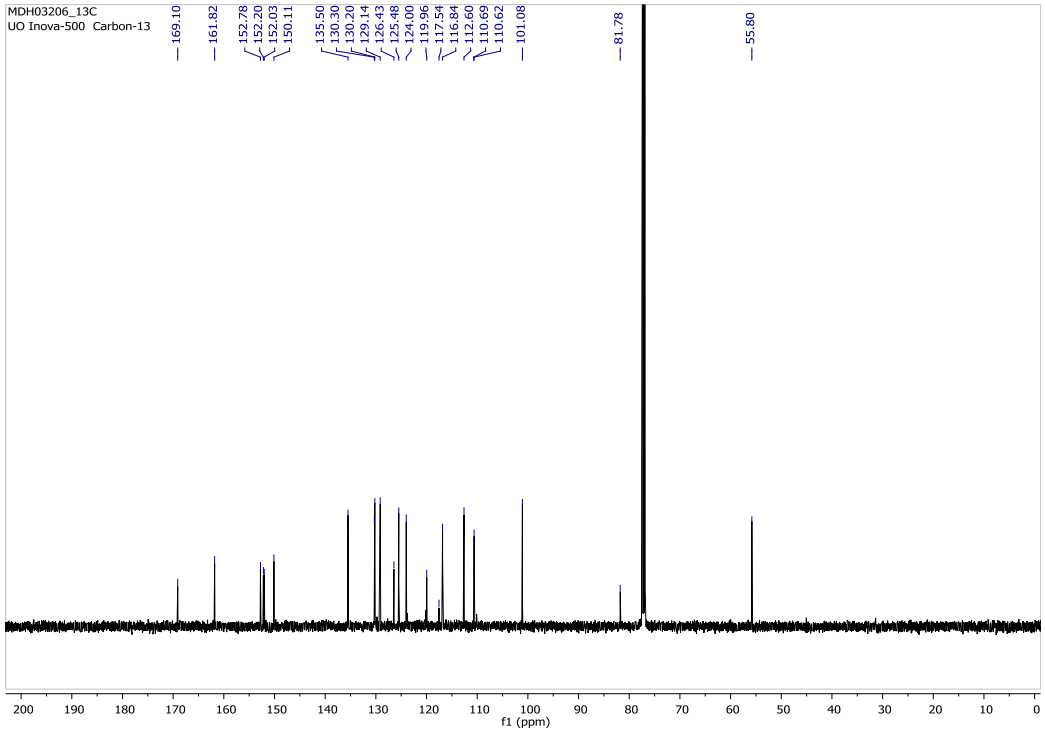

^{1}H (500 MHz, $CDCl_3$) and $^{13}C\{^{1}H\}$ (125 MHz, $CDCl_3$) NMR Spectra of MeRho

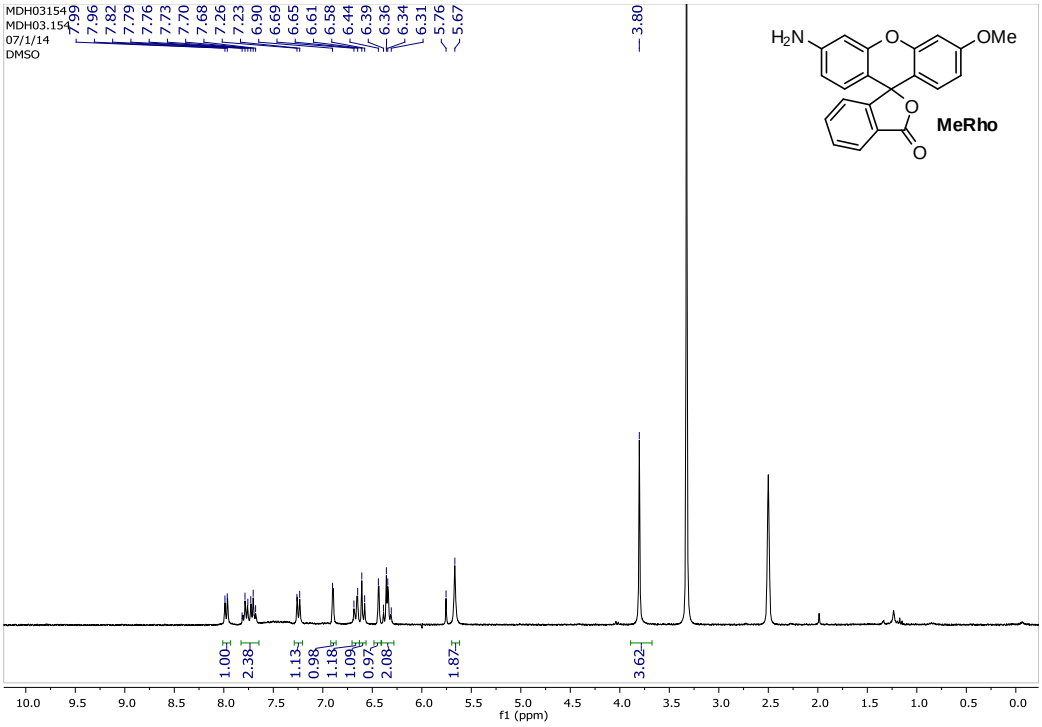

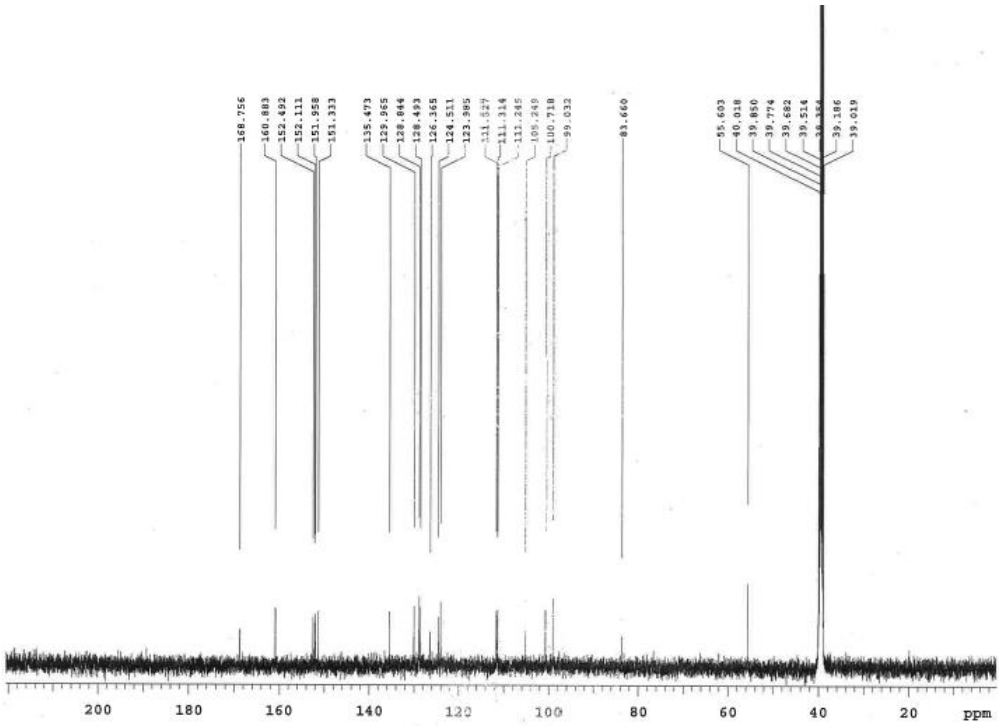

^{1}H (600 MHz, $CDCl_3$) and $^{13}C\{^{1}H\}$ (125 MHz, $CDCl_3$) NMR Spectra of MeRho-Az

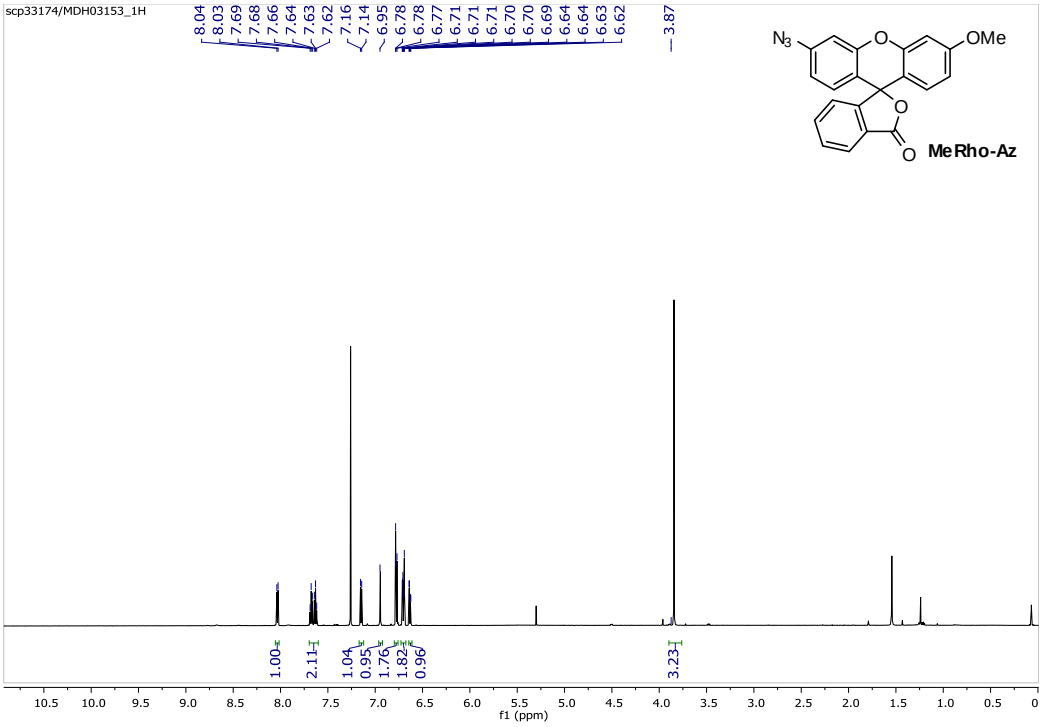

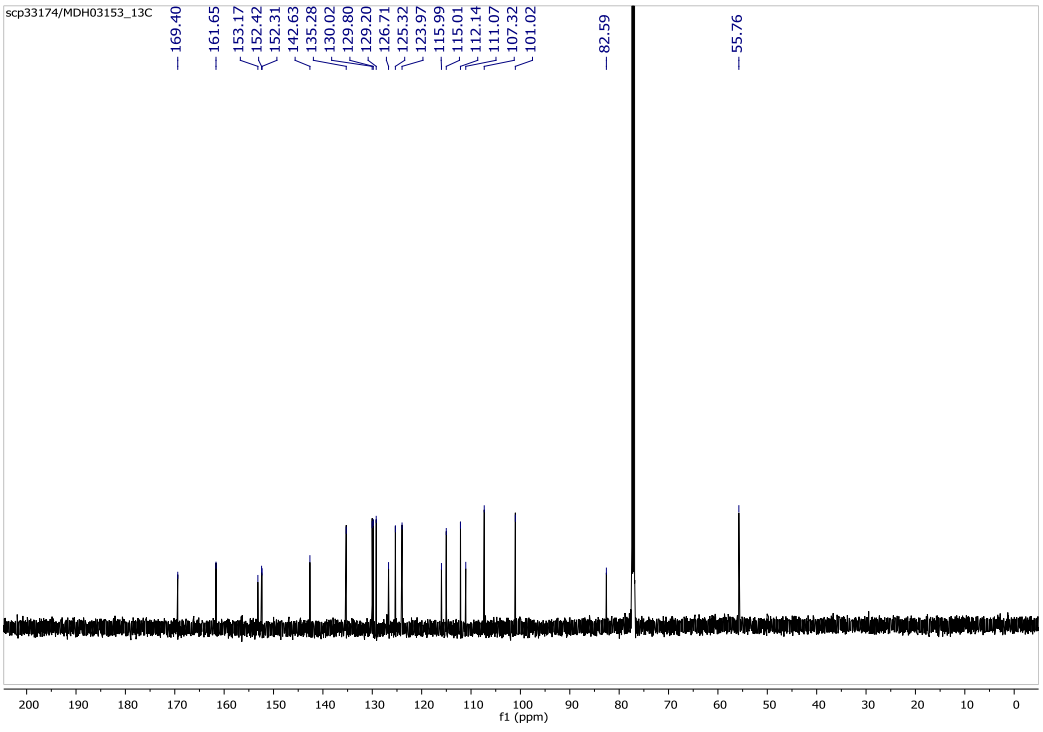

APPENDIX B

CHAPTER III SUPPLEMENTARY INFORMATION AND SPECTRA

Supplementary Figures

None

NMR Spectra

^{1}H (500 MHz, DMSO) and $^{13}C\{^{1}H\}$ (125 MHz, DMSO) NMR Spectra of NBD-Coum

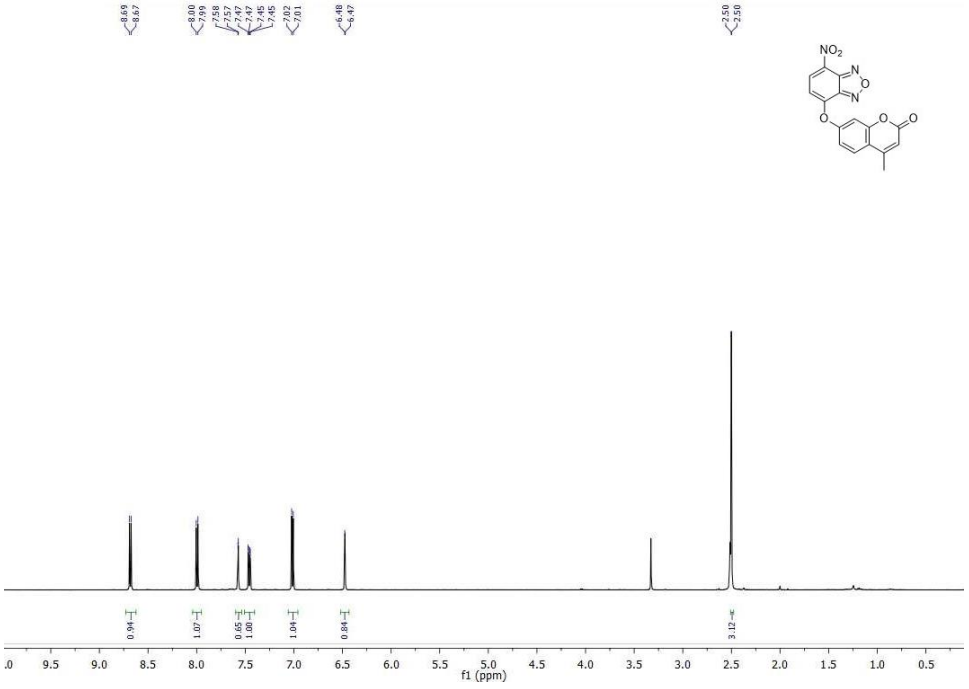

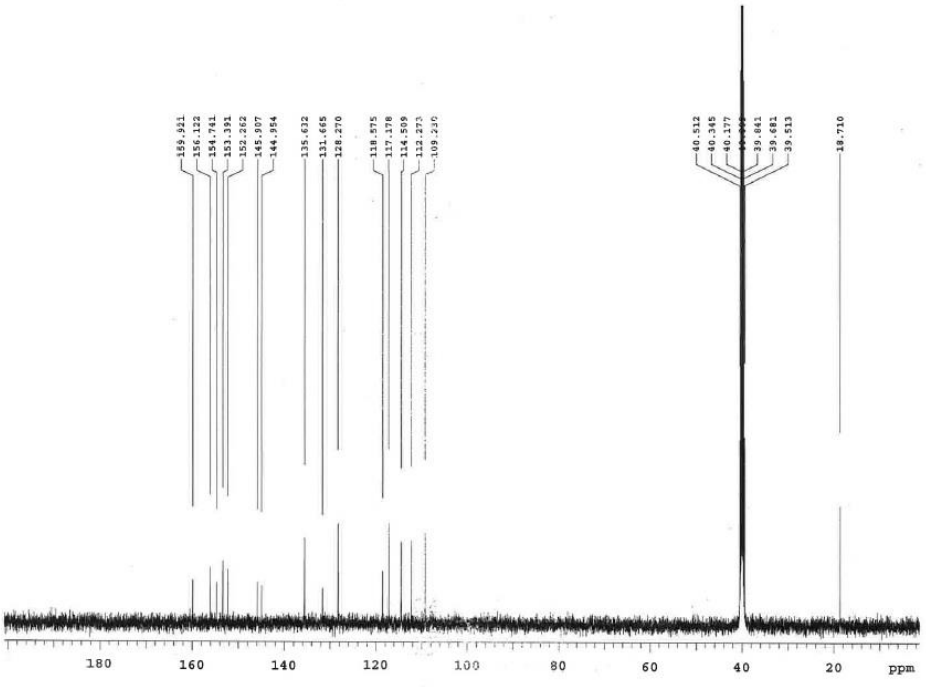

APPENDIX C

CHAPTER IV SUPPLEMENTARY INFORMATION AND SPECTRA

Supplementary Figures

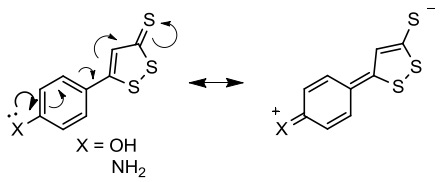

Scheme C.1. Resonance contribution in ADT-OH and ADT-NH_2 from lone pair delocalization.

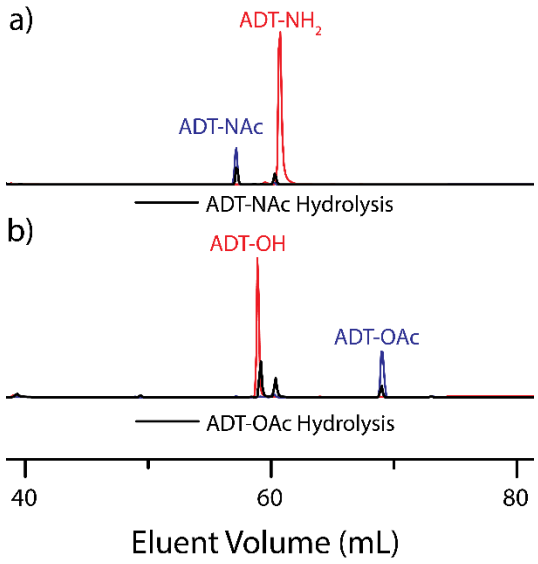

Figure C.1. HPLC analysis of a) ADT-NH_2, ADT-NAc, and the reaction products of ADT-NAc hydrolysis, b) ADT-OH, ADT-OAc, and the reaction products of ADT-OAc hydrolysis. Conditions: 20 µM analyte, 18 hour hydrolysis in 0.1 M HCl, H_2O:acetonitrile eluent gradient from 4 to 100 % with 10 mM triethylammonium acetate. Hydrolysis of ADT-OAc does not appear to be entirely clean, as a reaction byproduct was also observed on HPLC.

NMR Spectra

^{1}H NMR (500 MHz, DMSO) and ^{13}C{^{1}H} NMR (125 MHz, DMSO) of 5-(4-methoxyphenyl)-3H-1,2-dithiole-3-thione (ADT-OMe)

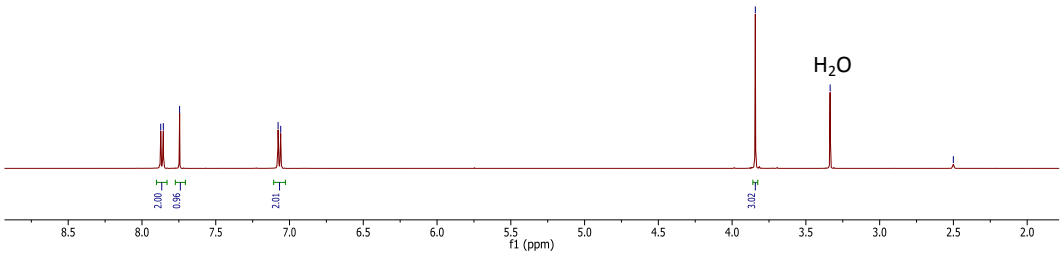

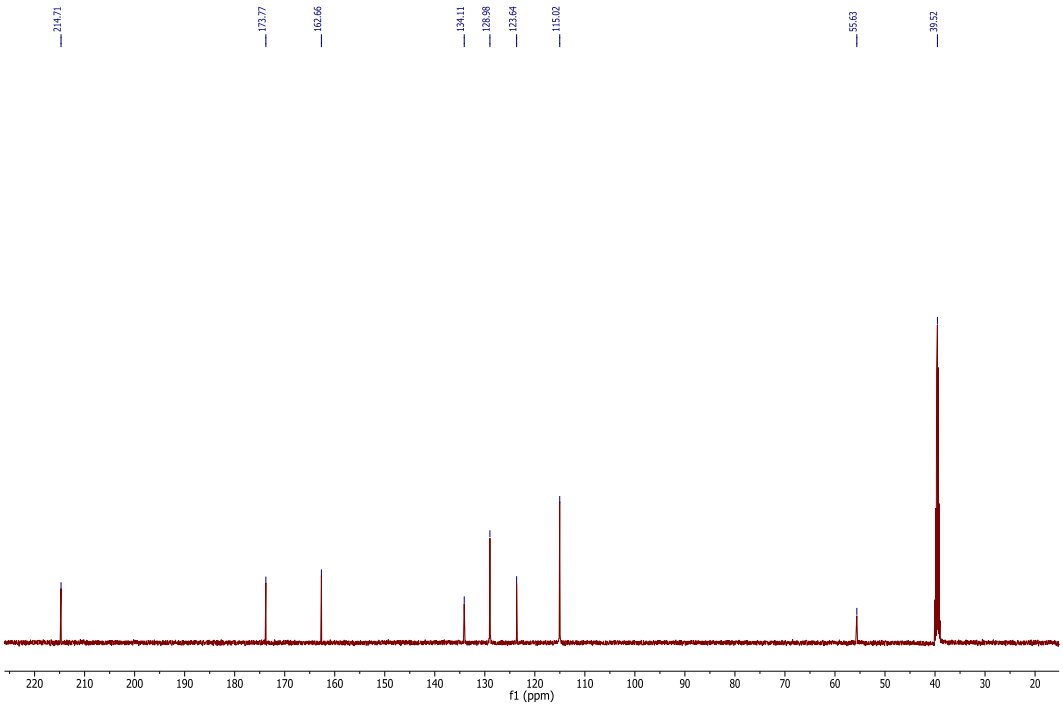

^{1}H NMR (500 MHz, DMSO) and ^{13}C{^{1}H} NMR (125 MHz, DMSO) of 5-(4-hydroxyphenyl)-3H-1,2-dithiole-3-thione (ADT-OH)

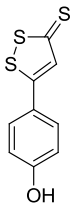

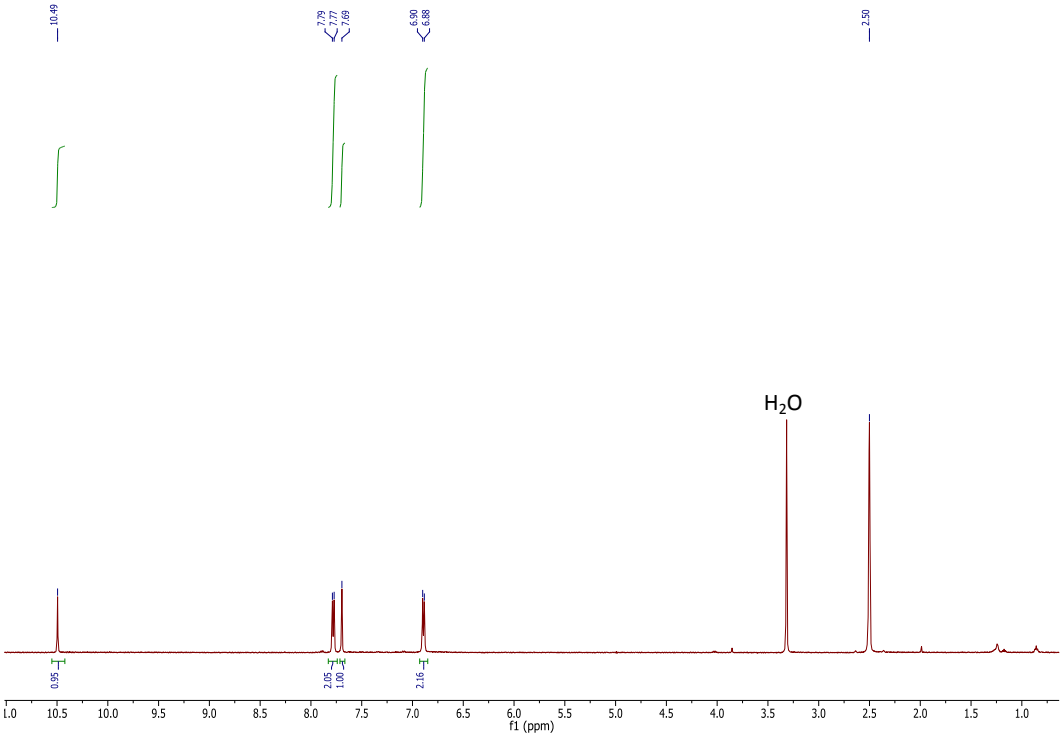

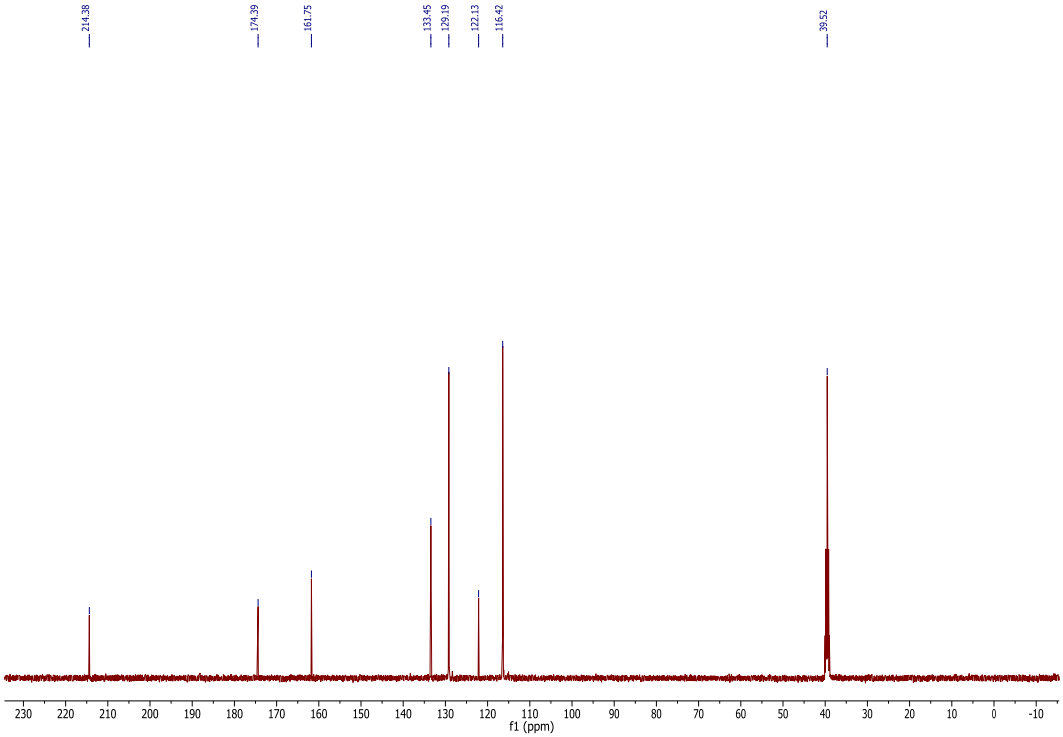

^{1}H NMR (500 MHz, DMSO) and ^{13}C{^{1}H} NMR (125 MHz, DMSO) of(E)-tert-butyl (4-(prop-1-en-1-yl)phenyl)carbamate (1)

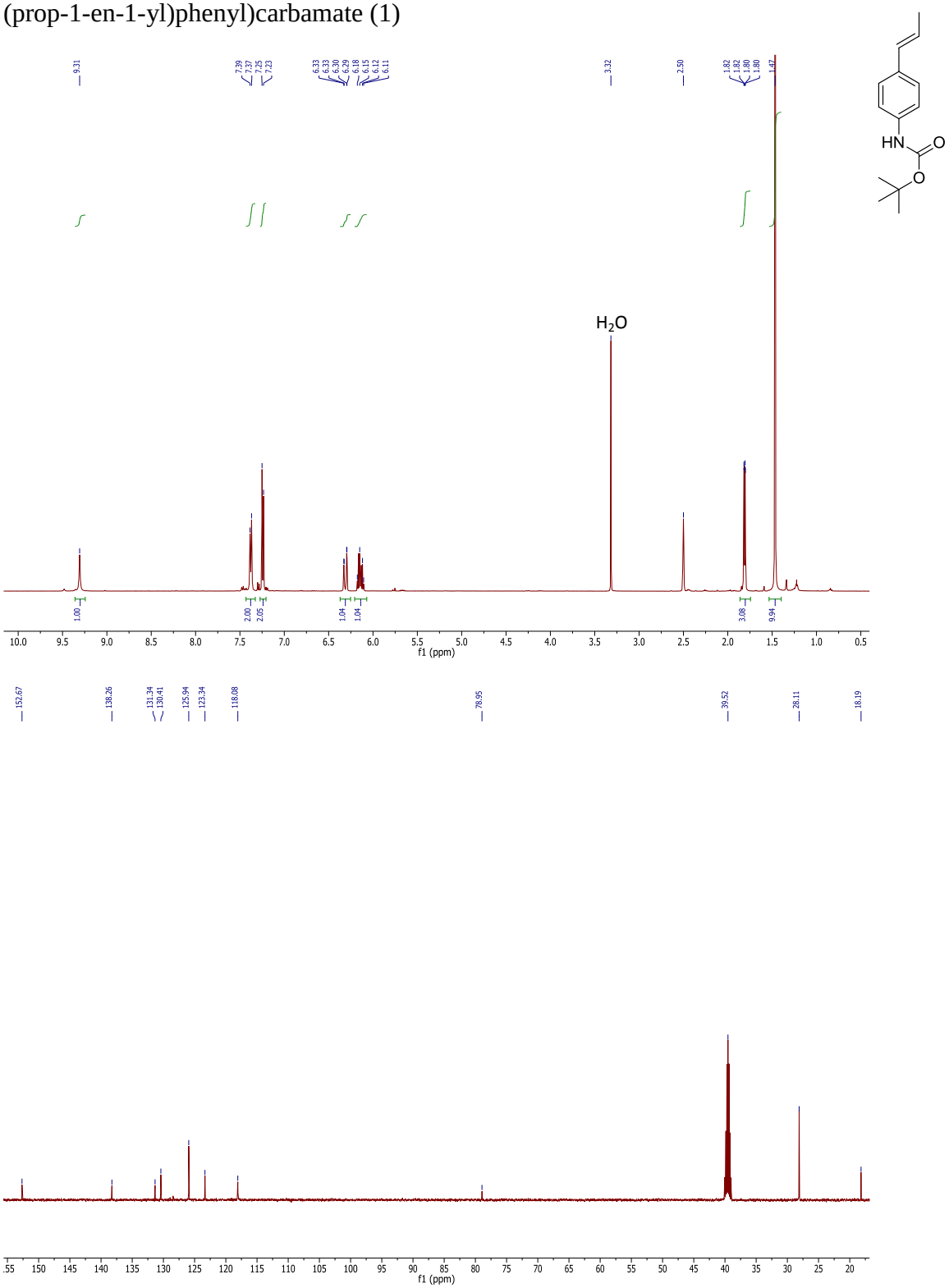

^{1}H NMR (500 MHz, CD_2Cl_2) and $^{13}C\{^{1}H\}$ NMR (125 MHz, CD_2Cl_2) of 5-(4-aminophenyl)-3H-1,2-dithiole-3-thione (ADT-NH_2)

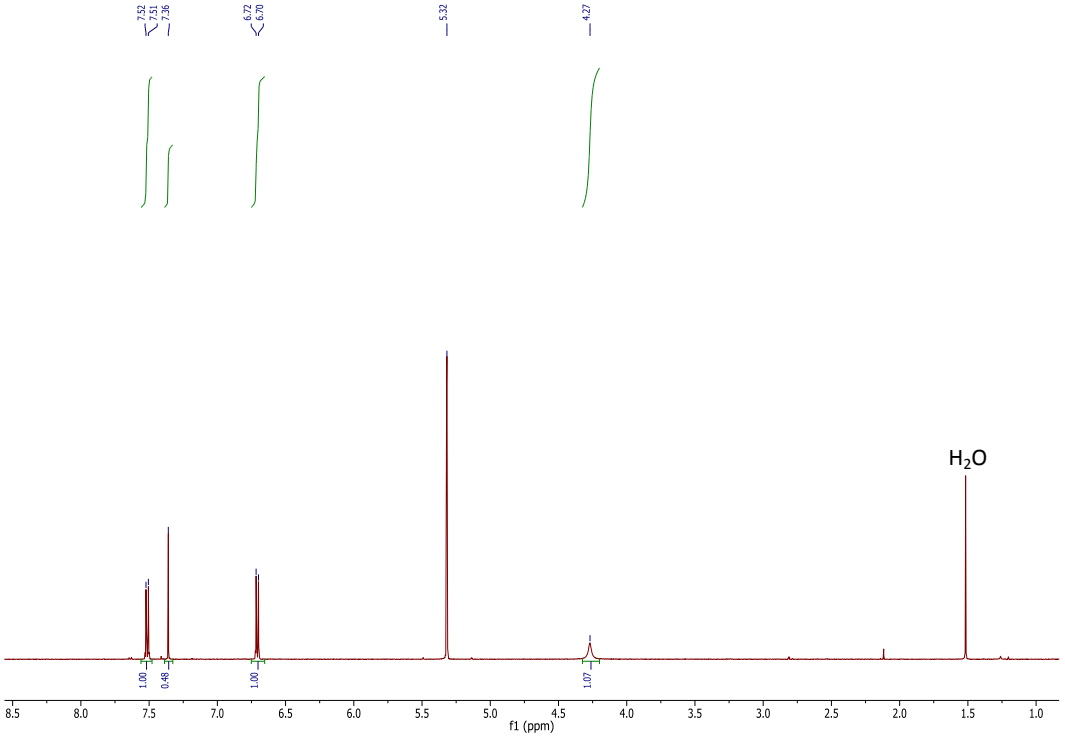

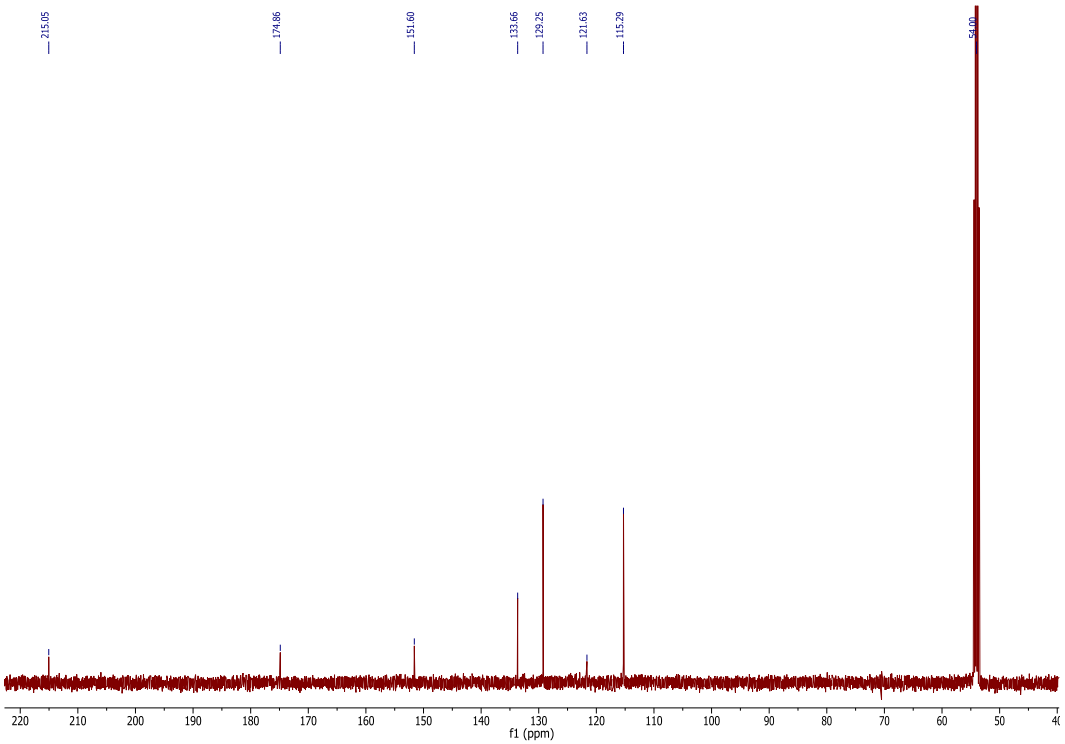

^{1}H NMR (500 MHz, CD_2Cl_2) and $^{13}C\{^{1}H\}$ NMR (125 MHz, CD_2Cl_2)of (E)-N,N-dimethyl-4-(prop-1-en-1-yl)aniline (N,N-Dimethyl Propenylaniline)

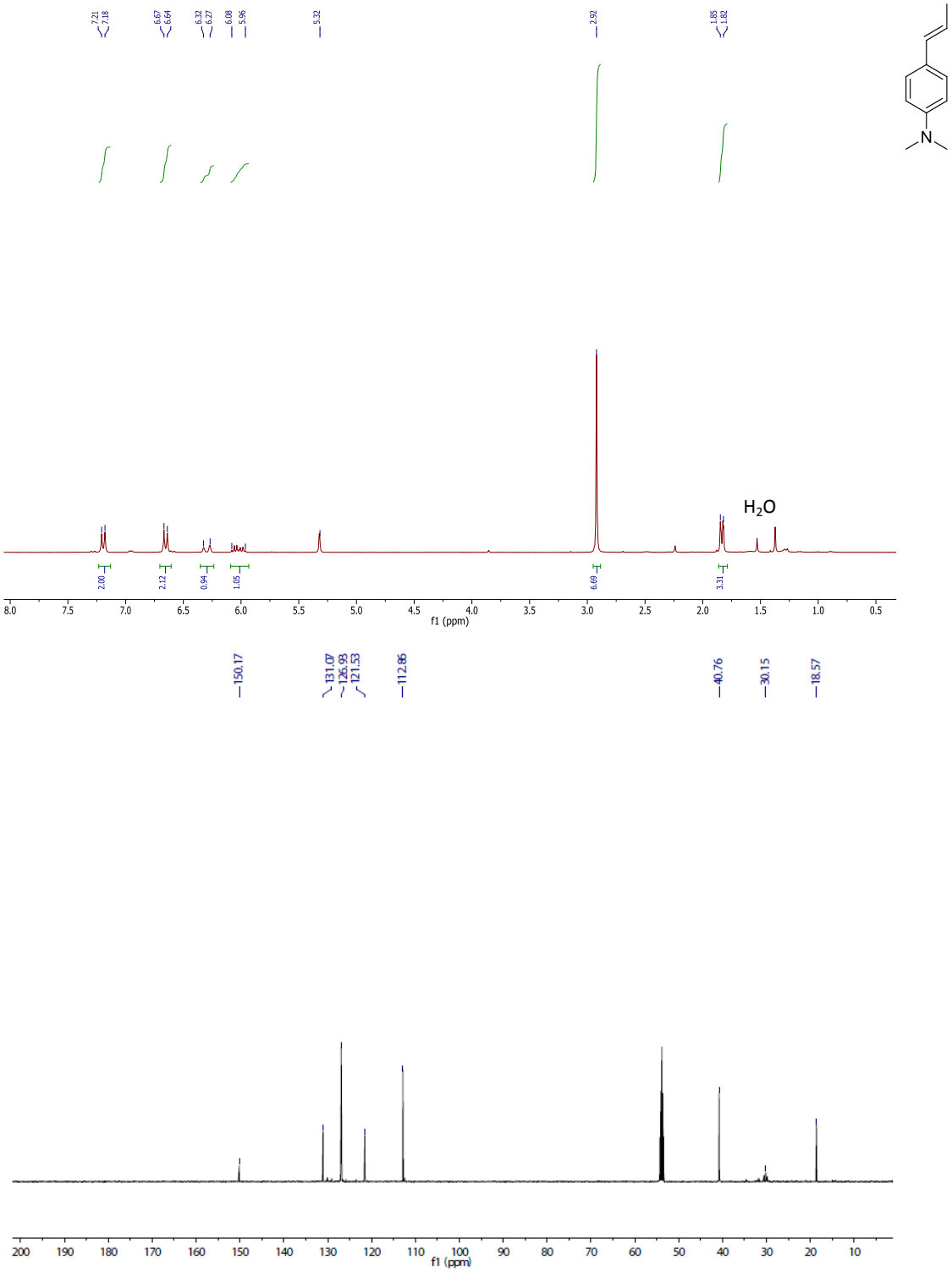

^{1}H NMR (500 MHz, CD_2Cl_2) and $^{13}C\{^{1}H\}$ NMR (125 MHz, CD_2Cl_2) of 5-(4-(dimethylamino)phenyl)-3H-1,2-dithiole-3-thione (ADT-NMe_2)

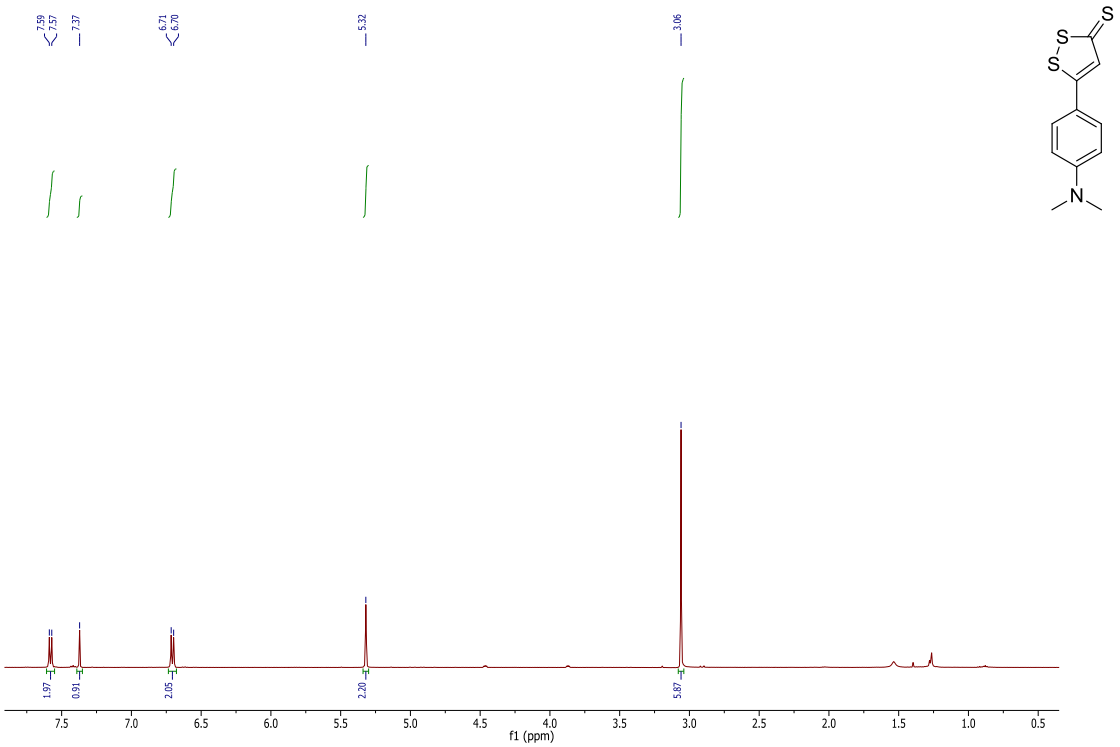

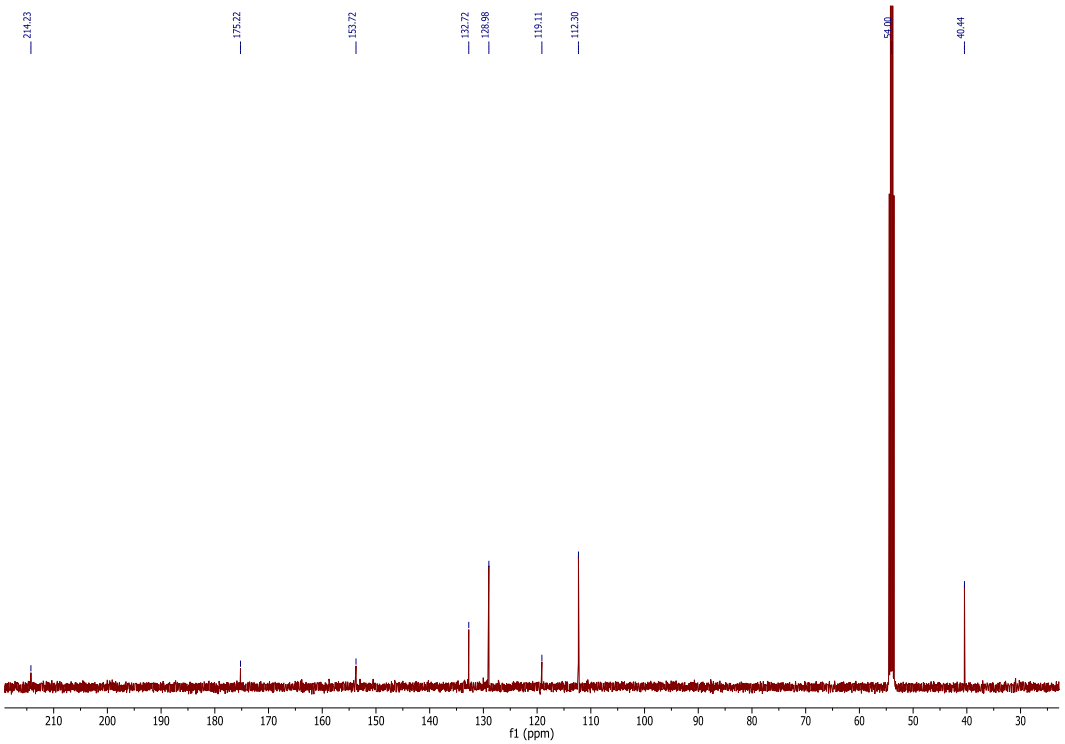

^{1}H NMR (500 MHz, CD_2Cl_2) and $^{13}C\{^{1}H\}$ NMR (125 MHz, CD_2Cl_2) of 4-(3-thioxo-3H-1,2-dithiol-5-yl)phenyl acetate (ADT-OAc)

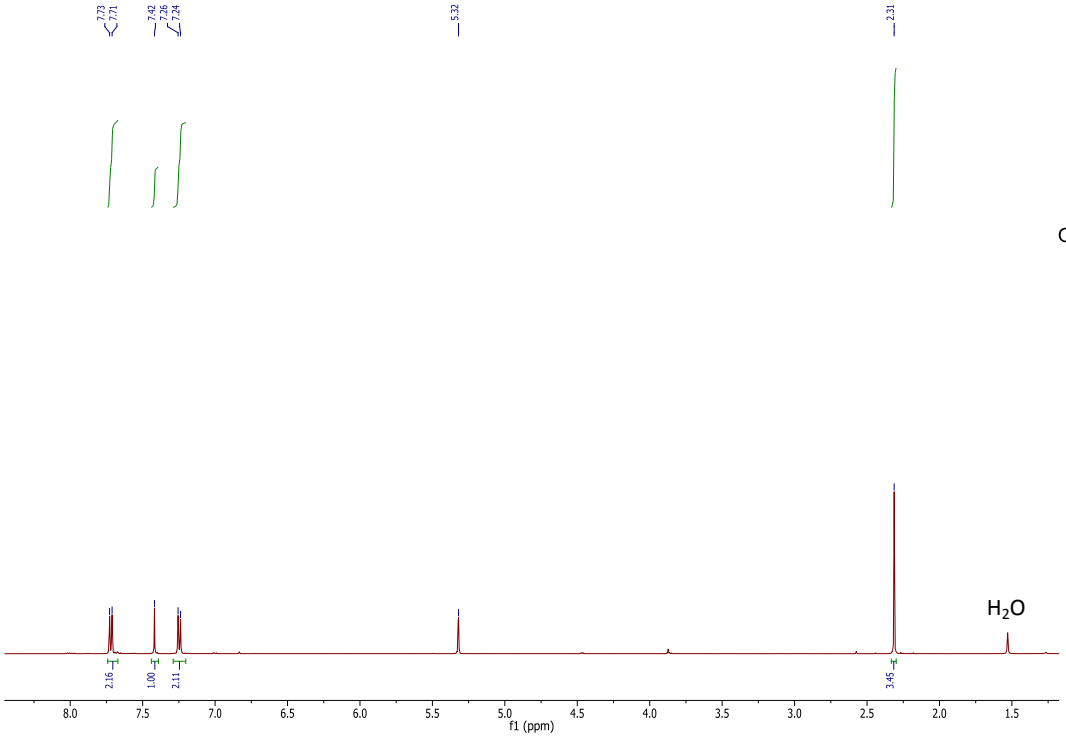

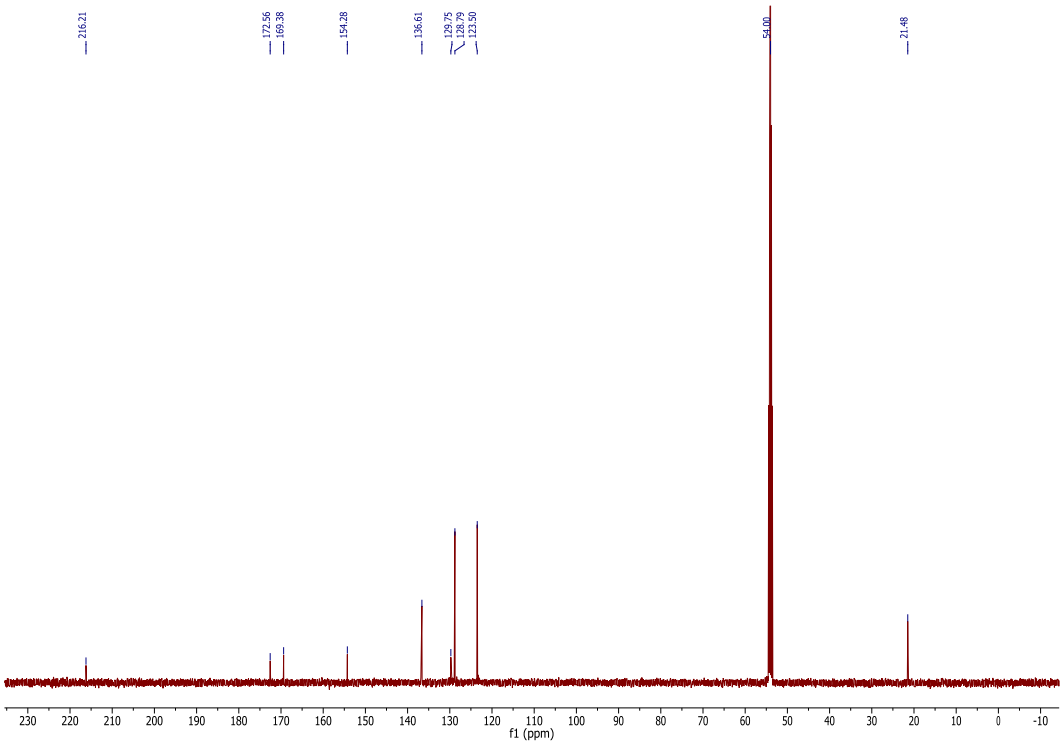

^{1}H NMR (500 MHz, $(CD_3)_2CO$) and $^{13}C\{^{1}H\}$ NMR (125 MHz, $(CD_3)_2CO$) of N-(4-(3-thioxo-3H-1,2-dithiol-5-yl)phenyl)acetamide (ADT-NAc)

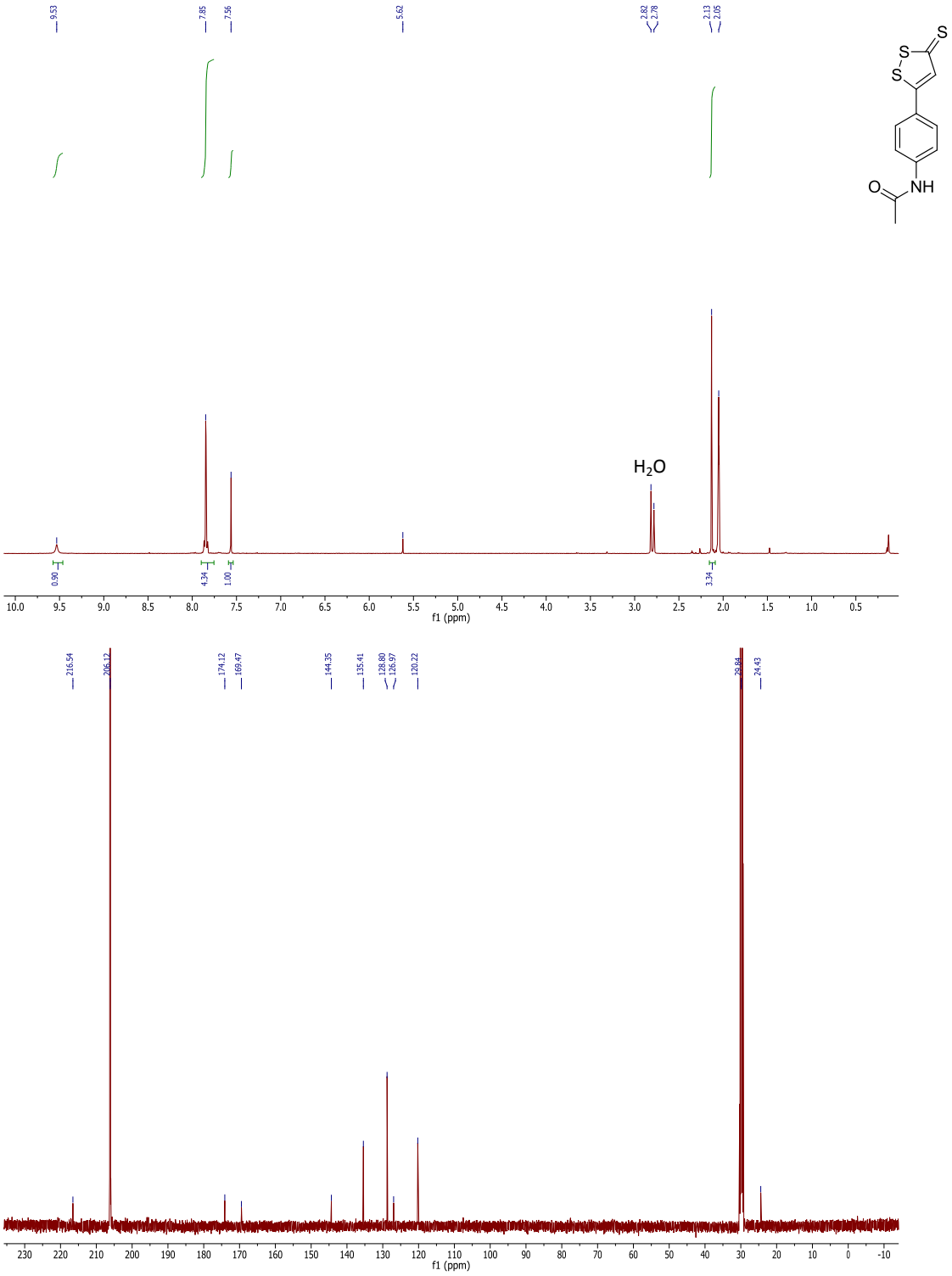

^{1}H NMR (500 MHz, CD_2Cl_2) and $^{13}C\{^{1}H\}$ NMR (125 MHz, CD_2Cl_2) of (S)-4-(3-thioxo-3H-1,2-dithiol-5-yl)phenyl 2-(6-methoxynaphthalen-2-yl)propanoate (ADT-ORox)

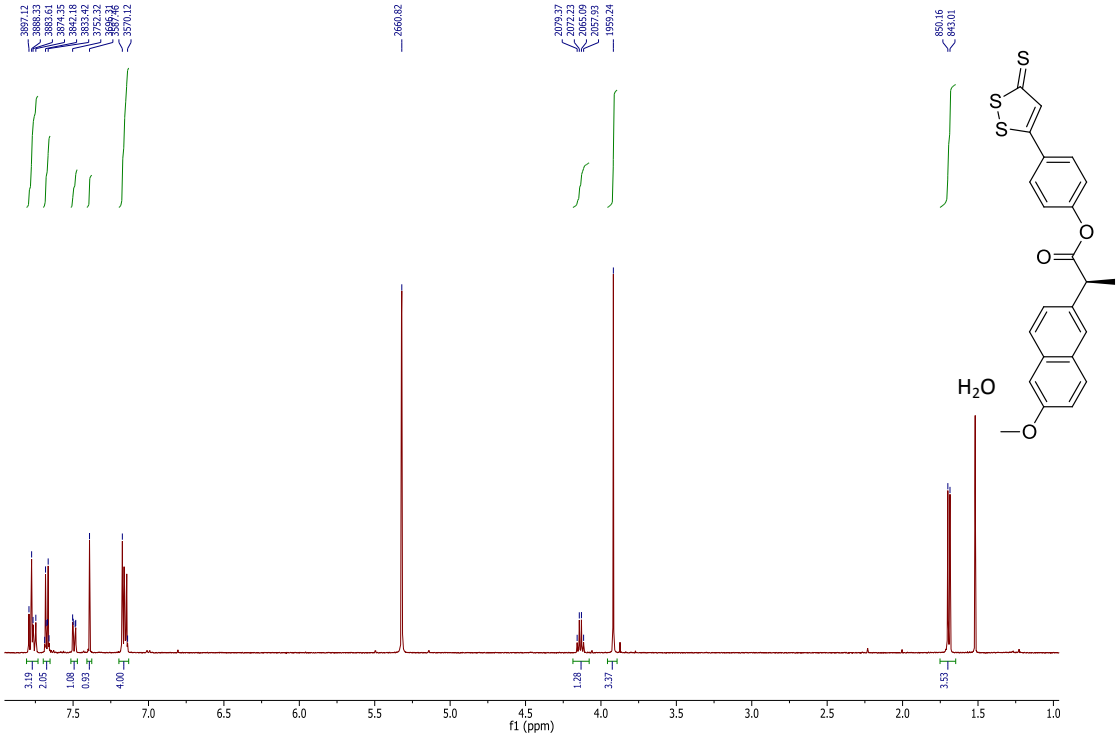

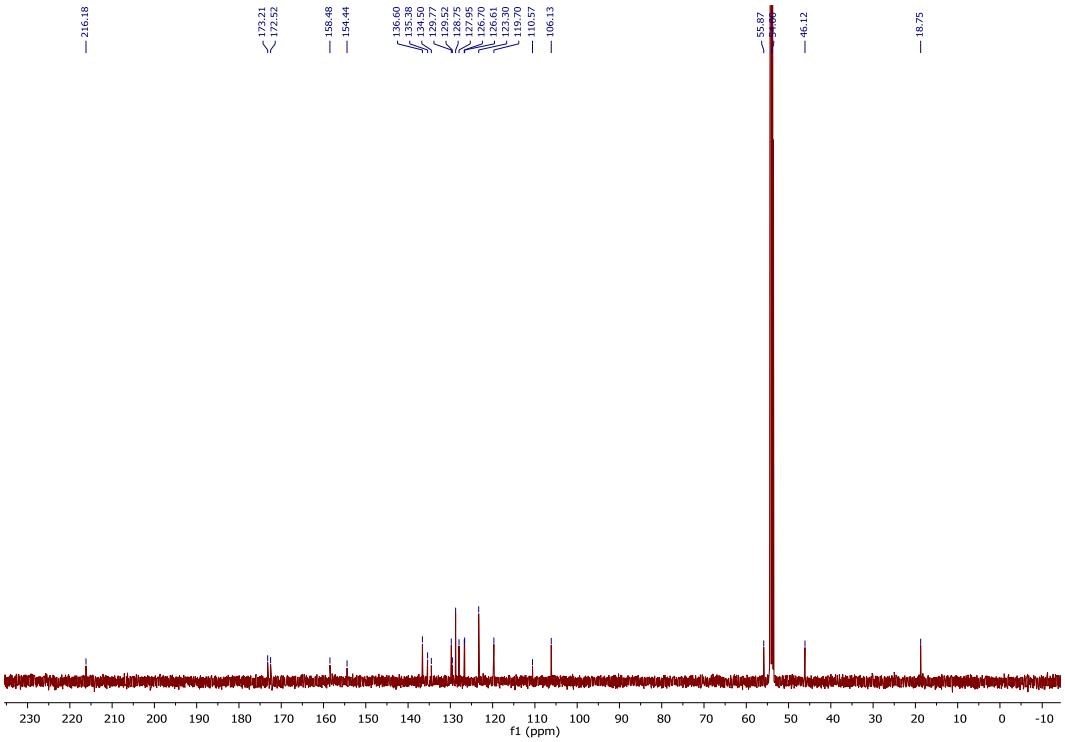

^{1}H NMR (500 MHz, CD_2Cl_2) and $^{13}C\{^{1}H\}$ NMR (125 MHz, CD_2Cl_2) of 4-(3-thioxo-3H-1,2-dithiol-5-yl)phenyl 2-propylpentanoate (ADT-OVal)

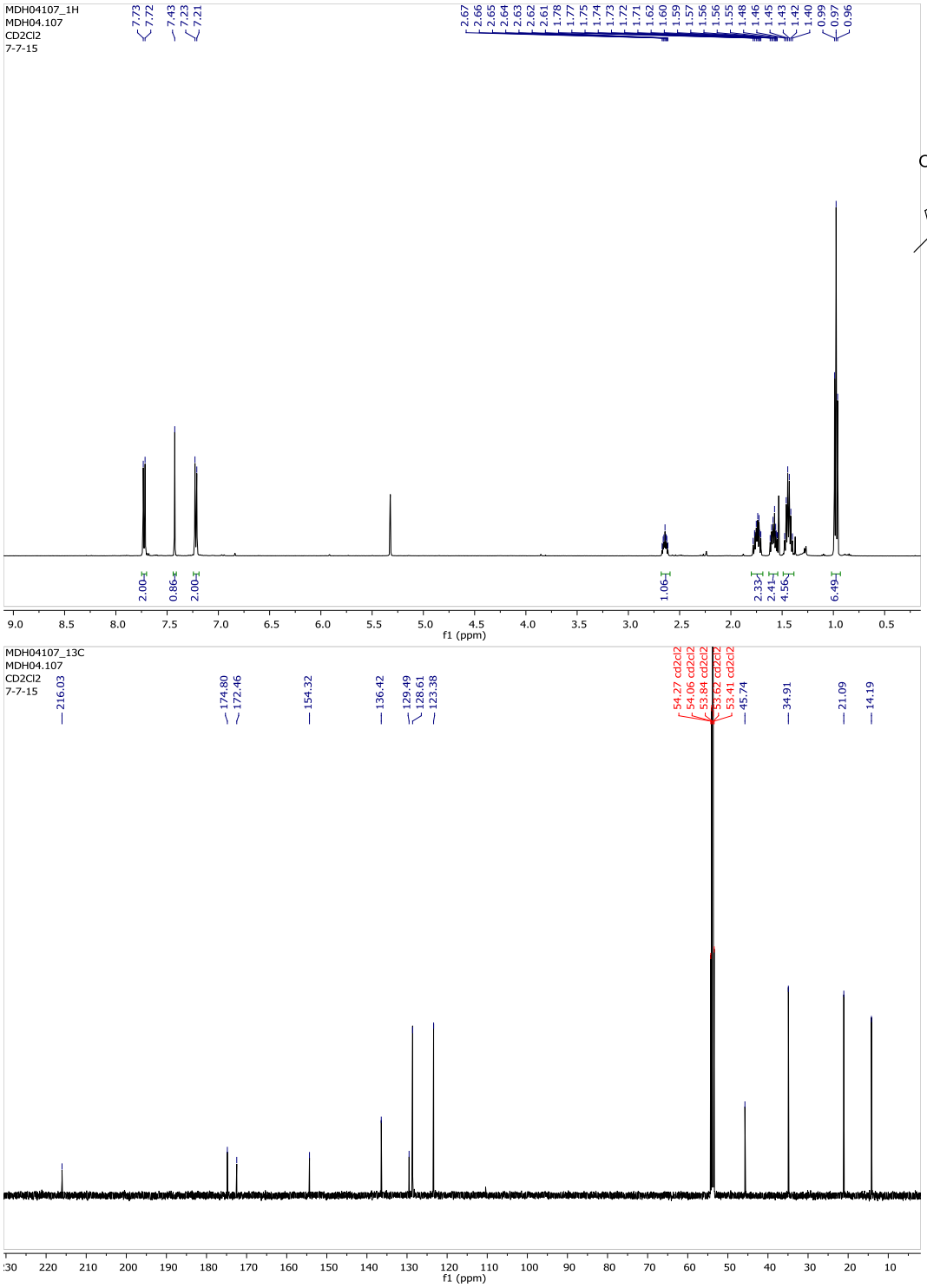

^{1}H NMR (500 MHz, CD_2Cl_2) and $^{13}C\{^{1}H\}$ NMR (125 MHz, CD_2Cl_2) of (S)-2-(6-methoxynaphthalen-2-yl)-N-(4-(3-thioxo-3H-1,2-dithiol-5-yl)phenyl)propanamide (ADT-NRox)

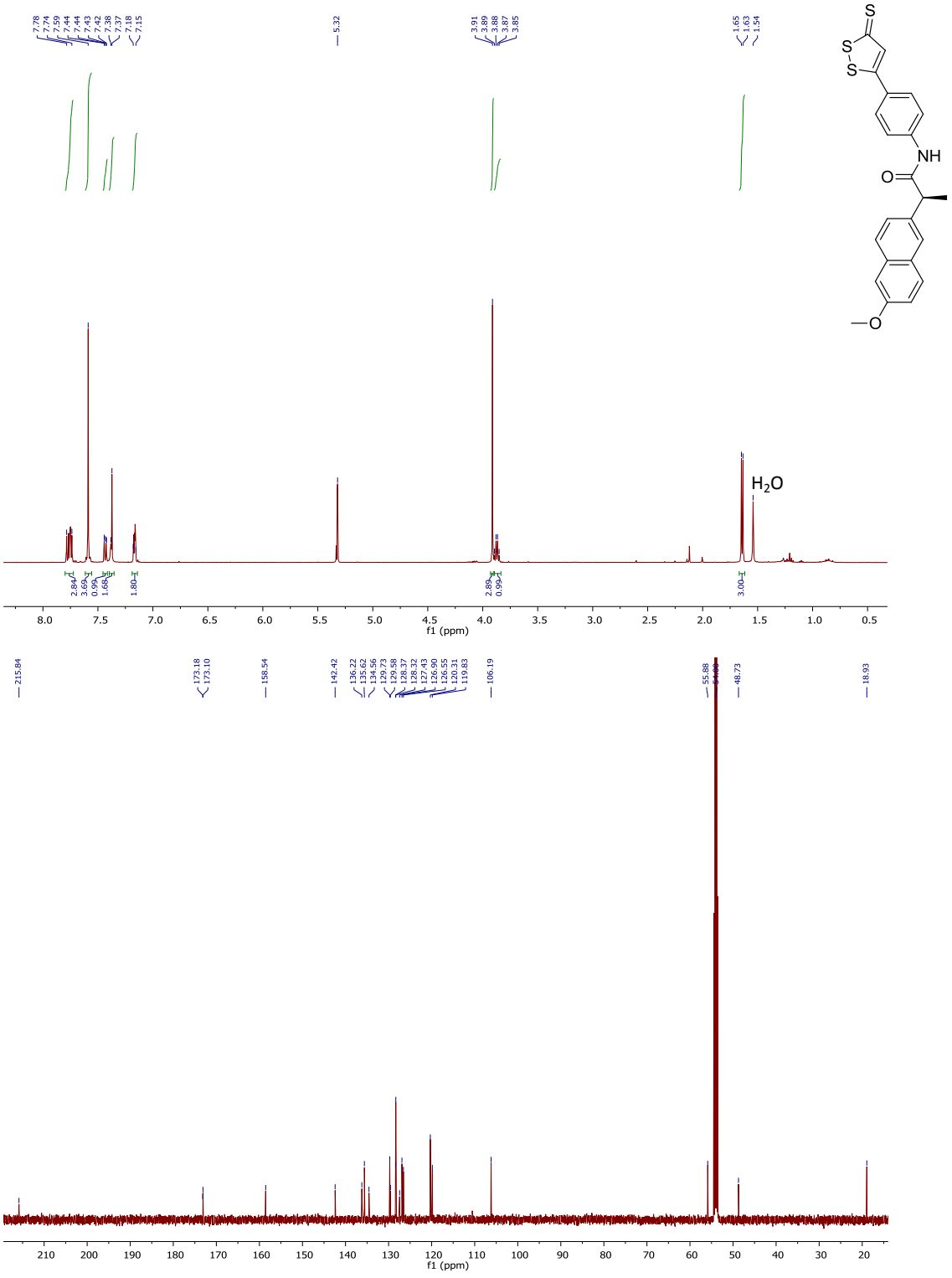

^{1}H NMR (500 MHz, CD_2Cl_2) and $^{13}C\{^{1}H\}$ NMR (125 MHz, CD_2Cl_2) of 2-propyl-N-(4-(3-thioxo-3H-1,2-dithiol-5-yl)phenyl)pentanamide (ADT-NVal)

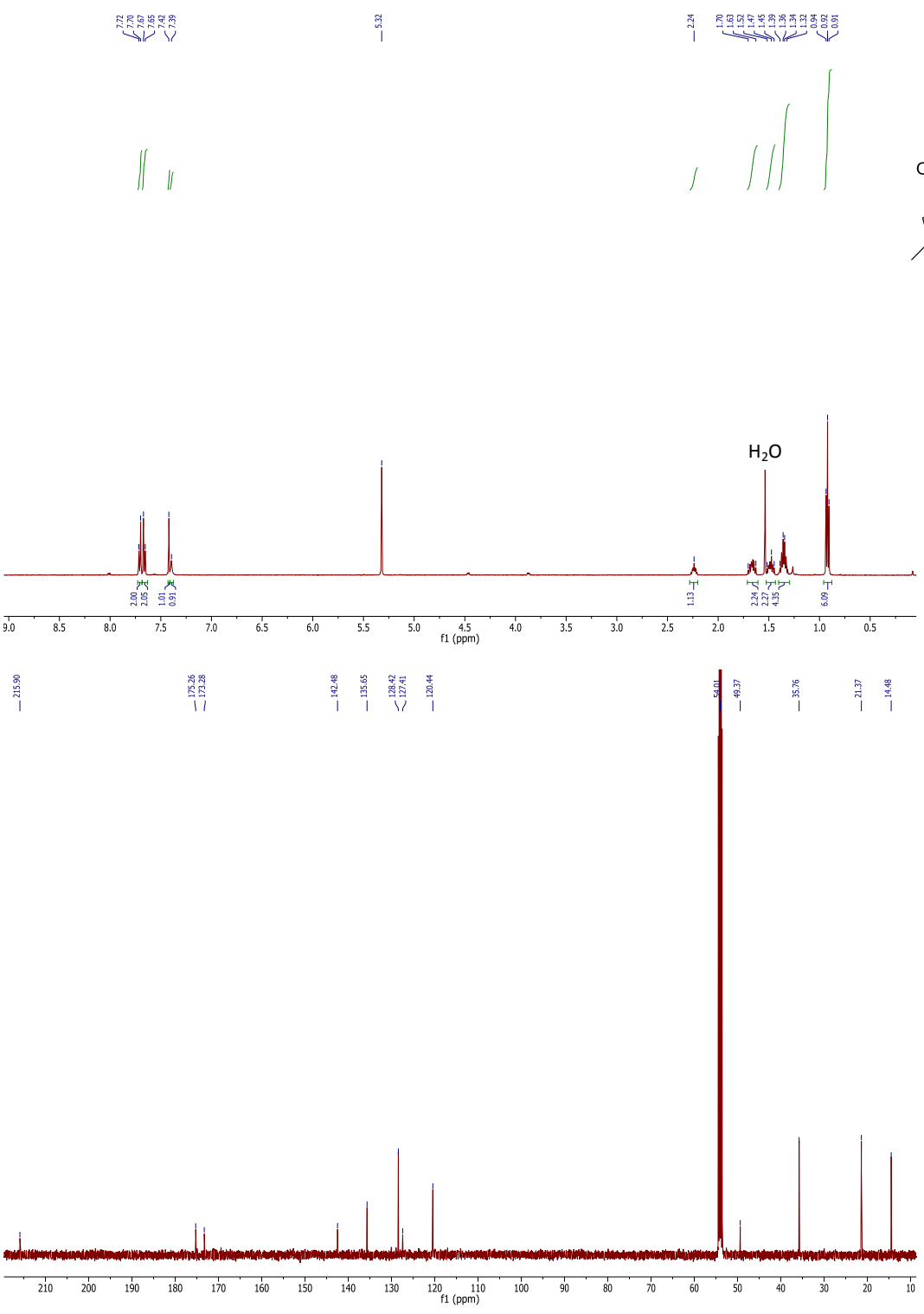

APPENDIX D

CHAPTER V SUPPLEMENTARY INFORMATION AND SPECTRA

Supplementary Figures

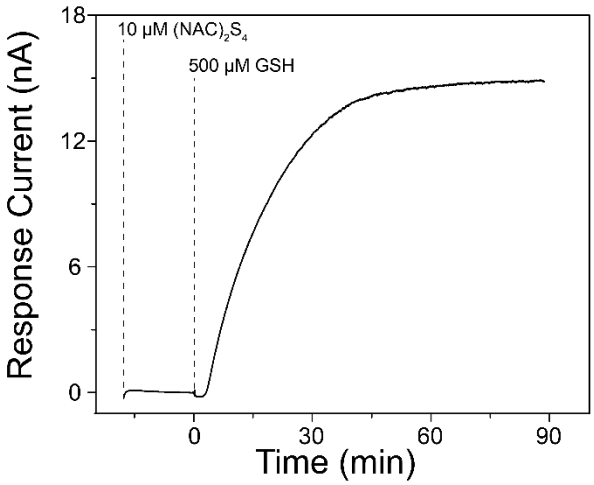

Figure D.1. Aqueous stability and thiol dependent H_2S release from $(NAC)_2S_4$. Electrode signal was allowed to equilibrate for 15 minutes after injection of $(NAC)_2S_4$ (10 μM) into PBS buffer (pH 7.4, 1 mM CTAB) while no H_2S was observed. Immediately after GSH injection (500 μM), H_2S release was observed from tetrasulfide.

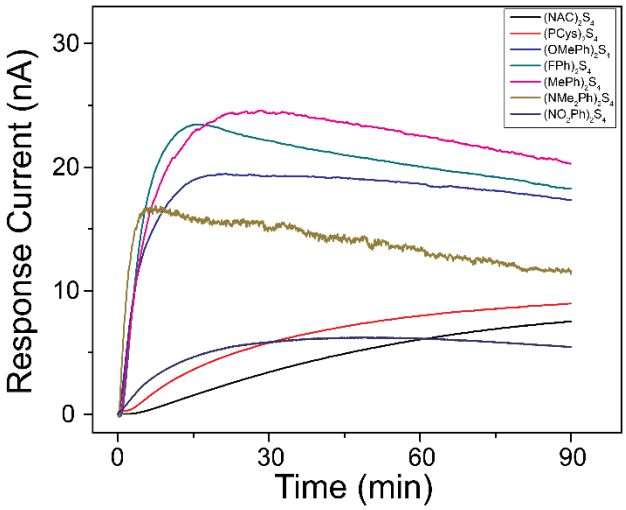

Figure D.2. H_2S release rates of tetrasulfide derivatives. Alkyl tetrasulfides $(NAC)_2S_4$, $(PCys)_2S_4$ and $_p$-functionalized aryl tetrasulfides containing –OMe, –F, –Me, $–NMe_2$, and $–NO_2$ substituents (10 µM) were treated with GSH (100 µM) in PBS buffer (pH 7.4, 1 mM CTAB), and the H_2S release was observed over 90 minutes.

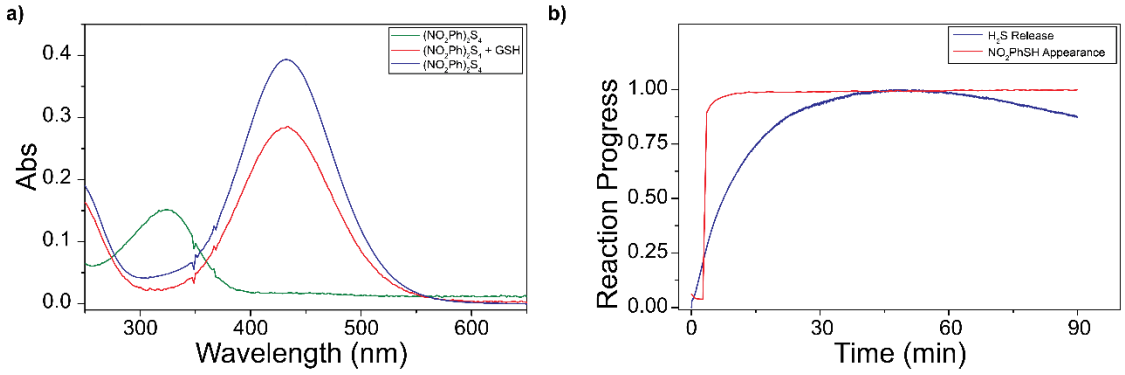

Figure D.3. Conversion of $(NO_2Ph)_2S_4$, 7, to *p*-nitrothiophenol after reaction with GSH. a) UV-vis spectra of $(NO_2Ph)_2S_4$ (10 µM) before (green) and after (red) treatment with GSH (100 µM) in PBS buffer (pH 7.4, 1 mM CTAB) overlaid with the UV-vis spectrum of *p*-nitrothiophenol (20 µM, blue), b) Normalized appearance of *p*-nitrothiophenol absorbance at 431 nm (red) and electrode signal for H_2S release (blue).

NMR Spectra

^{1}H NMR (500 MHz, DMSO) and ^{13}C{^{1}H} NMR (125 MHz, DMSO) of 3,3'-tetrasulfanediylbis(2-acetamidopropanoic acid) ($(NAC)_2S_4$, 1)

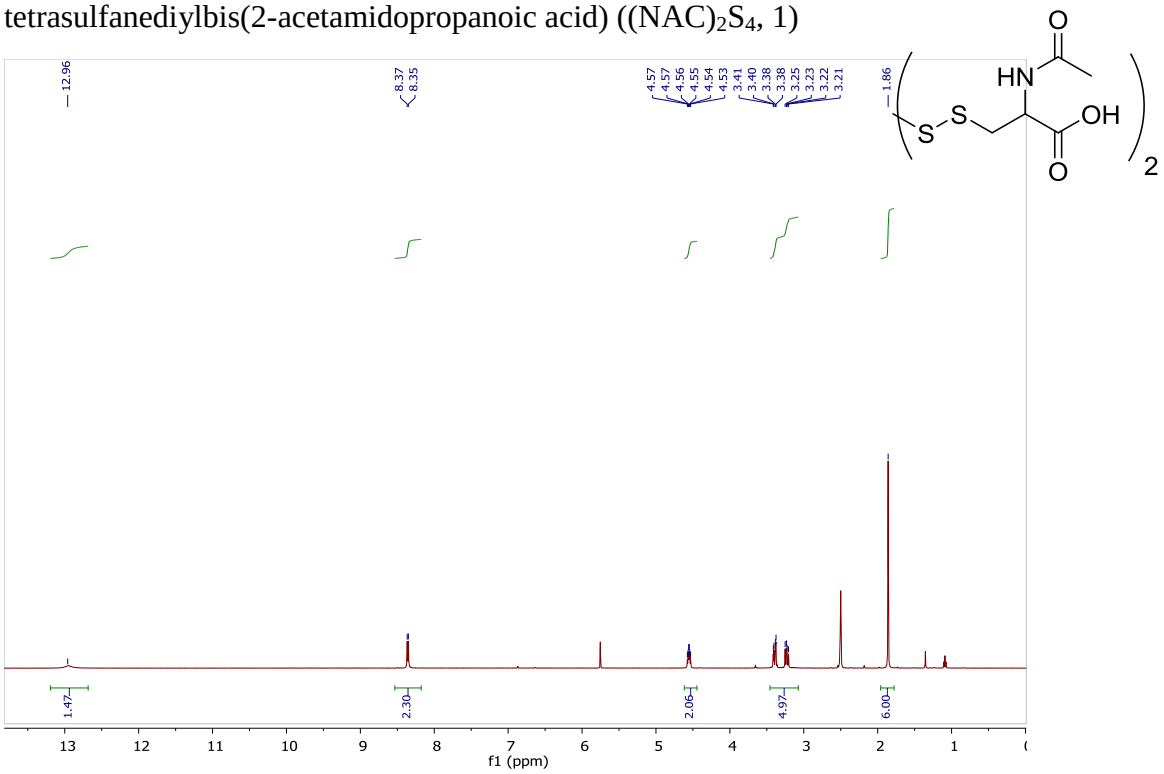

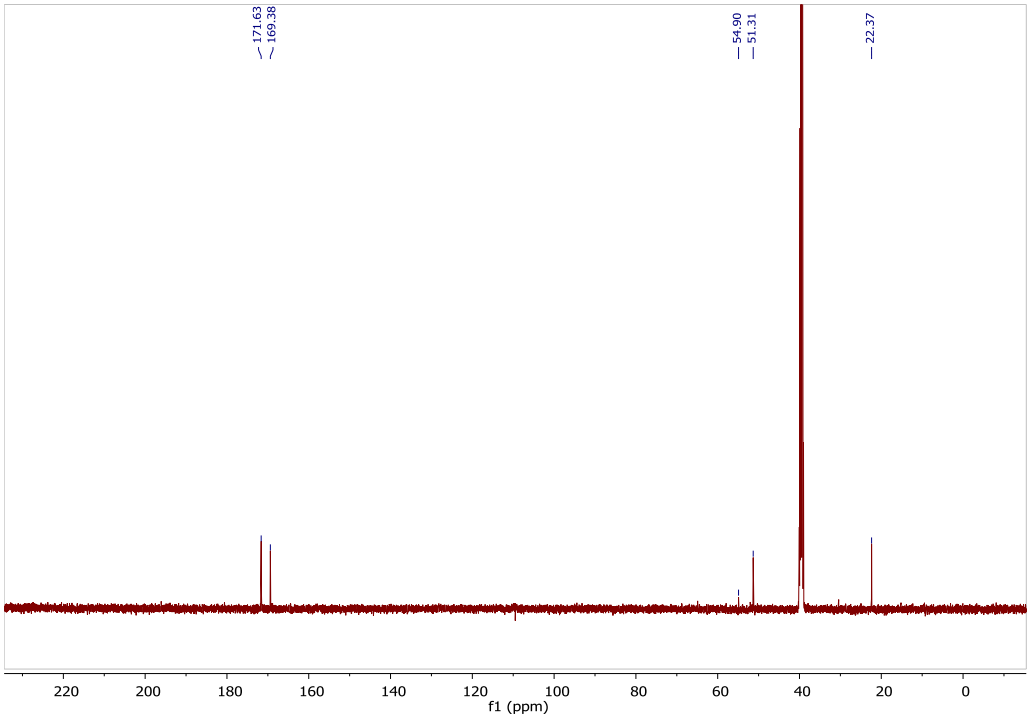

^{1}H NMR (500 MHz, DMSO) and ^{13}C{^{1}H} NMR (125 MHz, DMSO) of Dimethyl 3,3'-tetrasulfanediylbis(2-acetamidopropanoate) ((PCys)$_2$S$_4$, 2)

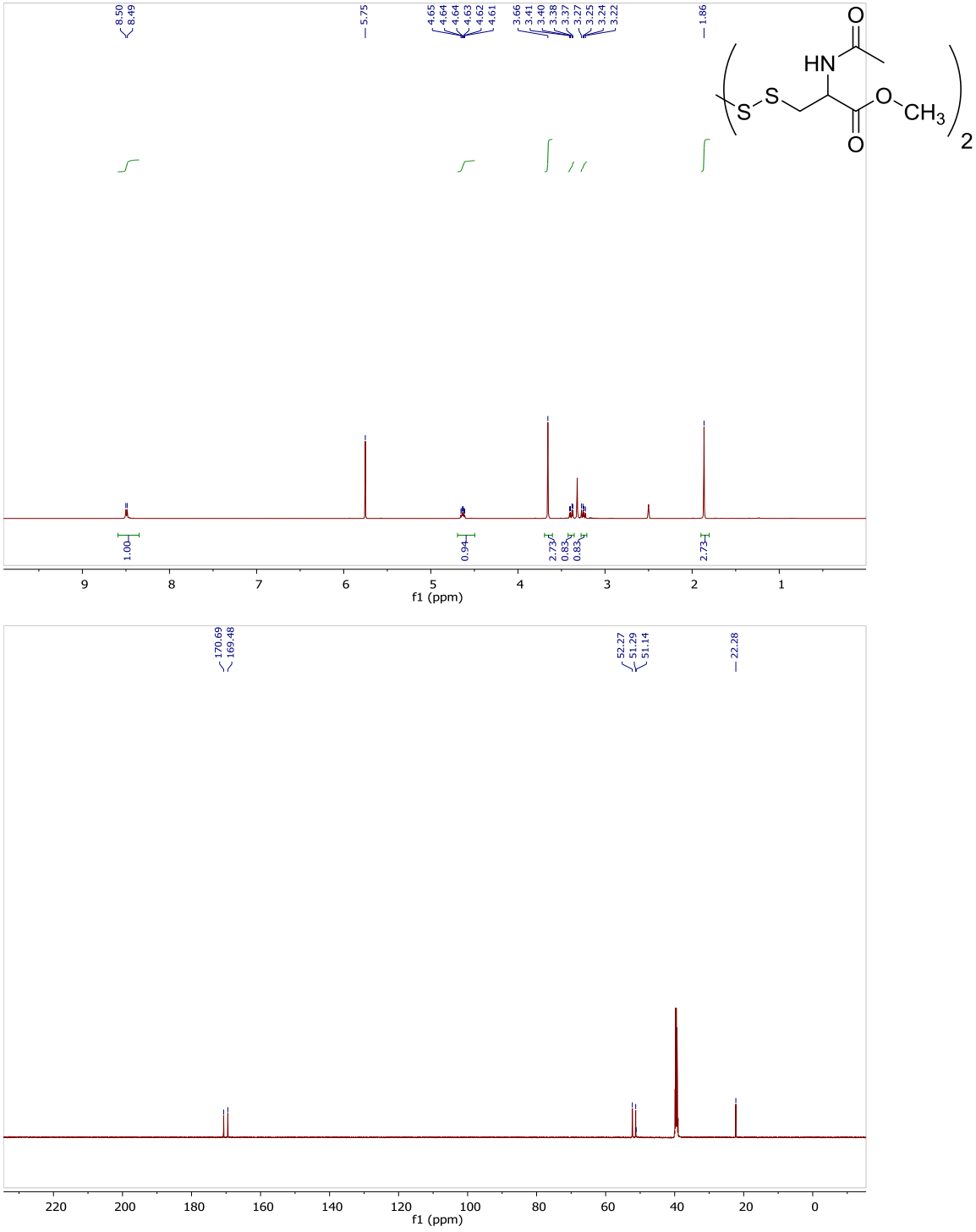

^{1}H NMR (500 MHz, $CDCl_3$) and $^{13}C\{^{1}H\}$ NMR (125 MHz, $CDCl_3$) of 4,4'-Tetrasulfanediylbis(N,N-dimethylaniline) (3)

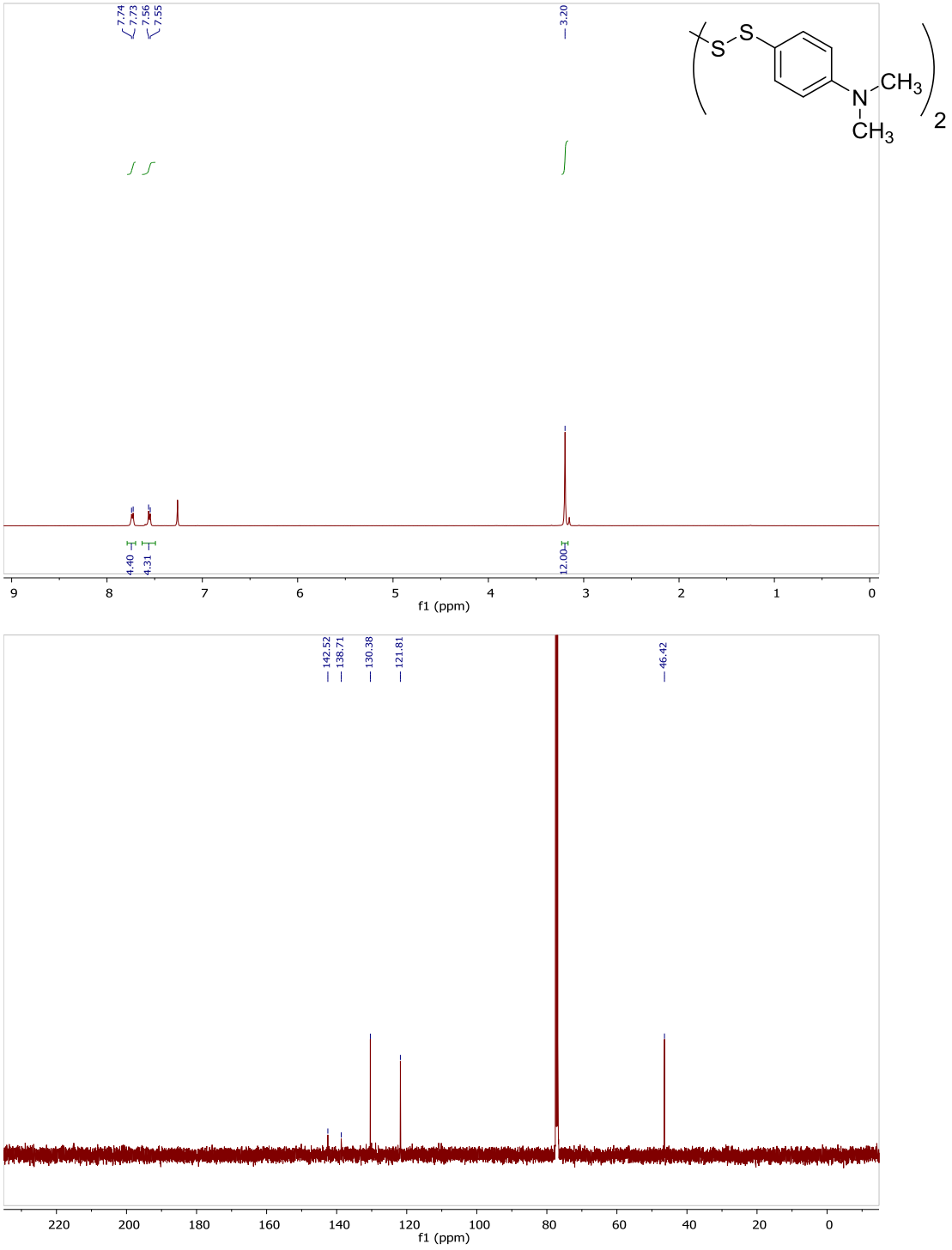

^{1}H NMR (500 MHz, $CDCl_3$) of 1,4-Bis(4-methoxyphenyl)tetrasulfane (4)

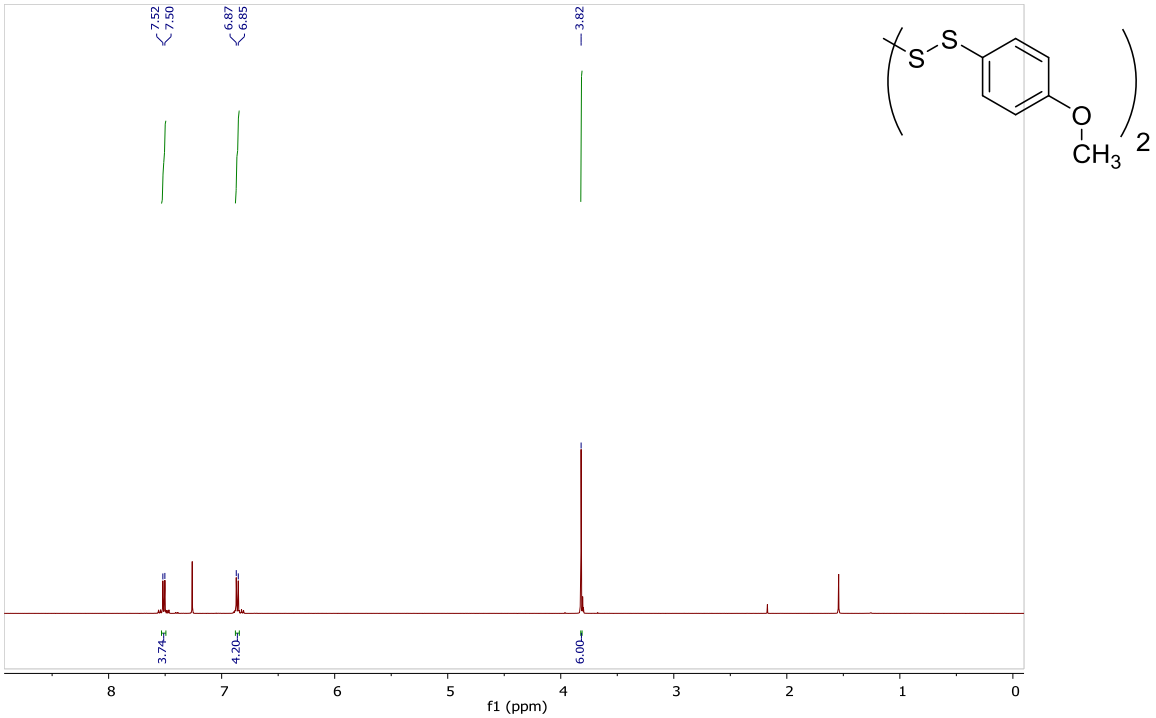

^{1}H NMR (500 MHz, $CDCl_3$) and $^{13}C\{^{1}H\}$ NMR (125 MHz, $CDCl_3$) of 1,4-Di-p-tolyltetrasulfane (5)

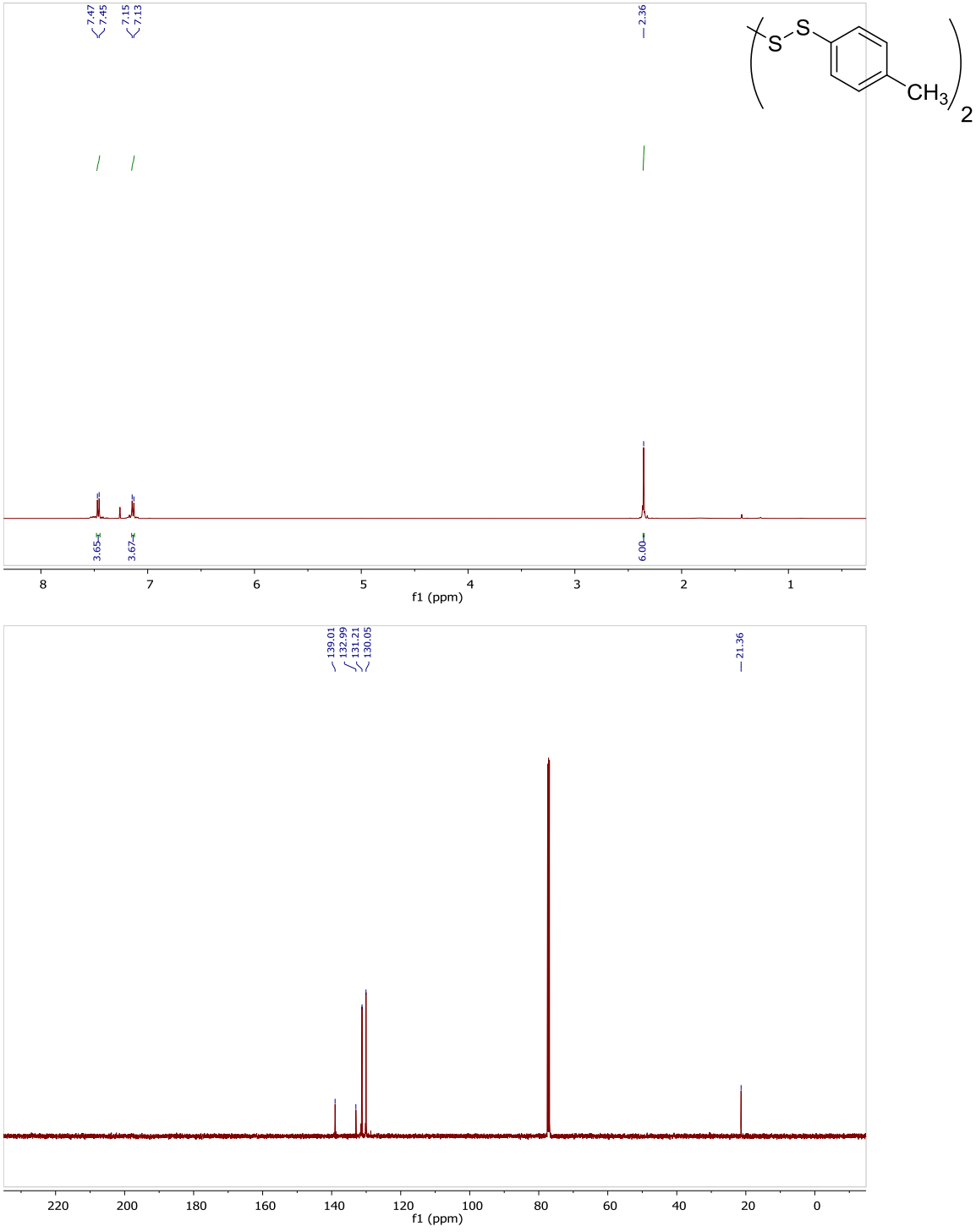

^{1}H NMR (500 MHz, $CDCl_3$) of 1,4-Bis(4-fluorophenyl)tetrasulfane (6)

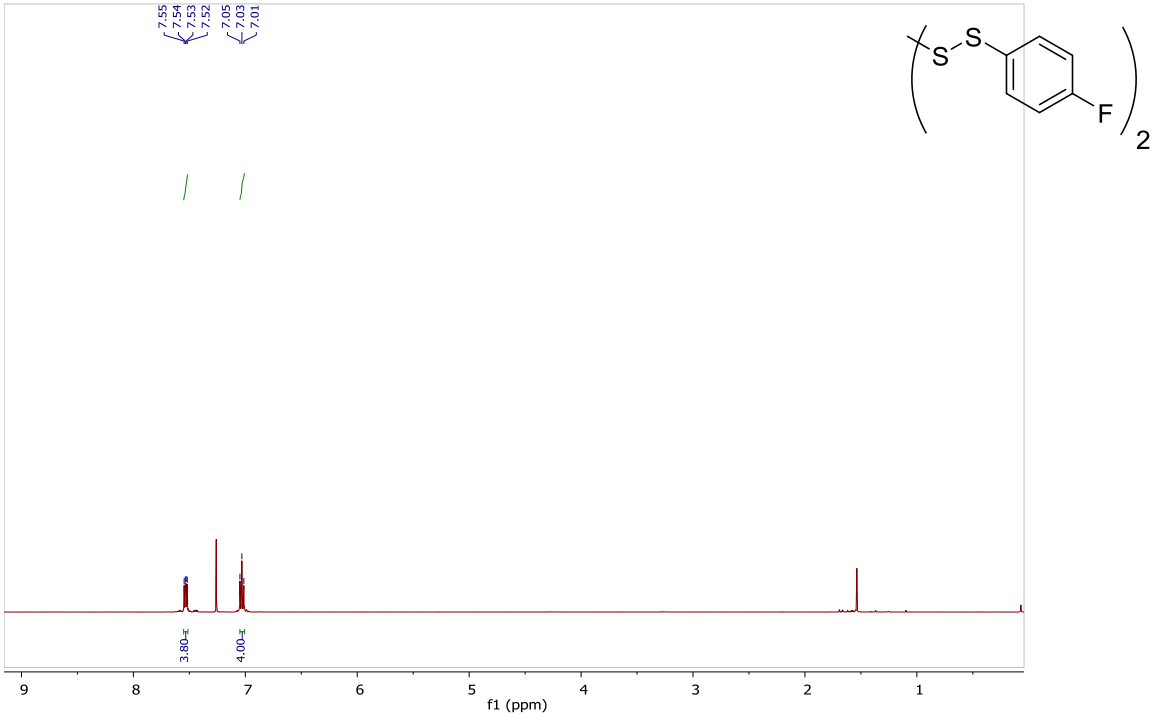

^{1}H NMR (500 MHz, $CDCl_3$) and $^{13}C\{^{1}H\}$ NMR (125 MHz, $CDCl_3$) of 1,4-Bis(4-nitrophenyl)tetrasulfane (7)

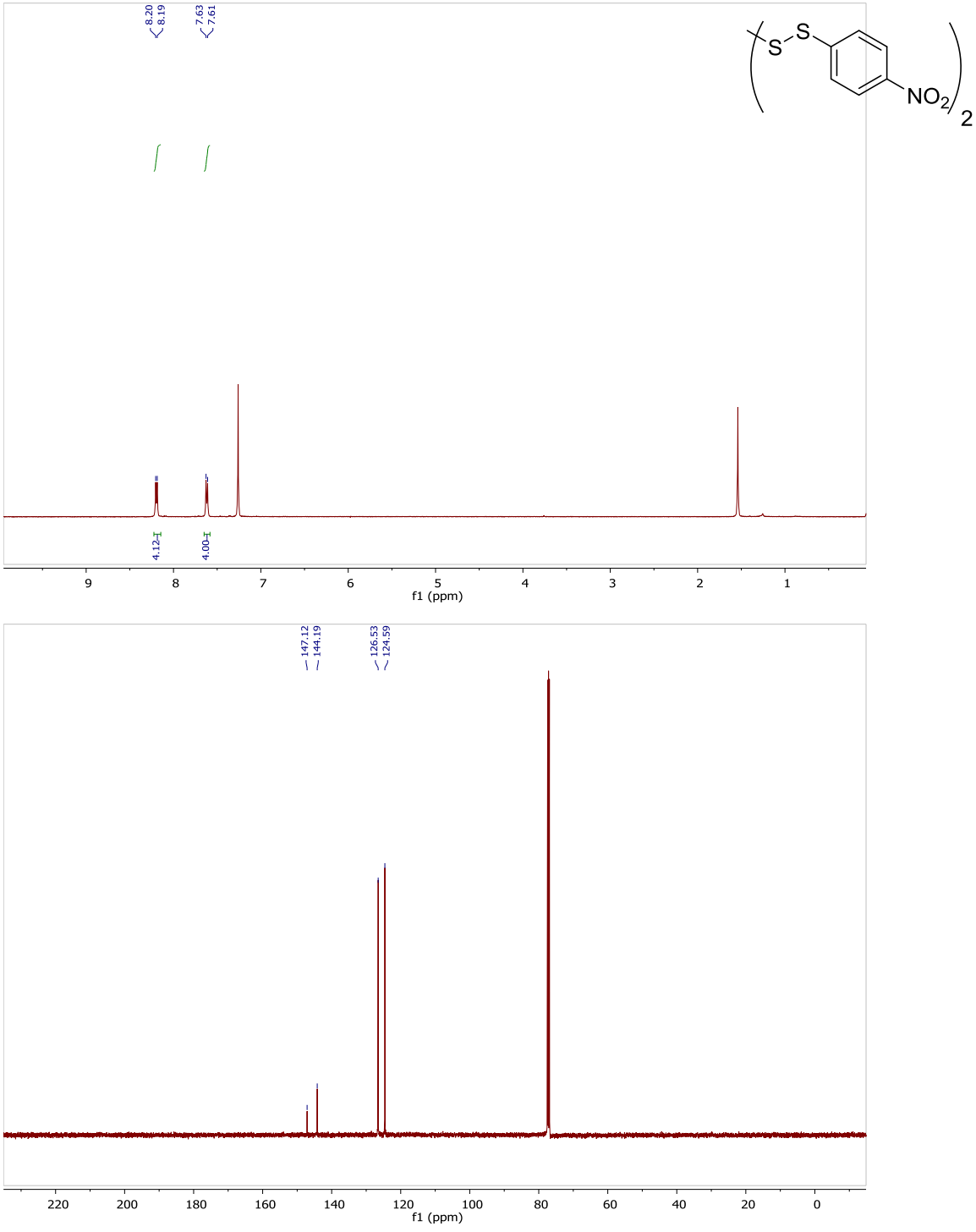

REFERENCES CITED

(1) Abe, K.; Kimura, H. *J. Neurosci.* **1996**, *16*, 1066-1071.
(2) Wang, R. *Antioxid. Redox. Sign.* **2003**, *5*, 493-501.
(3) Kimura, H.; Nagai, Y.; Umemura, K.; Kimura, Y. *Antioxid. Redox. Sign.* **2005**, *7*, 795-803.
(4) Wang, R. *Physiol. Rev.* **2012**, *92*, 791-896.
(5) Braunstein, A. E.; Goryachenkova, E. V.; Lac, N. D. *B.B.A.-Enzym.* **1969**, *171*, 366-368.
(6) Stipanuk, M. H.; Beck, P. W. *Biochem. J.* **1982**, *206*, 267-277.
(7) Shibuya, N.; Tanaka, M.; Yoshida, M.; Ogasawara, Y.; Togawa, T.; Ishii, K.; Kimura, H. *Antioxid. Redox. Sign.* **2009**, *11*, 703-714.
(8) Siebert, N.; Cantre, D.; Eipel, C.; Vollmar, B. *Am. J. Physiol. Gastrointest. Liver Physiol.* **2008**, *295*, G1266-1273.
(9) Teague, B.; Asiedu, S.; Moore, P. K. *Br. J. Pharmacol.* **2002**, *137*, 139-145.
(10) Yang, G.; Wu, L.; Wang, R. *FASEB J.* **2006**, *20*, 553-555.
(11) Yang, G.; Sun, X.; Wang, R. *FASEB J.* **2004**, *18*, 1782-1784.
(12) Whiteman, M.; Winyard, P. G. *Expert Rev. Clin. Pharmacol.* **2011**, *4*, 13-32.
(13) Li, L.; Bhatia, M.; Moore, P. K. *Curr. Opin. Pharmacol.* **2006**, *6*, 125-129.
(14) Wallace, J. L.; Ferraz, J. G. P.; Muscara, M. N. *Antioxid. Redox. Sign.* **2012**, *17*, 58-67.
(15) Wallace, J. L.; Blackler, R. W.; Chan, M. V.; Da Silva, G. J.; Elsheikh, W.; Flannigan, K. L.; Gamaniek, I.; Manko, A.; Wang, L.; Motta, J. P.; Buret, A. G. *Antioxid. Redox. Sign.* **2015**, *22*, 398-410.
(16) Kimura, H. *Mol. Neurobiol.* **2002**, *26*, 13-19.
(17) Wei, H.-J.; Li, X.; Tang, X.-Q. *J. Clin. Neurosci.* **2014**, *21*, 1665-1669.
(18) Xue, X.; Bian, J.-S. In *Method. Enzymol.*; Enrique, C., Lester, P., Eds.; Academic Press: 2015; Vol. Volume 554, p 169-186.
(19) Ichinohe, A.; Kanaumi, T.; Takashima, S.; Enokido, Y.; Nagai, Y.; Kimura, H. *Biochem. Bioph. Res. Co.* **2005**, *338*, 1547-1550.
(20) Cooper, C. E.; Brown, G. C. *J. Bioenerg. Biomembr.* **2008**, *40*, 533-539.
(21) Kabil, O.; Banerjee, R. *J. Biol. Chem.* **2010**, *285*, 21903-21907.
(22) Fogo, J. K.; Popowsky, M. *Anal. Chem.* **1949**, *21*, 732-734.
(23) Shen, X.; Pattillo, C. B.; Pardue, S.; Bir, S. C.; Wang, R.; Kevil, C. G. *Free Radic. Biol. Med.* **2011**, *50*, 1021-1031.
(24) Shen, X.; Peter, E. A.; Bir, S.; Wang, R.; Kevil, C. G. *Free Radic. Biol. Med.* **2012**, *52*, 2276-2283.
(25) Wardencki, W. *J. Chromatogr. A* **1998**, *793*, 1-19.
(26) Doeller, J. E.; Isbell, T. S.; Benavides, G.; Koenitzer, J.; Patel, H.; Patel, R. P.; Lancaster Jr, J. R.; Darley-Usmar, V. M.; Kraus, D. W. *Anal. Biochem.* **2005**, *341*, 40-51.
(27) García-Calzada, M.; Marbán, G.; Fuertes, A. B. *Anal. Chim. Acta* **1999**, *380*, 39-45.
(28) Xuan, W.; Sheng, C.; Cao, Y.; He, W.; Wang, W. *Angew. Chem. Int. Ed.* **2012**, *51*, 2282-2284.

(29) Michael, D. P.; Bailey, T. S.; Matthew, D. H.; Leticia, A. M. In *Biochalcogen Chemistry: The Biological Chemistry of Sulfur, Selenium, and Tellurium*; American Chemical Society: 2013; Vol. 1152, p 15-32.
(30) Peng, H.; Chen, W.; Burroughs, S.; Wang, B. *Curr. Org. Chem.* **2013**, *17*, 641-653.
(31) Kumar, N.; Bhalla, V.; Kumar, M. *Coordin. Chem. Rev.* **2013**, *257*, 2335-2347.
(32) Duan, C. X.; Liu, Y. G. *Curr. Med. Chem.* **2013**, *20*, 2929-2937.
(33) Lippert, A. R. *J. Inorg.Biochem.* **2014**, *133*, 136-142.
(34) Yu, F.; Han, X.; Chen, L. *Chem. Commun.* **2014**, *50*, 12234-12249.
(35) Wang, K.; Peng, H.; Wang, B. *J. Cell. Biochem.* **2014**, *115*, 1007-1022.
(36) Lin, V. S.; Chen, W.; Xian, M.; Chang, C. J. *Chem. Soc. Rev.* **2015**, *44*, 4596-4618.
(37) Shimamoto, K.; Hanaoka, K. *Nitric Oxide* **2015**, *46*, 72-79.
(38) Guo, Z.; Chen, G.; Zeng, G.; Li, Z.; Chen, A.; Wang, J.; Jiang, L. *Analyst* **2015**, *140*, 1772-1786.
(39) Feng, W.; Dymock, B. W. *Handb. Exp. Pharmacol.* **2015**, *230*, 291-323.
(40) Olson, K. R. *Am. J. Physiol. Regul. Integr. Comp. Physiol.* **2011**, *301*, R297-312.
(41) Predmore, B. L.; Lefer, D. J.; Gojon, G. *Antioxid. Redox. Sign.* **2012**, *17*, 119-140.
(42) Song, Z. J.; Ng, M. Y.; Lee, Z.-W.; Dai, W.; Hagen, T.; Moore, P. K.; Huang, D.; Deng, L.-W.; Tan, C.-H. *MedChemComm.* **2014**, *5*, 557-570.
(43) Zhao, Y.; Biggs, T. D.; Xian, M. *Chem. Commun.* **2014**, *50*, 11788-11805.
(44) Giustarini, D.; Del Soldato, P.; Sparatore, A.; Rossi, R. *Free Radic. Biol. Med.* **2010**, *48*, 1263-1272.
(45) Wallace, J. L.; Caliendo, G.; Santagada, V.; Cirino, G. *Br. J. Pharmacol.* **2010**, *159*, 1236-1246.
(46) Szabo, C. *Nat. Rev. Drug. Discov.* **2007**, *6*, 917-935.
(47) Whiteman, M.; Perry, A.; Zhou, Z.; Bucci, M.; Papapetropoulos, A.; Cirino, G.; Wood, M. E. *Handb. Exp. Pharmacol.* **2015**, *230*, 337-363.
(48) WANG, R. *FASEB J.* **2002**, *16*, 1792-1798.
(49) Yang, W.; Yang, G.; Jia, X.; Wu, L.; Wang, R. *J. Physiol.* **2005**, *569*, 519-531.
(50) Hegde, A.; Bhatia, M. *Inflamm. Allergy. Drug. Targets.* **2011**, *10*, 118-122.
(51) Wilinski, B.; Wilinski, J.; Somogyi, E.; Piotrowska, J.; Opoka, W. *Pharmacol. Rep.* **2013**, *65*, 737-742.
(52) Mustafa, A. K.; Gadalla, M. M.; Sen, N.; Kim, S.; Mu, W.; Gazi, S. K.; Barrow, R. K.; Yang, G.; Wang, R.; Snyder, S. H. *Sci. Signal.* **2009**, *2*, ra72.
(53) Paul, B. D.; Snyder, S. H. *Nat. Rev. Mol. Cell Biol.* **2012**, *13*, 499-507.
(54) Bailey, T. S.; Zakharov, L. N.; Pluth, M. D. *J. Am. Chem. Soc.* **2014**, *136*, 10573-10576.
(55) Ishigami, M.; Hiraki, K.; Umemura, K.; Ogasawara, Y.; Ishii, K.; Kimura, H. *Antioxid. Redox. Sign.* **2009**, *11*, 205-214.
(56) Lin, V. S.; Chang, C. J. *Curr. Opin. Chem. Biol.* **2012**, *16*, 595-601.
(57) Liu, C.; Pan, J.; Li, S.; Zhao, Y.; Wu, L. Y.; Berkman, C. E.; Whorton, A. R.; Xian, M. *Angew. Chem. Int. Ed.* **2011**, *50*, 10327-10329.
(58) Qian, Y.; Karpus, J.; Kabil, O.; Zhang, S.-Y.; Zhu, H.-L.; Banerjee, R.; Zhao, J.; He, C. *Nat. Commun.* **2011**, *2*, 495.

(59) Liu, C.; Peng, B.; Li, S.; Park, C.-M.; Whorton, A. R.; Xian, M. *Org. Lett.* **2012**, *14*, 2184-2187.
(60) Xu, Z.; Xu, L.; Zhou, J.; Xu, Y.; Zhu, W.; Qian, X. *Chem. Commun.* **2012**, *48*, 10871-10873.
(61) Qian, Y.; Zhang, L.; Ding, S.; Deng, X.; He, C.; Zheng, X. E.; Zhu, H.-L.; Zhao, J. *Chem. Sci.* **2012**, *3*, 2920-2923.
(62) Zhang, J.; Sun, Y.-Q.; Liu, J.; Shi, Y.; Guo, W. *Chem. Commun.* **2013**, *49*, 11305-11307.
(63) Wei, C.; Zhu, Q.; Liu, W.; Chen, W.; Xi, Z.; Yi, L. *Org. Biomol. Chem.* **2014**, *12*, 479-485.
(64) Sasakura, K.; Hanaoka, K.; Shibuya, N.; Mikami, Y.; Kimura, Y.; Komatsu, T.; Ueno, T.; Terai, T.; Kimura, H.; Nagano, T. *J. Am. Chem. Soc.* **2011**, *133*, 18003-18005.
(65) Gu, X.; Liu, C.; Zhu, Y.-C.; Zhu, Y.-Z. *Tetrahedron Lett.* **2011**, *52*, 5000-5003.
(66) Qu, X.; Li, C.; Chen, H.; Mack, J.; Guo, Z.; Shen, Z. *Chem. Commun.* **2013**, *49*, 7510-7512.
(67) Lippert, A. R.; New, E. J.; Chang, C. J. *J. Am. Chem. Soc.* **2011**, *133*, 10078-10080.
(68) Peng, H.; Cheng, Y.; Dai, C.; King, A. L.; Predmore, B. L.; Lefer, D. J.; Wang, B. *Angew. Chem. Int. Ed.* **2011**, *50*, 9672-9675.
(69) Cao, X.; Lin, W.; Zheng, K.; He, L. *Chem. Commun.* **2012**, *48*, 10529-10531.
(70) Chen, B.; Lv, C.; Tang, X. *Anal. Bioanal. Chem.* **2012**, *404*, 1919-1923.
(71) Chen, S.; Chen, Z.-j.; Ren, W.; Ai, H.-w. *J. Am. Chem. Soc.* **2012**, *134*, 9589-9592.
(72) Das, S. K.; Lim, C. S.; Yang, S. Y.; Han, J. H.; Cho, B. R. *Chem. Commun.* **2012**, *48*, 8395-8397.
(73) Hartman, M. C. T.; Dcona, M. M. *Analyst* **2012**, *137*, 4910-4912.
(74) Wang, R.; Yu, F.; Chen, L.; Chen, H.; Wang, L.; Zhang, W. *Chem. Commun.* **2012**, *48*, 11757-11759.
(75) Zheng, K.; Lin, W.; Tan, L. *Org. Biomol. Chem.* **2012**, *10*, 9683-9688.
(76) Bailey, T. S.; Pluth, M. D. *J. Am. Chem. Soc.* **2013**, *135*, 16697-16704.
(77) Chen, B.; Li, W.; Lv, C.; Zhao, M.; Jin, H.; Jin, H.; Du, J.; Zhang, L.; Tang, X. *Analyst* **2013**, *138*, 946-951.
(78) Li, W.; Sun, W.; Yu, X.; Du, L.; Li, M. *J. Fluoresc.* **2013**, *23*, 181-186.
(79) Lin, V. S.; Lippert, A. R.; Chang, C. J. *Proc. Natl. Acad. Sci. U. S. A.* **2013**, *110*, 7131-7135.
(80) Sun, W.; Fan, J.; Hu, C.; Cao, J.; Zhang, H.; Xiong, X.; Wang, J.; Cui, S.; Sun, S.; Peng, X. *Chem. Commun.* **2013**, *49*, 3890-3892.
(81) Zhou, G.; Wang, H.; Ma, Y.; Chen, X. *Tetrahedron* **2013**, *69*, 867-870.
(82) Santos-Figueroa, L. E.; de laTorre, C.; El Sayed, S.; Sancenón, F.; Martínez-Máñez, R.; Costero, A. M.; Gil, S.; Parra, M. *Eur. J. Org. Chem.* **2014**, *2014*, 1848-1854.
(83) Cao, J.; Lopez, R.; Thacker, J. M.; Moon, J. Y.; Jiang, C.; Morris, S. N. S.; Bauer, J. H.; Tao, P.; Mason, R. P.; Lippert, A. R. *Chem. Sci.* **2015**, *6*, 1979-1985.
(84) Wan, Q.; Song, Y.; Li, Z.; Gao, X.; Ma, H. *Chem. Commun.* **2013**, *49*, 502-504.
(85) Dufton, N.; Natividad, J.; Verdu, E. F.; Wallace, J. L. *Sci. Rep.* **2012**, *2*.

(86) Huisken, J.; Stainier, D. Y. *Development* **2009**, *136*, 1963-1975.
(87) Keller, P. J.; Schmidt, A. D.; Wittbrodt, J.; Stelzer, E. H. *Science* **2008**, *322*, 1065-1069.
(88) Huisken, J. *BioEssays* **2012**, *34*, 406-411.
(89) Jemielita, M.; Taormina, M. J.; Delaurier, A.; Kimmel, C. B.; Parthasarathy, R. *J. Biophotonics* **2013**, *6*, 920-928.
(90) Santi, P. A. *J. Histochem. Cytochem.* **2011**, *59*, 129-138.
(91) Grunwald, D. J.; Eisen, J. S. *Nat. Rev. Genet.* **2002**, *3*, 717-724.
(92) Taormina, M. J.; Jemielita, M.; Stephens, W. Z.; Burns, A. R.; Troll, J. V.; Parthasarathy, R.; Guillemin, K. *Biol. Bull.* **2012**, *223*, 7-20.
(93) Jemielita, M.; Taormina, M. J.; Burns, A. R.; Hampton, J. S.; Rolig, A. S.; Guillemin, K.; Parthasarathy, R. *mBio* **2014**, *5*.
(94) Chan, J.; Dodani, S. C.; Chang, C. J. *Nat. Chem.* **2012**, *4*, 973-984.
(95) Whitaker, J. E.; Haugland, R. P.; Ryan, D.; Hewitt, P. C.; Haugland, R. P.; Prendergast, F. G. *Anal. Biochem.* **1992**, *207*, 267-279.
(96) Dickinson, B. C.; Huynh, C.; Chang, C. J. *J. Am. Chem. Soc.* **2010**, *132*, 5906-5915.
(97) Kamiya, M.; Asanuma, D.; Kuranaga, E.; Takeishi, A.; Sakabe, M.; Miura, M.; Nagano, T.; Urano, Y. *J. Am. Chem. Soc.* **2011**, *133*, 12960-12963.
(98) Kawai, K.; Ieda, N.; Aizawa, K.; Suzuki, T.; Miyata, N.; Nakagawa, H. *J. Am. Chem. Soc.* **2013**, *135*, 12690-12696.
(99) Yang, X.-F.; Huang, Q.; Zhong, Y.; Li, Z.; Li, H.; Lowry, M.; Escobedo, J. O.; Strongin, R. M. *Chem. Sci.* **2014**, *5*, 2177-2183.
(100) Peng, T.; Yang, D. *Org. Lett.* **2010**, *12*, 496-499.
(101) Zhu, D.; Xue, L.; Li, G.; Che, Y.; Jiang, H. *Org. Chem. Front.* **2014**, *1*, 501-505.
(102) Montoya, L. A.; Pluth, M. D. *Chem. Commun.* **2012**, *48*, 4767-4769.
(103) Szczesny, B.; Módis, K.; Yanagi, K.; Coletta, C.; Le Trionnaire, S.; Perry, A.; Wood, M. E.; Whiteman, M.; Szabo, C. *Nitric Oxide* **2014**, *41*, 120-130.
(104) Asimakopoulou, A.; Panopoulos, P.; Chasapis, C. T.; Coletta, C.; Zhou, Z.; Cirino, G.; Giannis, A.; Szabo, C.; Spyroulias, G. A.; Papapetropoulos, A. *Br. J. Pharmacol.* **2013**, *169*, 922-932.
(105) Benavides, G. A.; Squadrito, G. L.; Mills, R. W.; Patel, H. D.; Isbell, T. S.; Patel, R. P.; Darley-Usmar, V. M.; Doeller, J. E.; Kraus, D. W. *Proc. Natl. Acad. Sci. U. S. A.* **2007**, *104*, 17977-17982.
(106) Cocchiaro, J. L.; Rawls, J. F. *J. Vis. Exp.* **2013**, e4434.
(107) Mugherli, L.; Burchak, O. N.; Chatelain, F.; Balakirev, M. Y. *Bioorg. Med. Chem. Lett.* **2006**, *16*, 4488-4491.
(108) Ritter, J. M. *Br. J. Clin. Pharmacol.* **2010**, *69*, 573-575.
(109) Jhee, K. H.; Kruger, W. D. *Antioxid. Redox. Sign.* **2005**, *7*, 813-822.
(110) Eto, K.; Asada, T.; Arima, K.; Makifuchi, T.; Kimura, H. *Biochem. Bioph. Res. Co.* **2002**, *293*, 1485-1488.
(111) Singh, S.; Padovani, D.; Leslie, R. A.; Chiku, T.; Banerjee, R. *J. Biol. Chem.* **2009**, *284*, 22457-22466.
(112) Gadalla, M. M.; Snyder, S. H. *J. Neurochem.* **2010**, *113*, 14-26.
(113) Ju, Y.; Zhang, W.; Pei, Y.; Yang, G. *Can. J. Physiol. Pharmacol.* **2013**, *91*, 8-14.
(114) M. F. Choi, M. *Analyst* **1998**, *123*, 1631-1634.

(115) Zhang, D.; Jin, W. *Specrochim. Acta. A.* **2012**, *90*, 35-39.
(116) Hou, F.; Huang, L.; Xi, P.; Cheng, J.; Zhao, X.; Xie, G.; Shi, Y.; Cheng, F.; Yao, X.; Bai, D.; Zeng, Z. *Inorg. chem.* **2012**, *51*, 2454-2460.
(117) Zhu, A.; Luo, Z.; Ding, C.; Li, B.; Zhou, S.; Wang, R.; Tian, Y. *Analyst* **2014**, *139*, 1945-1952.
(118) Yu, F.; Li, P.; Song, P.; Wang, B.; Zhao, J.; Han, K. *Chem. Commun.* **2012**, *48*, 2852-2854.
(119) Liu, J.; Sun, Y.-Q.; Zhang, J.; Yang, T.; Cao, J.; Zhang, L.; Guo, W. *Chem. Eur. J.* **2013**, *19*, 4717-4722.
(120) Bae, S. K.; Heo, C. H.; Choi, D. J.; Sen, D.; Joe, E. H.; Cho, B. R.; Kim, H. M. *J. Am. Chem. Soc.* **2013**, *135*, 9915-9923.
(121) Yu, C.; Li, X.; Zeng, F.; Zheng, F.; Wu, S. *Chem. Commun.* **2013**, *49*, 403-405.
(122) Wu, M.-Y.; Li, K.; Hou, J.-T.; Huang, Z.; Yu, X.-Q. *Org. Biomol. Chem.* **2012**, *10*, 8342-8347.
(123) Montoya, L. A.; Pearce, T. F.; Hansen, R. J.; Zakharov, L. N.; Pluth, M. D. *J. Org. Chem.* **2013**, *78*, 6550-6557.
(124) Niu, L.-Y.; Guan, Y.-S.; Chen, Y.-Z.; Wu, L.-Z.; Tung, C.-H.; Yang, Q.-Z. *J. Am. Chem. Soc.* **2012**, *134*, 18928-18931.
(125) Liu, J.; Sun, Y.-Q.; Huo, Y.; Zhang, H.; Wang, L.; Zhang, P.; Song, D.; Shi, Y.; Guo, W. *J. Am. Chem. Soc.* **2013**, *136*, 574-577.
(126) Chen, Y.-H.; Tsai, J.-C.; Cheng, T.-H.; Yuan, S.-S.; Wang, Y.-M. *Biosens. Bioelectron.* **2014**, *56*, 117-123.
(127) Ghosh, P. B.; Whitehouse, M. W. *Biochem. J.* **1968**, *108*, 155-156.
(128) Giuliani, D.; Ottani, A.; Zaffe, D.; Galantucci, M.; Strinati, F.; Lodi, R.; Guarini, S. *Neurobiol. Learn. Mem* **2013**, *104*, 82-91.
(129) Li-Fang, H.; Ming, L.; Chi Xin, T.; Dawe, G. S.; Gang, H.; Jin-Song, B. *Aging Cell* **2010**, *9*, 135-146.
(130) Szabo, C.; Papapetropoulos, A. *Br. J. Pharmacol.* **2011**, *164*, 853-865.
(131) Zanardo, R. C. O.; Brancaleone, V.; Distrutti, E.; Fiorucci, S.; Cirino, G.; Wallace, J. L. *FASEB J.* **2006**, *20*, 2118-2120.
(132) Hui, Y.; Du, J.; Tang, C.; Bin, G.; Jiang, H. *J. Infection* **2003**, *47*, 155-160.
(133) Li, L.; Bhatia, M.; Zhu, Y. Z.; Zhu, Y. C.; Ramnath, R. D.; Wang, Z. J.; Anuar, F. B. M.; Whiteman, M.; Salto-Tellez, M.; Moore, P. K. *FASEB J.* **2005**, *19*, 1196-1198.
(134) Collin, M.; Anuar, F. B. M.; Murch, O.; Bhatia, M.; Moore, P. K.; Thiemermann, C. *Br. J. Pharmacol.* **2005**, *146*, 498-505.
(135) Gardiner, S. M.; Kemp, P. A.; March, J. E.; Bennett, T. *Br. J. Pharmacol.* **1999**, *128*, 1772-1778.
(136) Cai, W. J.; Wang, M. J.; Moore, P. K.; Jin, H. M.; Yao, T.; Zhu, Y. C. *Cardiovasc. Res.* **2007**, *76*, 29-40.
(137) Papapetropoulos, A.; Pyriochou, A.; Altaany, Z.; Yang, G.; Marazioti, A.; Zhou, Z.; Jeschke, M. G.; Branski, L. K.; Herndon, D. N.; Wang, R.; Szabó, C. *Proc. Natl. Acad. Sci. U. S. A.* **2009**, *106*, 21972-21977.
(138) Jang, H.; Oh, M.-Y.; Kim, Y.-J.; Choi, I.-Y.; Yang, H. s.; Ryu, W.-S.; Lee, S.-H.; Yoon, B.-W. *J. Neurosci. Res.* **2014**, *92*, 1520-1528.

(139) Pluth, M. D.; Bailey, T. S.; Hammers, M. D.; Hartle, M. D.; Henthorn, H. A.; Steiger, A. K. *Synlett* **2015**, *26*, 2633-2643.
(140) Li, L.; Rossoni, G.; Sparatore, A.; Lee, L. C.; Del Soldato, P.; Moore, P. K. *Free Radic. Biol. Med.* **2007**, *42*, 706-719.
(141) Isenberg, J. S.; Jia, Y.; Field, L.; Ridnour, L. A.; Sparatore, A.; Del Soldato, P.; Sowers, A. L.; Yeh, G. C.; Moody, T. W.; Wink, D. A.; Ramchandran, R.; Roberts, D. D. *Br. J. Pharmacol.* **2007**, *151*, 63-72.
(142) Muzaffar, S.; Jeremy, J. Y.; Sparatore, A.; Del Soldato, P.; Angelini, G. D.; Shukla, N. *Br. J. Pharmacol.* **2008**, *155*, 984-994.
(143) Fiorucci, S.; Orlandi, S.; Mencarelli, A.; Caliendo, G.; Santagada, V.; Distrutti, E.; Santucci, L.; Cirino, G.; Wallace, J. L. *Br. J. Pharmacol.* **2007**, *150*, 996-1002.
(144) Hasegawa, U.; van der Vlies, A. J. *Bioconjugate Chem.* **2014**, *25*, 1290-1300.
(145) Mizuno, M.; Yamano, M. *Org. Lett.* **2005**, *7*, 3629-3631.
(146) Molander, G. A.; Ellis, N. *Accounts Chem. Res.* **2007**, *40*, 275-286.
(147) Doucet, H. *Eur. J. Org. Chem.* **2008**, *2008*, 2013-2030.
(148) Alacid, E.; Nájera, C. *J. Org. Chem.* **2009**, *74*, 8191-8195.
(149) Molander, G. A.; Barcellos, T.; Traister, K. M. *Org. Lett.* **2013**, *15*, 3342-3345.
(150) Chollet, M.; Legouin, B.; Burgot, J.-L. *J. Chem. Soc. Perk. T. 2* **1998**, 2227-2232.
(151) Mosmann, T. *J. Immunol. Methods* **1983**, *65*, 55-63.
(152) Motawi, T. M. K.; Bustanji, Y.; El-Maraghy, S.; Taha, M. O.; Al-Ghussein, M. A. S. *J. Enzym. Inhib. Med. Ch.* **2014**, *29*, 153-161.
(153) Correia, I.; Arantes-Rodrigues, R.; Pinto-Leite, R.; Gaivão, I. *Toxicol. Env. Heal. A.* **2014**, *77*, 916-923.
(154) Maleszewska, M.; Steranka, A.; Kaminska, B. *Pharmacol. Rep.* **2014**, *66*, 107-113.
(155) Condorelli, F.; Gnemmi, I.; Vallario, A.; Genazzani, A. A.; Canonico, P. L. *Br. J. Pharmacol.* **2008**, *153*, 657-668.
(156) Bruce King, S. *Free Radic. Biol. Med.* **2013**, *55*, 1-7.
(157) Pietri, R.; Román-Morales, E.; López-Garriga, J. *Antioxid. Redox. Sign.* **2010**, *15*, 393-404.
(158) Lo Faro, M. L.; Fox, B.; Whatmore, J. L.; Winyard, P. G.; Whiteman, M. *Nitric Oxide* **2014**, *41*, 38-47.
(159) Kimura, H. *Antioxid. Redox. Sign.* **2014**, *20*, 783-793.
(160) Li, L.; Whiteman, M.; Guan, Y. Y.; Neo, K. L.; Cheng, Y.; Lee, S. W.; Zhao, Y.; Baskar, R.; Tan, C.-H.; Moore, P. K. *Circulation* **2008**, *117*, 2351-2360.
(161) Lee, Z. W.; Zhou, J.; Chen, C.-S.; Zhao, Y.; Tan, C.-H.; Li, L.; Moore, P. K.; Deng, L.-W. *PLoS ONE* **2011**, *6*, e21077.
(162) Zhao, Y.; Wang, H.; Xian, M. *J. Am. Chem. Soc.* **2011**, *133*, 15-17.
(163) Zhao, Y.; Bhushan, S.; Yang, C.; Otsuka, H.; Stein, J. D.; Pacheco, A.; Peng, B.; Devarie-Baez, N. O.; Aguilar, H. C.; Lefer, D. J.; Xian, M. *ACS Chem. Biol.* **2013**, *8*, 1283-1290.
(164) Devarie-Baez, N. O.; Bagdon, P. E.; Peng, B.; Zhao, Y.; Park, C.-M.; Xian, M. *Org. Lett.* **2013**, *15*, 2786-2789.
(165) Liang, D.; Wu, H.; Wong, M. W.; Huang, D. *Org. Lett.* **2015**, *17*, 4196-4199.
(166) Clennan, E. L.; Stensaas, K. L. *Org. Prep. Proced. Int.* **1998**, *30*, 551-600.

(167) Austad, B. C. In *Encyclopedia of Reagents for Organic Synthesis*; John Wiley & Sons, Ltd: 2001.
(168) Zysman-Colman, E.; Harpp, D. N. *J. Org. Chem.* **2003**, *68*, 2487-2489.
(169) Elbini Dhouib, I.; Jallouli, M.; Annabi, A.; Gharbi, N.; Elfazaa, S.; Lasram, M. M. *Life Sci.* **2016**, *151*, 359-363.